

WEAK STABILITY BOUNDARY TRANSFERS TO MOON AND MARS

*A Thesis submitted
in partial fulfilment for the degree of*

DOCTOR OF PHILOSOPHY

by

POOJA DUTT



DEPARTMENT OF MATHEMATICS

INDIAN INSTITUTE OF SPACE SCIENCE AND TECHNOLOGY

Thiruvananthapuram – 695547

May 2017

CERTIFICATE

This is to certify that the thesis entitled **Weak Stability Boundary Transfers to Moon and Mars** submitted by **Mrs. Pooja Dutt**, to the Indian Institute of Space Science and Technology, Thiruvananthapuram, in partial fulfillment for the award of the degree of **Doctor of Philosophy** is a *bona fide* record of research work carried out by her under our supervision. The contents of this thesis, in full or in parts, have not been submitted to any other Institution or University for the award of any degree or diploma.

Dr. Raju K. George
Supervisor
Dean R&D
IIST

Dr. A.K.Anilkumar
Co-supervisor
Head, APMD
VSSC

Thiruvananthapuram

Counter signature of HOD with seal

May 2017

DECLARATION

I declare that this thesis entitled **Weak Stability Boundary Transfers to Moon and Mars** submitted in partial fulfillment of the degree of **Doctor of Philosophy** is a record of original work carried out by me under the supervision of **Dr. Raju K. George** and **Dr. A. K. Anilkumar**, and has not formed the basis for the award of any other degree, diploma, associateship, fellowship or other titles in this or any other Institution or University. In keeping with the ethical practice in reporting scientific information, due acknowledgements have been made wherever the findings of others have been cited.

Pooja Dutt

SC12D002

Thiruvananthapuram - 695547

May 2017

ACKNOWLEDGMENTS

I would like to express my heartfelt gratitude to my advisors Dr. Raju K. George and Dr. A. K. Anilkumar for giving me the opportunity to work under their expert supervision. I extend my deepest regards to them for their help, care, guidance and continuous support which seamlessly encouraged me in exploring the different ideas leading to this research work.

This gives me the opportunity to thank Dr. Vinay Kumar Dadhwal, Director, IIST and Dr. K. S. Dasgupta, former Director, IIST for providing me with all the necessary facilities. I thank the former and present deans of IIST for their support and encouragement during my work. I extend my sincere thanks to Dr. K.S. Subrahmanian Moosath, Head of the Department of Mathematics, IIST for his support and valuable suggestions.

I am thankful to Dr. K. Sivan, Director, Vikram Sarabhai Space Centre; and Shri. P.S. Veeraraghavan, Shri. S. Ramakrishnan and Shri. M. C. Dathan, former Directors of VSSC for their endorsement to initiate and continue my Ph.D. work. Support and encouragements from Shri. S. Pandian, Associate Director (R&D), VSSC and Deputy Director (AERO) VSSC and Shri. Abhay Kumar Group Director AFDG are gratefully appreciated.

My profound thanks and regards to the doctoral committee members, Dr. Debashish Ghosh, IISc, Bangalore, Dr. T.R.Ramamohan, C-MMACS, Bangalore and Dr. P. Sudheesh Chethil, IIST, Dr. C.V.Anilkumar, IIST, Chairman doctoral committee and reviewers of this thesis. I am very grateful to their helpful advices, suggestions and enthusiastic support which helped me to substantially improve the quality of present work. I am indebted to all the faculty members of Department of Mathematics, IIST for their whole hearted support. I thank Anish, Nisha, Karim and Pournami, the staff members in the department, for their support and prompt help. I am also thankful to the all other departments of IIST who extended their help in many forms.

I am deeply indebted to Dr. R.K. Sharma, former Division Head, Applied Mathematics Division (APMD) and Dr.V. Adimurthy, former Associate Director, VSSC for their help, support and knowledge sharing. I thank Dr.M.Xavier James Raj, Shri. N.I.Vishnu Namboodiri, Shri. Deepak Negi, Dr. M.Mutyalarao, Smt. Shraddha Gupta, Smt. P.Bhanumathy and Smt. T.R.Saritha Kumari members of APMD, VSSC and Shri. A.Sabarinath, STS, VSSC for their help and support.

In retrospection, this is also an occasion for me to thank each and every one who has taught me at various levels for their motivating lectures. Especially I would like to thank Dr. Kiran Shrivastava, former HOD, Mathematics Department, Sarojini Naidu Girls PG College, Bhopal for her guidance, encouragement and support. I also offer my sincere appreciation to all my friends for their sincere help, support and good wishes.

Last but most important, I would like to thank my parents, brother, husband for their constant love, inspiration and support; and my special thanks to my daughter and new born baby for their profound and unconditional love.

Pooja Dutt

ABSTRACT

The conventional method to design an interplanetary trajectory is by using patched conic technique in two-body problem. It mainly consists of two impulses namely, trans-planetary injection (ΔV_{TPI}) to send the spacecraft from an Earth Parking Orbit (EPO) into heliocentric trajectory towards the destination planet, and Planetary Orbit Insertion (ΔV_{POI}) to put the spacecraft from a heliocentric trajectory to an orbit around the destination planet. Low-energy transfers are non-conventional methods for interplanetary transfers, and are associated with low-energy with respect to the given major body. Weak Stability Boundary (WSB) transfers, belong to the category of low-energy transfers which take advantage of WSB regions where gravitational attractions of the influencing bodies tend to balance each other, to reduce ΔV_{POI} (to almost zero in case of lunar transfers). The benefits of using WSB transfer over the conventional transfers are less fuel requirement, more flexibility in arrival orbits, extended launch periods and relaxed operational timeline (Parker and Anderson, 2013). WSB transfer has a major disadvantage of long flight duration.

WSB transfer to Moon was first discovered by Belbruno for the Lunar Get-a-Way Special (LGAS) spacecraft which was proposed to use electric propulsion to reach Moon and search for water at its polar regions (Belbruno, 1987). The spacecraft's thrusters were too weak to perform a conventional capture manoeuvre at Moon, so Belbruno proposed an alternative trajectory which would slowly spiral out from Earth, coast to the WSB region so that the spacecraft would be captured into an orbit around Moon. Then it would use its thrusters to spiral down to the final orbit at Moon.

WSB is described by Belbruno and Miller (1993) as “a generalization of Lagrange points and a complicated region surrounding the Moon”; Belbruno (2004) as “a region in phase space supporting a special type of chaotic motion for special choices of elliptic initial conditions with respect to m_2 ”; Yagasaki (2004) as “a transition region between the gravitational capture and escape from the Moon in the phase space”. WSB region is locus of points in the phase space of

restricted three-body problem; these points are functions of energy of infinitesimal body and its position such that its state with respect to the smaller primary transitions between ‘capture’ (its Keplerian energy with respect to the smaller primary in inertial sense, C_3 is negative), and ‘escape’ (C_3 is positive). WSB transfers take advantage of WSB region where the gravitational attraction of influencing bodies tend to balance each other, to reduce the impulse required by the spacecraft on an interplanetary trajectory to establish an orbit around the destination planet/Moon. The invariant manifold structure associated with the Lyapunov orbits near the collinear Lagrange points play an important role in this type of low-energy transfers (Belbruno, 1990; Koon et al., 2007; Anderson and Lo, 2004; Belbruno, 2004; Gomez et al., 2004; Garcia and Gomez, 2007; Topputo et al., 2008; Alessi, 2009 a,b; Fantino et al., 2010).

Belbruno’s WSB theory was demonstrated in 1990 when Japanese first Moon mission suffered a failure. This mission consisted of two spacecraft MUSES A and MUSES B. The smaller one, MUSES B was to go to Moon, while the larger one, MUSES A was to remain in Earth orbit as a communication relay. Unfortunately, MUSES B failed and MUSES A did not have sufficient fuel to reach Moon. WSB trajectory was designed for MUSES A which took advantage of gravitational forces of Sun along with Earth and Moon to reach Moon (Belbruno and Miller 1990; Uesugi 1991). In April 1991, MUSES A, renamed as Hiten fired its engines to reach Moon on 2nd October 1991.

Awareness regarding unconventional trajectories in spaceflight was again highlighted by AsiaSat3 in 1998. Due to an upper stage malfunction of Proton rocket, AsiaSat3 was stranded in an elliptical transfer orbit instead of GEO. Although the spacecraft lacked necessary propellant to reach GEO, its controllers were able to perform a series of manoeuvres that sent it around Moon twice and finally to GEO (Ocampo, 2005). The spacecraft was able to operate in limited capacity for several years. Next ESA’s SMART-1 (Schoenmaekers et al., 2001) was launched on 27 Sep 2003 reached Moon utilizing a low-energy transfer trajectory like the one designed for LGAS. NASA’s Gravity Recovery and Interior Laboratory (GRAIL) Mission in 2011 (Roncoli and Fujii 2010, Chung et

al. 2010 and Hatch et al. 2010) was the first mission launched to Moon directly on a low energy transfer. GRAIL launched two spacecraft on board a single launch vehicle and used the long flight duration (~90-114 days) to separate their orbit insertion epochs by 25 hours. Low energy transfer is proposed for missions like Multi Moon Orbiter (Ross et al., 2003; Ross et al., 2004), Europa Orbiter (Sweetser et al., 1997; Johannesen and D'Amario, 1999; Heaton et al., 2002) and BepiColombo (Jehn et al., 2004; Campagnola and Lo, 2007; Jehn et al., 2008).

Using the dynamical system theory some natural phenomena like resonance hopping and capture observed in Jupiter comets has been explained (Belbruno and Marsden, 1997; Lo and Ross, 1997; Howell et al., 2000; Koon et al., 2007). Further, Belbruno and Gott (2005) attempt to explain the BigSplat hypothesis and Belbruno et al. (2008) explain the lithopanspermia hypothesis using the dynamical system theory.

The work carried out in this thesis mainly concerns with the design of WSB transfers to Moon and Mars and studies their dynamics. In order to study the dynamics of WSB trajectories to Moon, lunar capture trajectories and geocentric elliptical orbits are represented on phase space diagrams. These results will be useful for mission designers as the phase space diagrams with colour code on time of flight (and capture) enables the selection of departure (and arrival) orbits and total time of flight can be approximated without actually constructing the complete trajectory. It is known that the positional phase angle of perilune of lunar capture trajectories lies within -55° to 55° and 125° to 235° (Yamakawa, 1992). With the help of numerical simulations it is found that this holds good for lower altitudes but it is violated to some extent for higher apolune altitudes.

Dynamics of capture orbits at Mars are studied in the framework of restricted three-body problem. It is found that for higher periapsis altitudes ($\geq 10,000$ km) almost all ranges positional phase angle of periapsis in Sun-Mars fixed rotating frame yields capture orbits. Hence in order to obtain WSB trajectories to Mars, the algorithm has to be targeted to high periapsis altitudes to increase the possibility of finding capture orbits.

Numerical algorithms are developed to obtain WSB trajectories to Moon and Mars in real world scenario. These algorithms start from an EPO, use forward propagation to reach a capture trajectory at Moon/Mars. Literature is flooded with back-propagation algorithms to find WSB trajectories, which face major problem of launch vehicle constraint satisfaction. Back-propagated trajectories may lead to a patching point, too expensive for a launch vehicle to satisfy its maximum payload constraints (mainly AOP and inclination). This drawback is eliminated in this case and these algorithms can be applied to both circular and elliptical EPO. Also given a departure date and EPO conditions, a number of WSB arrival orbits can be found using the given algorithm with marginal difference in impulse requirements but varying arrival orbits. In case of conventional transfers, the inclination of arrival orbit depends on declination of incoming hyperbola. But for WSB transfers different inclination arrival orbits are obtained for the same incoming trajectory. The one suiting our requirements can be selected. Another advantage of this algorithm is that the WSB trajectories are developed in high fidelity force model which can be used for actual missions.

ORGANIZATION OF THE THESIS

This thesis consists of the following chapters

Chapter 1 introduces the conventional method for the design of interplanetary trajectories, fly-by and orbiter trajectories and alternative methods to reduce ΔV for interplanetary methods like gravity assist, aerobraking, aerocapture and weak stability boundary transfers.

Chapter 2 gives a literature survey of works and important contributions in the area of low energy transfers. This work is under review with the journal “Astrophysics and Space Science”.

In Chapter 3, as first step towards orbiter missions, planar fly-by trajectories to Moon are studied in the framework of R3BP. A number of initial conditions (x, y, \dot{x}, \dot{y}) of the form $(x_0, 0, 0, y_0)$ and $(-\mu, y_0, \dot{x}_0, 0)$ close to Earth are propagated for 1000 days and plotted on phase space with colour code on time of flight. It is observed that the trajectories with similar flight duration appear in clusters in the phase space. This result is published in Advances in Space Research.

In Chapter 4, the dynamics of WSB trajectories to Moon is studied in the framework of R3BP. A number of Lunar Capture trajectories (LCT) and highly elliptical geocentric (HEG) orbits are studied and eligible candidates for design of WSB trajectories to Moon are represented on the phase space. Also fly-by Moon on the way to apogee for a HEG is investigated. In bicircular restricted three-body problem, WSB trajectory to Moon is constructed using fixed time of arrival targeting for patching HEG with LCT. Some optimization techniques are evaluated to find optimal patching points to reduce total impulse requirement. These results are published in Astrophysics and Space Science and IAC 2015.

Chapter 5 presents an algorithm to find WSB trajectories to Moon in high fidelity force model using forward propagation. The algorithm starts from an EPO (circular or elliptical), varies control parameters at EPO and on its way to Moon to arrive at a capture trajectory at Moon. Importance of forward propagation for

determination of WSB to Moon is highlighted. Results are accepted for publication in the journal “Astrophysics and Space Science”.

In Chapter 6 the dynamics of capture orbits at Mars is studied in the framework of R3BP. Then an algorithm to find WSB transfer to Mars in high fidelity force model using forward propagation is developed. Using this algorithm a number of capture trajectories to Mars are determined and their characteristics are noted. A paper consolidating these results is under review with the journal “Journal of Spacecraft and Rockets”.

Chapter 7 provides the conclusions of the present studies and also gives an outline for future studies.

TABLE OF CONTENT

CERTIFICATE	v
DECLARATION	vii
ACKNOWLEDGEMENT	ix
ABSTRACT	xi
ORGANIZATION OF THE THESIS	xv
LIST OF FIGURES	xxi
LIST OF TABLES	xxix
ABBREVIATIONS	xxxix
NOTATIONS	xxxv
CONSTANTS	xxxvii
1. DESIGN OF INTERPLANETARY TRAJECTORIES	1
1.1. Introduction	1
1.2. Interplanetary Trajectory Design Methodology	1
1.3. Fly-by and Orbiter Trajectories	7
1.3.1. Injection Conditions	8
1.3.1.1. Tangential Injection from Perigee ($i \geq \delta_\infty$)	9
1.3.1.2. Tangential Injection from Perigee ($i < \delta_\infty$)	10
1.4. Methods to reduce ΔV Requirements for Interplanetary Missions	11
1.4.1. Gravity Assist Manoeuvre	11
1.4.2. Aerobraking	12
1.4.3. Aerocapture	13
1.4.4. Weak Stability Boundary Transfers	14
1.5. Conclusion	15
2. REVIEW OF WEAK STABILITY BOUNDARY TRANSFER TRAJECTORIES	17
2.1 Introduction	17
2.2 Review of WSB	19
2.2.1 Circular Restricted Three-Body Problem	19
2.2.1.1 Analytical definition of Capture and WSB given by	21

Belbruno (2004)	
2.2.1.2 Numerical Algorithmic definition of WSB given by Belbruno (2004)	23
2.2.1.3 Definition of WSB given by García-Gómez (2007)	25
2.2.2. WSB Trajectory Design	26
2.2.3. Dynamical System Theory	32
2.2.4. Optimization for computation of WSB trajectories	35
2.3. Notable Missions/Planned Missions	37
2.4. Low Thrust Trajectories	39
2.5. Conclusion	41
3. ANALYSIS OF PLANAR FLY-BY TRAJECTORIES TO MOON	43
3.1. Introduction	43
3.2. Methodology	44
3.3. Results	46
3.4. Conclusion	53
4. DYNAMICS OF WEAK STABILITY BOUNDARY TRANSFER TRAJECTORIES TO MOON	55
4.1. Introduction	55
4.2. Equations of Motion	56
4.2.1 Conditions for Easy Capture at Moon	58
4.3. Dynamics of WSB Trajectories	59
4.3.1 Lunar Capture Trajectories	59
4.3.2 Enlargement of perigee from LEO to Earth-Moon distance	60
4.3.3. Fly-by Moon on the way to apogee	63
4.4. Construction of WSB Trajectory	65
4.5. Conclusions	69

5. DESIGN OF WSB TRAJECTORY TO MOON USING FORWARD PROPAGATION	71
5.1 Introduction	71
5.2 Methodology	71
5.3 Results	74
5.3.1. Analysis of WSB transfers to Moon	74
5.3.2. Analysis of capture orbits for a particular case	75
5.4 Conclusion	76
6. WEAK STABILITY BOUNDARY TRANSFERS TO MARS	93
6.1. Introduction	93
6.2. Dynamics of WSB capture orbits at Mars	95
6.3. Algorithm for Numerical Computation of WSB Trajectories	98
6.4. Results	102
6.5. Conclusion	107
7. CONCLUDING REMARKS AND FUTURE WORKS	121
References	123
Appendix	139
Appendix A: Restricted Three-Body Problem	139
Appendix B: Restricted three-body problem in polar form	143
Appendix C: Bi-circular Restricted Three-Body Problem	148
Appendix D: Fixed Time of Arrival Targeting	149
Appendix E: Lambert Conic Method	151
Appendix F: Program listing	153
List of Publications based on the Thesis	177

LIST OF FIGURES

FIGURE NO.	TITLE	PAGE NO.
1.1	Hohmann Transfer Geometry	2
1.2	Lambert conic transfer geometry	4
1.3	Pseudostate transfer geometry	5
1.4	Patched conic transfer geometry	6
1.5	C3 Departure contour plots for the launch opportunity to Mars during 2018	8
1.6	C3 Total contour plots for the launch opportunity to Mars during 2018	8
1.7	Mechanics of Aerobraking	12
1.8	Mechanism of Aerocapture	13
1.9	Hiten spacecraft	14
1.10	Trajectory GRAIL spacecraft	15
2.1	Stable, unstable motion and primary interchange escape (Belbruno, 2004)	25
3.1(a)	Initial condition space along with the periodic orbits contained in the white regions	47
3.1(b)	Initial condition space along with the fly-by trajectories with $TOF \leq 90$ days	48
3.2(a)	Poincaré surface of section for $C=2.7$ and corresponding periodic orbits	48
3.2(b)	Poincaré surface of section for $C=3.1$ and corresponding periodic orbits	49
3.3	A typical trajectory with $C=2.6$, $x=0.48368684$, $TOF=37$ days, $r_2=408$ km	50
3.4(a)	Initial condition space for set (ii) ICs along with PO contained in the white regions	51
3.4(b)	Initial condition space for set (ii) along with some fly-by trajectories	51
3.5(a)	Fly-by trajectories for IC of set (ii) whose TOF lies between 15 to 30 days	52
3.5(b)	Fly-by trajectories for set (ii) of IC whose TOF lies between	52

	30 to 40 days	
3.6	A typical trajectory of set (ii) IC with $C=3.09$, $y=-0.32154006$, $TOF=16.8$ days, $r_2=421$ km	53
4.1	Variation in error due to initial step size for different tolerance values	57
4.2	Variation of step-size within the RKF integrator for a given initial step size (H)	57
4.3	Lunar capture trajectories obtained by back propagation for 50 days. The initial conditions which lead to a capture trajectory are plotted in the phase space with colour code on time of capture. (a) Direct motion about m_2 , (b) Retrograde motion about m_2 .	59
4.4	EPO whose perigee rose from 200 km to about 384400 km propagated in bi-circular R3BP (Initial lunar phase angle is 0°) with colour code on time of flight	61
4.5	Comparison of phase space re presentation of EPO whose perigee rose from 200 km to 384400 km for initial lunar phase angle (θ_{M0}) 0° and 90° .	62
4.6	EPO which encounter Moon on return to perigee	62
4.7	Fly-by Moon on the way to apogee with colour code on time of flight	63
4.8 (a-j)	Dependence of time of flight on the angular position of Moon during flyby on the way to apogee	63-65
4.9	An Earth centred orbit	66
4.10	Lunar Capture orbit	66
4.11	Patching Earth centred orbit with Lunar capture orbit using FTAT	66
4.12	Patching points A and B obtained by GA	67
5.1	Control parameters for trajectory optimization – WSB Moon	72
5.2	Flowchart of the process for computation of WSB trajectory to Moon	73
5.3	WSB trajectory to Moon for example 1 (launch date 20 Nov 2017) in 2D space	81
5.4	WSB trajectory to Moon for example 1 (launch date 20 Nov 2017) in 3D space	81

5.5	WSB trajectory to Moon for example 2 (launch date 2 Dec 2017) in 2D space	82
5.6	WSB trajectory to Moon for example 2 (launch date 2 Dec 2017) in 3D space	82
5.7	WSB trajectory to Moon for example 3 (launch date 10 Dec 2017) in 2D space	83
5.8	WSB trajectory to Moon for example 3 (launch date 10 Dec 2017) in 3D space	83
5.9	WSB trajectory to Moon for example 4 (launch date 19 Dec 2017) in 2D space	84
5.10	WSB trajectory to Moon for example 4 (launch date 19 Dec 2017) in 3D space	84
5.11	WSB trajectory to Moon for example 1 (launch date 30 Dec 2017) in 2D space	85
5.12	WSB trajectory to Moon for example 1 (launch date 30 Dec 2017) in 3D space	85
5.13	Total ΔV histogram for capture orbits in case 3	86
5.14	ΔV_C histogram for capture orbits in case 3	86
5.15	Total time of flight histogram for capture orbits for case 3	86
5.16	Histogram of minimum eccentricity attained by the capture orbits for case 3	86
5.17	Histogram of Perilune altitude of capture orbit at minimum eccentricity for case 3	86
5.18	Histogram of inclination of capture orbits at minimum eccentricity for case 3	86
5.19	Variation in C3 of the spacecraft with respect to Moon as a function of iteration number for some of the outer and inner loops in case 3	87
5.20	Variation in objective function value as a function of inner loop number for some outer loops for case 3	88-89
5.21	Mean variation in ΔV_2 for all the outer loops in case 3	90
5.22(a-c)	Mean variation in ΔV_{2x} , ΔV_{2y} and ΔV_{2z} for all the outer loops in case 3	90
5.23	Variation in min. ΔV_2 for all the outer loops in case 3	90
5.24	Variation in min. C3 of spacecraft wrt Moon for all the outer	90

	loops in case 3	
5.25	AOP varied by the outer loops and corresponding distance from Moon	91
5.26	RAAN varied by the outer loops and corresponding distance from Moon	91
5.27	Perilune and apolune profiles for minimum eccentricity orbit attained by various outer loops (same color and marker denotes same outer loop)	91
5.28	zoomed version of Fig. 5.27	91
5.29	semi-major axis and eccentricity profiles for minimum eccentricity orbit attained by various outer loops	91
5.30	Perilune and ΔV_3 profiles for minimum eccentricity orbit attained by various outer loops	91
6.1	Structure of the ballistic capture transfers to Mars	94
6.2	Time of capture (TOC in days) as a function of Apoapsis Altitude and positional phase angle of periapsis (θ) for periapsis altitude 1000 km (a) direct motion about m_2 (b) retrograde motion about m_2 .	96
6.3	Time of capture (TOC in days) as a function of Apoapsis Altitude and θ for periapsis altitude 5000 km (a) direct motion about m_2 (b) retrograde motion about m_2 .	96
6.4	Time of capture (TOC in days) as a function of Apoapsis Altitude and θ for periapsis altitude 10,000 km (a) direct motion about m_2 (b) retrograde motion about m_2 .	97
6.5	Time of capture (TOC in days) as a function of Apoapsis Altitude and θ for periapsis altitude 25,000 km (a) direct motion about m_2 (b) retrograde motion about m_2 .	97
6.6	Time of capture (TOC in days) as a function of Apoapsis Altitude and θ for periapsis altitude 1,00,000 km (a) direct motion about m_2 (b) retrograde motion about m_2 .	97
6.7	Time of capture (TOC in days) as a function of Apoapsis Altitude and θ for periapsis altitude 5,00,000 km (a) direct motion about m_2 (b) retrograde motion about m_2 .	98
6.8	Sample trajectory from Earth to Mars with ΔV_c leading to capture	99

6.9	Control variables for WSB trajectory optimization	99
6.10	Flowchart of the process to obtain WSB transfers from Earth to Mars	101
6.11	C3 Departure contour plots for the launch opportunity to Mars during 2018	102
6.12	C3 Total contour plots for the launch opportunity to Mars during 2018	102
6.13	2D representation of WSB trajectory to Mars case 1 launch date 25 Mar 2018	113
6.14	3D representation of WSB trajectory to Mars case 1 launch date 25 Mar 2018	113
6.15	2D representation of WSB trajectory to Mars case 2 launch date 10 Apr 2018	113
6.16	3D representation of WSB trajectory to Mars case 2 launch date 10 Apr 2018	113
6.17	2D representation of WSB trajectory to Mars case 3 launch date 24 Apr 2018	113
6.18	3D representation of WSB trajectory to Mars case 3 launch date 24 Apr 2018	113
6.19	2D representation of WSB trajectory to Mars case 4 launch date 9 May 2018	114
6.20	3D representation of WSB trajectory to Mars case 4 launch date 9 May 2018	114
6.21	2D representation of WSB trajectory to Mars case 5 launch date 20 May 2018	114
6.22	3D representation of WSB trajectory to Mars case 5 launch date 20 May 2018	114
6.23	2D representation of WSB trajectory to Mars case 6 launch date 1 Jun 2018	114
6.24	3D representation of WSB trajectory to Mars case 6 launch date 1 Jun 2018	114
6.25	2D representation of WSB trajectory to Mars case 7 launch date 15 Jun 2018	115
6.26	3D representation of WSB trajectory to Mars case 7 launch date 15 Jun 2018	115

6.27	2D representation of WSB trajectory to Mars case 8 launch date 27 Jun 2018	115
6.28	3D representation of WSB trajectory to Mars case 8 launch date 27 Jun 2018	115
6.29	2D representation of WSB trajectory to Mars case 9 launch date 11 Jul 2018	115
6.30	3D representation of WSB trajectory to Mars case 9 launch date 11 Jul 2018	115
6.31	Variation in distance from Mars for direct and WSB trajectories for case 1	116
6.32	Velocity of the spacecraft with respect to Mars for direct and WSB trajectories for case 1	116
6.33	Converged values of launch epoch for each outer loop for case 7	116
6.34	Converged values of flight duration from launch epoch to time of ΔV_c maneuver for each outer loop for case 7	116
6.35	Converged values of ΔV_{TMI} for each outer loop for case 7	116
6.36	Converged values of RAAN and AOP for each outer loop for case 7	116
6.37	Converged values of ΔV_c for each outer loop for case 7	117
6.38	Objective function value for each outer loop for case 7	117
6.39	Variation in all the three components of ΔV_c corresponding to each outer loop for case 7	117
6.40	Variation of C3 of the spacecraft wrt Mars by the inner loop for some outer loops (OL) namely, 89, 167, 256, 291, 301, 302, 312, 327, 342	118-119
6.41	Histogram of semi-major axis of capture orbits for case 7	119
6.42	Histogram of inclination of capture orbits for case 7	119
6.43	Histogram of capture time (from ΔV_c epoch till capture epoch) for case 7	119
6.44	Histogram of altitude R_c at which ΔV_c is applied for case 7	119
6.45	Capture ΔV_c and altitude R_c at which ΔV_c is applied - case 7	120
6.46	Capture ΔV_c vs capture duration (no. of days from ΔV_c to capture) – case 7	120
6.47	Minimum eccentricity attained after ΔT days after being	120

	captured in orbit around Mars - case 7	
6.48	Histogram of periapsis altitude of minimum eccentricity orbits for case 7	120
6.49	DeltaV required to reduce from captured orbit to 1000 km circular and 500X80,000 km orbits- case 7	120
A.1	R3BP - Earth-Moon system with Lagrange Points	140
B.1	R3BP (Cartesian and Polar Coordinates)	143
C.1	Bi-circular restricted three-body problem	149
D.1	Fixed time of arrival targeting	150
E.1	Transfer arc obtained by Lambert conic from Earth to Mars	151

LIST OF TABLES

TABLE NO.	TITLE	PAGE NO.
1.1	Synodic Period for some planets	3
1.2	SOI radius for some planets and Moon	6
4.1	Comparison between optimization methods – Pattern Search, Nelder-Mead Simplex algorithm and genetic algorithm	68
4.2	Comparison between Hohmann transfer, Invariant manifold theory (Topputo et al 2004) and present method using GA	69
5.1	Test cases	78
5.2	Details of Trajectory with minimum total ΔV – Part I	80
5.3	Details of Trajectory with minimum total ΔV – Part II	80
6.1	Input trajectory details for the test cases	108
6.2	WSB trajectory details for the test cases	109
6.3	WSB trajectory details of orbit obtained at capture for the test cases	110
6.4	WSB trajectory details of minimum eccentricity orbit obtained after capture for the test cases	111
6.5	Comparison of direct transfer and WSB transfer trajectory for case 1	112

ABBREVIATIONS

AOP	Argument of Perigee
AOPI	Argument of Perilune
ARTEMIS	Acceleration, Reconnection, Turbulence and Electrodynamics of the Moon's Interaction with the Sun (Mission)
COM	Centre of mass
CR3BP	Circular Restricted Three-Body Problem
JPL-DE421	JPL Development Ephemeris 421
EGM-96	Earth Gravitational Model 1996
EPO	Earth Parking Orbit
FTAT	Fixed Time of Arrival Targeting
GA	Genetic algorithm
GC	Gravitational Capture
GRAIL	Gravity Recovery and Interior Laboratory (Mission)
GTO	Geostationary Transfer Orbit
HEG	Highly Elliptical Geocentric (orbit)
IC	Initial Condition(s)
IS_p	Specific Impulse
JPL	Jet Propulsion Laboratory
LC	Lambert Conic
LCT	Lunar Capture Trajectory
LEO	Low Earth Orbit

LGAS	Lunar Get-a-way Special (spacecraft)
LOI	Lunar Orbit Insertion
LPO	Libration Point Orbit
LTP	Low Thrust Propulsion
LTT	Low Thrust Trajectory
MOI	Mars Orbit Insertion
MOM-1	Mars Orbiter Mission-1
NRLMSIS-00	2001 United States Naval Research Laboratory Mass Spectrometer and Incoherent Scatter Radar Exosphere atmospheric model
NSGA	Non-dominated sorting genetic algorithm
PO	Periodic Orbit
POI	Planetary Orbit Insertion
PS	Pattern Search (optimization method)
PSS	Poincaré Surface of Section
R3BP	Restricted three-body problem
RKF(7,8)	Runge-Kutta-Fehlberg 7 th order integration scheme with 8 th order error estimator
SEP	Solar Electric Propulsion
SMART-1	Small Missions for Advanced Research in Technology-1
SOI	Sphere of Influence
TCM	Trajectory Correction Manoeuvre
TLI	Trans-Lunar Injection
TMI	Trans-Mars Injection

TOC	Time of capture
TOF	Time of flight
TPI	Trans-planetary injection
wrt	with respect to
WSB	Weak Stability Boundary
Min.	Minimum

NOTATIONS

μ_S	gravitational constants of Sun
μ_E	gravitational constants of Earth
μ_P	gravitational constants of planet under consideration
r_{SOI}	Sphere of Influence radius
R_P	Distance between Sun and planet under consideration
m_P	Mass of the planet under consideration
m_S	Mass of Sun
V_∞	Hyperbolic excess velocity vector
C_3	Excess hyperbolic energy
α_∞	Right ascension of V_∞
δ_∞	Declination of V_∞
$\Delta v, \Delta V$	Magnitude of change in velocity, impulse
i	Inclination of EPO
Ω	Right ascension of ascending node of EPO
ω	Argument of perigee of EPO
u	Argument of injection points on EPO
θ_∞	True anomaly at ∞
β_∞	angle between the outgoing asymptote and the spin axis of the Earth
W	Weak Stability Boundary set
μ	Mass ratio of the system in R3BP
m_1, m_2	More massive and less massive primaries in R3BP

μ_1, μ_2	Mass of more massive and less massive primaries in R3BP.
$L_i, i=1,2,\dots,5$	Libration points in R3BP
ΔV_{TLI}	Trans-lunar Injection impulse
ΔV_{LOI}	Lunar Orbit Insertion impulse
ΔV_{TCM}	Trajectory correction manoeuvre
ΔV_L	Impulse required to reduce the capture orbit at Moon to 100 km circular orbit
ΔV_{TMI}	Trans-Mars Injection impulse
ΔV_{MOI}	Mars Orbit Insertion impulse required for 1000 km circular orbit at Mars
ΔV_{MOI_ell}	Mars Orbit Insertion impulse required for 500 km X 80,000 km orbit at Mars
ΔV_C	Impulse given at WSB region of Mars so that a ballistic capture trajectory is obtained within specified time period
ΔT	Time in days required for the spacecraft to travel from departure epoch to reach WSB region of Mars where ΔV_C is applied to obtain a ballistic capture orbit at Mars
ΔV_{ell}	Impulse required to reduce the minimum eccentricity ballistic capture orbit at Mars to 500 km X 80,000 km orbit
ΔV_{circ}	Impulse required to reduce the minimum eccentricity ballistic capture orbit at Mars to 1000 km circular orbit
ΔV_T	Sum of ΔV_C and ΔV_{circ}
ΔV_{T_ell}	Sum of ΔV_C and ΔV_{ell}

CONSTANTS

Astronomical constants	Values
mass ratio for Earth-Moon system (μ)	0.012150829
mass ratio for Sun-Mars system (μ)	$3.227136860121953 \times 10^{-7}$
gravitational constants of Sun (μ_S)	$1.32712428 \times 10^{11}$
gravitational constants of Earth (μ_E)	$398600.4415 \text{ km}^3/\text{s}^2$
gravitational constants of Mars (μ_M)	$42828.4 \text{ km}^3/\text{s}^2$
gravitational constants of Moon (μ_L)	$4902.799 \text{ km}^3/\text{s}^2$
Equatorial radius of Earth	6378.137 km
Equatorial radius of Moon	1738 km
Equatorial radius of Mars	3397.2 km
Distance between Earth and Moon	384400 km
Distance between Sun and Mars	227939186 km
SOI of Earth	924650 km
SOI of Mars	576000 km
SOI of Moon	66100 km

CHAPTER 1

DESIGN OF INTERPLANETARY TRAJECTORIES

1.1. Introduction

An interplanetary flight is the journey of a vehicle, spacecraft from Earth to a definite point of the solar system. Once the spacecraft escapes Earth, it becomes an independent member of solar system and therefore its motion can be first approximated by laws of two-body problem with Sun as the central body. The solution of two-body problem is a conic section – an ellipse, parabola or hyperbola. From all three types of conical sections elliptical orbit has the smallest initial velocity – hence most economic. Thus, a spacecraft launched from Earth towards any planet/moon should perform its journey in an arc of an ellipse with Sun at one of the foci, Earth on one end of the arc and the destination planet on the other end of the arc.

1.2. Interplanetary Trajectory Design Methodology

Interplanetary trajectory design is an iterative process which begins by finding simple baseline trajectory as a reference, which is improved by adding complexity in each step. The final phase of trajectory design is obtained by solving the four-body equations of motion, involving the departure and arrival planets, Sun and the spacecraft (Vallado, 2001).

$$\frac{d^2\vec{r}}{dt^2} = -\mu_S \frac{\vec{r}}{r^3} - \mu_E \left(\frac{\vec{r}_E}{r_E^3} + \frac{\vec{R}_E}{R_E^3} \right) - \mu_P \left(\frac{\vec{r}_P}{r_P^3} + \frac{\vec{R}_P}{R_P^3} \right), \quad (1.1)$$

where, μ_S , μ_E and μ_P are the gravitational constants of Sun, Earth and the destination planet, respectively, \vec{r} , \vec{r}_E and \vec{r}_P are the radius vector of spacecraft with respect to Sun, Earth and destination planet, respectively, and \vec{R}_E and \vec{R}_P are the radius vector of Earth and destination planet, respectively, with respect to Sun.

But this equation does not have closed form solution. If a baseline trajectory is not available, then searching for a favorable trajectory using numerical integration over search space for all the design variables will involve enormous computer time and often it is not possible. This necessitates analytical design methodologies for initial design phase.

If the orbits of the planets were circular and coplanar then *Hohmann transfer ellipse* is most economical. It is the ellipse in contact with the circular orbits of Earth and destination planet exactly at perihelion and apohelion (in case of exterior planet and vice versa for interior planet).

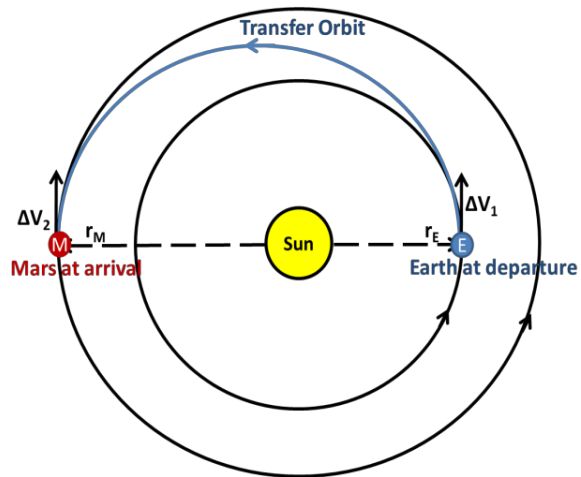


Fig. 1.1: Hohmann Transfer Geometry

That means in order to have a minimum energy transfer trajectory, the transfer angle between heliocentric positions of Earth on departure date and destination planet on arrival date should be 180° . The years for which such an approximation of position occurs are said to offer *launch opportunity*. Fig. 1.1 gives the Hohmann transfer geometry for transfer between Earth and Mars. The periapsis of the transfer orbit is the position of Earth at departure (r_E), which is diametrically opposite to the apoapsis of transfer orbit which is the position of Mars at arrival (r_M). ΔV_1 is the velocity change required to put the spacecraft from Earth's orbit to transfer orbit and ΔV_2 is the velocity change required to put the spacecraft from transfer orbit to Mars' orbit.

Hohmann geometry enables to locate the launch opportunity for interplanetary transfers. The minimum energy transfer occurs in the neighbourhood of Hohmann geometry. The *synodic period* is the time interval between launch opportunities and is characteristic of each planet. If ω_1 and ω_2 are the orbital angular

rates of the inner and outer planets, respectively, moving about Sun in circular orbits, then the mutual configuration of the two bodies changes at the following rate:

$$\omega_{12} = \omega_1 - \omega_2, \frac{rad}{s} \quad (1.2)$$

If a period of revolution P is defined as

$$P = \frac{2\pi}{\omega}, s \quad (1.3)$$

then,

$$\frac{1}{P_S} = \frac{1}{P_1} - \frac{1}{P_2}, \quad (1.4)$$

where P_S is the synodic period, ie, the period of planetary geometry recurrence, and P_1 and P_2 are the orbital sidereal periods of the inner and the outer planet considered, respectively. Since the planetary orbits are neither exactly circular nor coplanar, launch opportunities do not repeat exactly, some opportunities are better than others. *Synodic cycle* consists of a number of synodic periods when there is a complete repeat of trajectory characteristics. It occurs when exactly the same orbital geometry of departure and arrival body recurs (Sergeyevsky et al., 1983). Table 1.1 gives the synodic period for Mercury, Venus, Mars and Jupiter (<http://star.arm.ac.uk;www.opencourse.info>).

Table 1.1: Synodic Period for some planets

	Mercury	Venus	Mars	Jupiter
Synodic Period (days)	116	584	780	399

The basic assumption in Hohmann transfer is that the departure and arrival orbits are circular and coplanar. As first step, Hohmann transfer gives a good starting solution as the planets in the solar system lie very close to the ecliptic plane with small eccentricities. But in order to be more precise, *Lambert conic* or *point conic*

method (Fig. 1.2) is used which takes into account the actual positions of planets. Three dimensional transfer trajectory characteristics are obtained in the framework of two-body problem. Still the planets are considered as point masses, their gravity is not considered. The velocity requirements and orientation of elliptical Earth parking orbit are obtained using point conic method, described in the Appendix F.

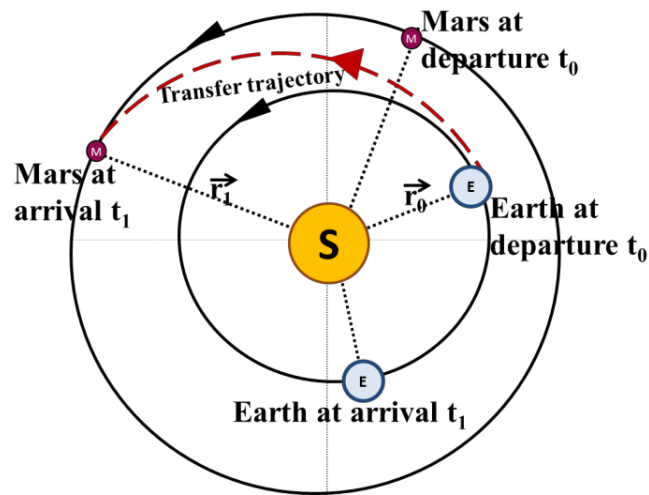


Fig. 1.2: Lambert conic transfer geometry

Further improvement is possible by the use of *pseudostate theory* (Fig. 1.3), first introduced by Wilson (1970) and modified by Byrnes (1979). Venkattaramanan (2006) has developed this method for lunar transfers. Pseudostate theory solves the Lambert problem, not between true planetary positions, but between two computed “pseudostates”. These are obtained by iteration on two displacement vectors of the planetary ephemeris positions on departure and arrival dates.

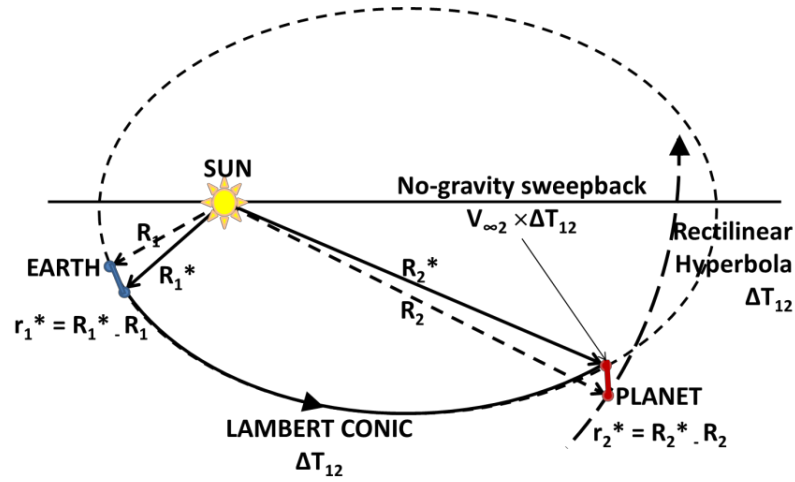


Fig. 1.3: Pseudostate transfer geometry

Further refinement comes from *patched conic technique* where the gravity of departure planet, Sun and arrival planets are considered one at a time. The trajectory is divided into heliocentric and planetocentric stages, depending on sphere of influence of planets where two-body approximation holds good. The *sphere of influence*, SOI of a planet is the radial distance surrounding the planet where its gravity becomes dominant over the Sun's. If m_s and m_p be the masses of Sun and the planet respectively, and R_p be the distance between the Sun and the planet then the SOI radius about that planet is given by (Curtis, 2005) –

$$r_{SOI} = R_p \left(\frac{m_p}{m_s} \right)^{2/5}. \quad (1.5)$$

SOI, in fact, is not quite a sphere. The distance to the SOI depends on the angular distance θ from the massive body. A more accurate formula is given by (Barrabés et al., 2004) –

$$r_{SOI}(\theta) \approx R_p \left(\frac{m_p}{m_s} \right)^{2/5} \frac{1}{\sqrt[10]{1 + 3\cos^2(\theta)}}, \quad (1.6)$$

Table 1.2 (from en.wikipedia.org) gives the SOI radius for some planets. SOI is more a concept than a physical reality.

Table 1.2: SOI radius for some planets and Moon

	Mercury	Venus	Earth	Moon	Mars	Jupiter
SOI radius (million km)	0.112	0.616	0.924	0.0661	0.576	48.2

In patched conic method, as shown in Fig. 1.4, the trajectory from departure planet to arrival planet is divided into three segments. When the spacecraft is within the SOI of departure planet, two-body equations of motion (considering departure planet and spacecraft) are solved. At an infinite distance ($r = \infty$ at the SOI), only the velocity determines the energy. It may be zero or some positive value, $V^2/2$. If the energy is positive, further motion is possible. The quantity $V^2/2$ is often called v -infinity, v_∞ , or *hyperbolic excess velocity* because it is the excess velocity at “infinity”, $C_3 = V_\infty^2 = -\mu/a$, ie, twice the injection energy per unit mass. Once outside the SOI of departure planet, the spacecraft is under influence of Sun, so two-body problem considering Sun and spacecraft are solved. When the spacecraft reaches the SOI of arrival planet, hyperbolic excess velocity with respect to arrival planet is computed and then equations of motion of two-body problem considering arrival planet and spacecraft are solved.

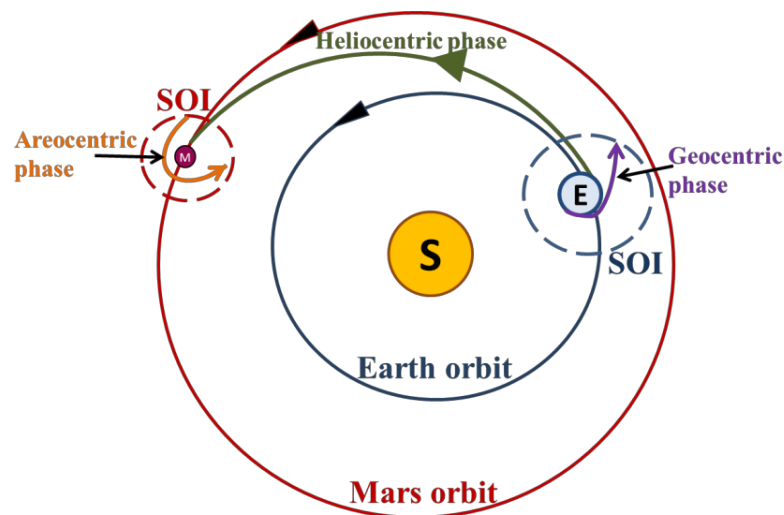


Fig. 1.4: Patched conic transfer geometry

The final phase of trajectory design is using numerical integration of the trajectory starting from Earth parking orbit (EPO) till the desired orbit around destination planet using full force model. The final trajectory obtained from above methods is the minimum energy trajectory satisfying the launch vehicle constraints at EPO and reaching the desired mapping orbit around destination planet and satisfying mission constraints, is refined using numerical integration of full force model considering gravity of all influencing planets and other perturbations acting on the spacecraft. Further details on the above methods can be obtained from Gurzadyan (1996); Venkattaramanan (2006); Curtis (2005); Battin (1999).

1.3. Fly-by and Orbiter Trajectories

Interplanetary transfer trajectory involves two Manoeuvres:

- (i) Trans-planetary Injection (ΔV_{TPI}) that enables spacecraft to escape from Earth's gravity and begin its journey towards destination planet
- (ii) Planetary Orbit Insertion (ΔV_{POI}) puts the spacecraft into an orbit around the destination planet.

On the course of travel, some corrections in the trajectory are carried out using Trajectory Correction Manoeuvres (ΔV_{TCM}).

Planetary missions are in general classified as (i) Fly-by missions, and (ii) Orbiter missions. In a fly-by mission, only ΔV_{TPI} velocity impulse is applied so that the spacecraft fly-bys the destination planet. In such cases only ΔV_{TPI} velocity impulse needs to be minimized to find minimum energy transfer trajectory. For orbiter missions, both ΔV_{TPI} and ΔV_{POI} velocity impulses are applied. Thus for orbiter mission, the sum of ΔV_{TPI} and ΔV_{POI} is to be minimized to find minimum energy transfer trajectory.

As mentioned in the previous section, the minimum energy launch opportunity occurs in the neighbourhood of Hohmann-like geometry. In order to find the desired minimum energy trajectory, a number of transfer trajectories are determined using

point-conic method, during a launch opportunity, by varying departure dates and flight durations. These trajectories are represented using “porkchop” plots for a given launch opportunity. Figs. 1.5 and 1.6 show porkchop plots for Mars mission launch opportunity during 2018 for fly-by and orbiter missions, respectively.

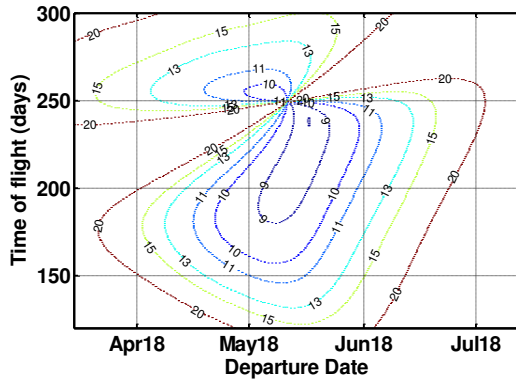


Fig. 1.5: C3 Departure contour plots for the launch opportunity to Mars during 2018

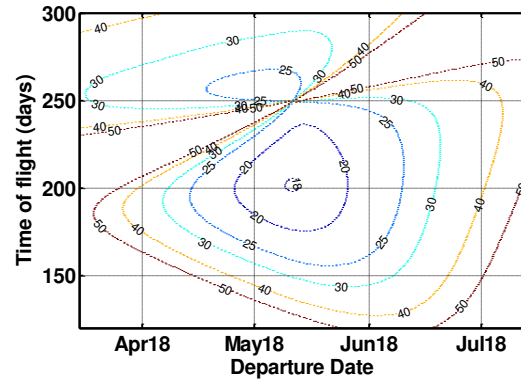


Fig. 1.6: C3 Total contour plots for the launch opportunity to Mars during 2018

Two regions of minimum exist and they are known as type 1 and type 2 opportunities. For type 1 opportunity, the transfer angle is less than 180^0 and for type 2 the angle is greater than 180^0 . The 180^0 transfer ridge, or pseudo-Hohmann (perihelion to aphelion) nodal transfer opportunity subdivides the two types of opportunities. This ridge is associated with all diametric, ie, near- 180^0 transfer trajectories because the planetary orbits are not strictly coplanar. At these ridges, high inclination transfers are found because the spacecraft velocity vector due to Earth’s orbital velocity must be rotated through large angles out of the ecliptic in addition to the need to acquire the required transfer trajectory energy. This high energy requirement for pseudo-Hohmann transfer can be eliminated using “broken-plane” Manoeuvres (Sergeyevsky et al., 1983).

1.3.1. Injection Conditions:

Consider a vehicle coasting in an Earth Parking Orbit (EPO). The radius of the circular EPO is r_1 and its inclination is i with respect to the equatorial plane. An

interplanetary orbit from Earth to target planet has been determined and it is desired to find the point on the coasting orbit where the minimum impulsive change in velocity can be made so that the vehicle can move away from the Earth along a hyperbola whose asymptotic velocity vector is $V_{\infty dep}$. Initial orbital speed of the vehicle is

$$v_0 = \sqrt{\frac{\mu_E}{r_1}}, \quad (1.7)$$

where, μ_E is Earth's gravitational constant. From the interplanetary orbit calculations the asymptotic relative velocity vector $V_{\infty dep}$ is determined. The unit excess hyperbolic velocity vector is given by

$$\hat{V}_{\infty} = \begin{bmatrix} \cos\alpha_{\infty} \cos\delta_{\infty} \\ \sin\alpha_{\infty} \cos\delta_{\infty} \\ \sin\delta_{\infty} \end{bmatrix}. \quad (1.8)$$

So from the components of \hat{V}_{∞} , the right ascension (α_{∞}) and declination (δ_{∞}) are computed. The magnitude of the velocity vector immediately following the injection impulse is

$$v_1 = \sqrt{\frac{2\mu}{r_1} + V_{\infty dep}^2} \quad (1.9)$$

Since v_0 and v_1 are fixed in magnitude, the velocity change $\Delta v = v_1 - v_0$ is minimized by making the angle ψ between them as small as possible. If a point on the coasting orbit can be found such that $r_1, v_0, V_{\infty dep}$ are coplanar, then the optimum point of injection occurs at the perigee of the escape.

1.3.1.1. Tangential Injection from Perigee ($i \geq \delta_{\infty}$)

In this case, there will be two opportunities to establish a departure hyperbola that satisfy the energy and orientation of the outgoing asymptote. One injection opportunity will be while the spacecraft is ascending and the other will be while the spacecraft is descending along the orbit. For the case where $i = \delta_{\infty}$, there will be a single injection opportunity. The EPO right ascension of ascending node (Ω) for each opportunity can be determined from (Battin, 1999) -

$$\Omega_1 = \pi + \alpha_\infty + \sin^{-1}\left(\frac{\cot(\beta_\infty)}{\tan(i)}\right), \quad (1.10)$$

$$\Omega_2 = 2\pi + \alpha_\infty - \sin^{-1}\left(\frac{\cot(\beta_\infty)}{\tan(i)}\right), \quad (1.11)$$

The arguments of the injection points (u) measured from their respective ascending nodes are (Battin, 1999),

$$u_1 = \cos^{-1}\left(\frac{\cos(\beta_\infty)}{\sin(i)}\right) - \theta_\infty, \quad (1.12)$$

$$u_2 = -\cos^{-1}\left(\frac{\cos(\beta_\infty)}{\sin(i)}\right) - \theta_\infty, \quad (1.13)$$

where, θ_∞ is the true anomaly at ∞ , and β_∞ is the angle between the outgoing asymptote and the spin axis of the Earth.

1.3.1.2. Tangential Injection from Perigee ($i < \delta_\infty$)

High declination trajectories require a non-tangential impulse because the angle between the EPO and departure hyperbola orbit planes is non-zero (Battin, 1999).

A unit vector normal to the EPO can be computed from

$$\hat{h} = \frac{\sin(i + \beta_\infty)}{\sin\beta_\infty} \hat{z} - \frac{\sin i}{\sin\beta_\infty} \hat{s}, \quad (1.14)$$

A unit vector in the direction of the ascending node of the EPO is given by

$$\hat{n} = \frac{\hat{z} \times \hat{h}}{\sin i}, \quad (1.15)$$

And hence

$$\Omega = \tan^{-1}(n_y, n_x), \quad (1.16)$$

and the true anomaly of the injection impulse on the EPO is given by

$$\theta = 2\pi - \sin^{-1}\left(\frac{\sin\theta_\infty}{\sin(i + \beta_\infty)}\right). \quad (1.17)$$

1.4. Methods to reduce ΔV requirements for Interplanetary Missions

Among the favourable trajectories for interplanetary missions the minimum energy (ΔV) transfer trajectories are evaluated because they provide a consistent starting point for the evaluation of the spacecraft's initial mass in the Low Earth Orbit (LEO). A significant fraction of the spacecraft's initial mass in LEO is the propellant mass required to accomplish the interplanetary transfer. Reduction in the ΔV requirements will reduce the propellant mass and thus increase the payload mass of the spacecraft.

1.4.1. Gravity Assist Manoeuvre

In Swing-by (SB) or Gravity Assist Manoeuvre, the spacecraft flies close to a planet or planet's natural satellite for gaining heliocentric velocity. This gain in heliocentric velocity helps in reducing the total impulse requirement of the spacecraft. SB Manoeuvre is not mandatory for reaching nearby planet eg. Mars and Venus, but it becomes necessary for farther planets like Mercury, Jupiter etc. Generally, SB Manoeuvres are unpowered. In certain cases, a powered SB (adding a small impulse at close approach to swing-by planet) provides flexibility to mission designers. The mathematical formulation of unpowered SB is in Longuski and Williams (1991) and of powered SB in Prado (1996).

Use of gravity assist trajectories for energy gain purposes has been utilized for a number of planetary missions including Voyagers 1 and 2, Pioneers 10 and 11, Galileo and others. Mariner 10 was the first spacecraft to make use of GA Manoeuvre in 1973. It used Venus swing-by to bend its flight path and bring its perihelion down to the level of Mercury's orbit for multiple fly-bys. Voyager 2, launched in 1977, was the first spacecraft to travel to Uranus and Neptune taking help of Saturn swing-by, thus completing the Planetary Grand Tour in just 12 years. Until Ulysses, launched in 1990, the Sun was only observed from low solar latitudes because a direct launch into

a high inclination solar orbit would require prohibitively large launch vehicle. Ulysses utilized Jupiter's GA to increase its inclination to the ecliptic by 80.2° .

1.4.2. Aerobraking

Aerobraking is a spaceflight manoeuvre that reduces the apoapsis of an elliptical orbit by flying the spacecraft through the atmosphere at the periapsis, using drag to slow its velocity. Aerobraking saves fuel, compared to the direct use of a rocket engine, when the spacecraft requires a low orbit after arriving at a planet with an atmosphere.

Aerobraking is accomplished in three phases (Fig 1.7):

- **Walk in Phase:** The spacecraft is captured into an orbit with a periapsis altitude, well above the atmosphere in order to accommodate navigational uncertainties associated with the approach trajectory. The periapsis is then lowered into the atmosphere.

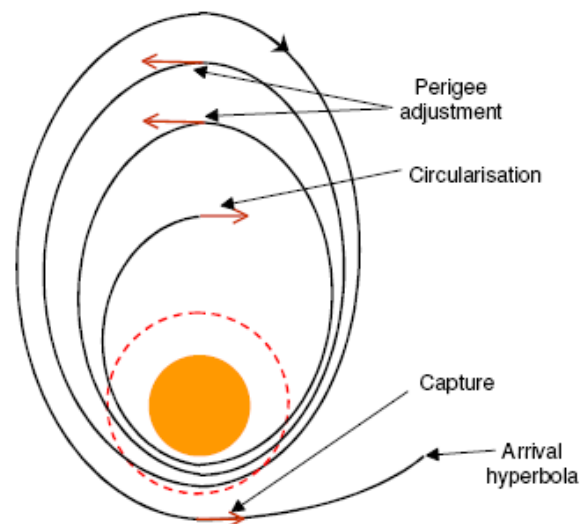


Fig. 1.7: Mechanics of Aerobraking

- **Main Phase:** The main phase begins when periapsis is lowered to an altitude where the drag is approximately equal to the planned, long term value required to shrink the orbit in the allocated time. Periodic propulsive “corridor control” Manoeuvres are required to maintain the drag in the appropriate range.
- **Walk out Phase:** The walk-out phase begins as the spacecraft approaches a circular orbit or the desired orbit. Aerobraking is terminated with a Manoeuvre which raises the periapsis out of the atmosphere and places it near the mapping orbit altitude.

Magellan in 1993 became the first planetary spacecraft to accomplish aerobraking as a demonstration. It used Venus atmosphere to reduce its apoapsis by nearly 8000 km using little propellant. Mars Global Surveyor was the first spacecraft to employ aerobraking at Mars to reach its desired mapping orbit. It was launched in 1996 with planned mission ΔV deficit of nearly 1250 m/s. It was followed by Mars Odyssey and Mars Reconnaissance Orbiter, which also utilized aerobraking at Mars. From these missions it is well known that about 30% impulse can be saved using aerobraking at Mars compared to the use of spacecraft thrusters to establish an orbit, but at the cost of flight duration. Mechanics of aerobraking and past mission details can be found in Repic et al, (1968); Schy and White (1969); Cook (1992); Striepe et al, (1993); Doody (1995); Beerer et al. (1996); Lyons (2000).

1.4.3. Aerocapture

Aerocapture (Fig. 1.8) is a technique used to reduce hyperbolic velocity of an incoming spacecraft using the planet's atmospheric drag so that it gets captured into an orbit around that planet. Only one pass in the atmosphere is required by this technique, in contrast with aerobraking. It requires significant thermal protection and precision closed-loop guidance during the Manoeuvre.

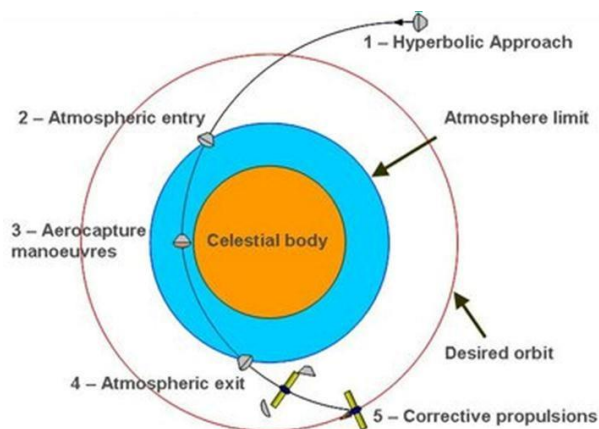


Fig. 1.8: Mechanism of Aerocapture

Aerocapture has not yet been tried on a planetary mission. Re-entry skip by Zond-6 and Zond-7 upon lunar return were aerocapture Manoeuvres. Aerocapture was originally planned for the Mars Odyssey orbiter, but later changed to aerobraking for reasons of cost and commonality with other missions. Aerocapture has been proposed for arrival at Saturn's moon Titan (Bailey et al., 2003).

1.4.4. Weak Stability Boundary Transfers

Belbruno in 1987 discovered this new type of transfer from Earth to Moon using ballistic lunar capture (ie, no ΔV for LOI). In Ballistic Capture the spacecraft goes into an unstable orbit around Moon automatically, for finite time. In weak capture state it is in the transitional boundary between capture and escape. Weak capture state can be mapped out as regions in the phase space. Initial orbit conditions depend on the location of the Sun relative to the Earth and the Moon.

Weak stability boundary transfers save about 150 m/s ΔV for lunar mission compared to conventional Hohmann transfers, which comes out to be 5% of spacecraft mass reduction (assuming 300s ISP). It offers wide range of possible lunar insertion points compared to Hohmann transfer. Circular Restricted Three-Body Problem is the base model for trajectory design. The Capture process is gradual and so there is no need of large thrusters. The major disadvantage of this method is high time of flight of about 3 to 4 months for lunar missions. This makes it suitable for rescue mission, cargo missions for permanent lunar base, sample return etc. and not suitable for manned missions. High reliability of sub-systems is required due to which overall mission cost increases. Also the spacecraft should have improved radiation protection. Long link-distance is required as spacecraft travels 15-20 lakh km away from Earth (Belbruno, 1987; Belbruno and Miller, 1993; Belbruno, 2005; Belbruno, 2007).

WSB transfer was first utilized by Hiten (Fig. 1.9) to reach Moon. The mission originally had two spacecraft, Muses-A and Muses-B; B was to go into orbit around the moon with A remaining in Earth orbit as a communication relay. B failed and A did not have sufficient fuel to make the journey. Utilizing a trajectory concept by Belbruno (1990), which is more energy-efficient than the one planned for B, Muses-A

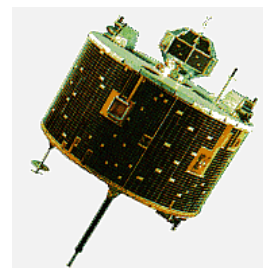


Fig. 1.9: Hiten spacecraft

(<https://en.wikipedia.org/wiki/Hiten>)

(renamed Hiten) left Earth orbit in April 1991 and reached Moon in Oct 1991.

Gravity Recovery and Interior Laboratory (GRAIL) in 2011 made use of WSB trajectory to reach the Moon. This trajectory enabled the mission to reduce fuel requirements, protect instruments and reduce the velocity of the two spacecraft at lunar arrival to help achieve the extremely low orbits with separation between the spacecraft (arriving 25 hours apart) of 175 to 225 km. Fig. 1.10 shows GRAIL-A and GRAIL-B trajectories for a launch at the open and close of the launch period.

GRAIL's trajectory from Earth follows a path towards the Sun, passing near the interior Sun-Earth L_1 before heading back towards the Earth-moon system. GRAIL's primary science objectives were to determine the structure of the lunar interior, from crust to core and to advance understanding of the thermal evolution of the Moon (Roncoli and Fuji, 2010; Chung et al., 2010; Hutch et al., 2010).

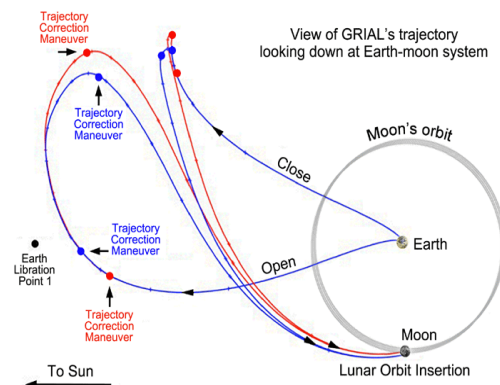


Fig. 1.10: Trajectory GRAIL spacecraft
(www.nasa.gov/pdf/582116main_GRAIL_launch_press_kit.pdf)

1.5. Conclusion

In this chapter, basics of interplanetary trajectory design process are explained in brief. Various methods like gravity assist, aerobraking, aerocapture and weak stability boundary methods are introduced which help in saving fuel in an interplanetary mission. Next chapter gives a flavour of important works carried out in the area of low energy transfers.

CHAPTER 2

REVIEW OF WEAK STABILITY BOUNDARY TRANSFER TRAJECTORIES

2.1. Introduction

Many space-faring nations are planning for solar system exploration missions which might use alternative methods to reach distant planets. The conventional method to design an interplanetary trajectory begins with Hohmann transfer ellipse which is further refined using patched conic method. Alternative techniques like aerobraking, gravity assist and ballistic capture trajectories can be employed for optimizing the fuel requirements. In some cases it has been proved that these alternative methods are better than conventional methods as they aid to reduce the total impulse requirement, provide extended launch opportunities, and give opportunity to observe natural satellites or planets. This is additional information about the GA planet or natural satellite on the way to distant planet. The theory of Weak Stability Boundary (WSB) Transfers or Ballistic Capture Trajectory is one such new unconventional technique which was used by Japanese Hiten Mission in 1991, NASA's ARTEMIS in 2009, NASA's GRAIL in 2011 and it is proposed for missions like Multi-Moon Orbiter, Europa Orbiter, BepiColombo etc. The trajectories designed using WSB theory have some benefits like decrease in total ΔV compared to direct transfers, longer view opportunity of enroute satellites/planets compared to gravity assist for example the MMO (Ross et al., 2003) and 3D Petit Grand Tour of Jovian moon system (Gomez et al., 2004); but suffer mainly from long flight durations and tracking difficulties as the spacecraft travels longer distances compared to direct transfers.

Basically the transfer approach to Moon can be broadly classified into four categories, namely, the direct, phasing loop, weak stability boundary and spiral

transfer (Lee, 2011). The ‘classical’ direct transfer trajectory to Moon starts from an Earth Parking Orbit (EPO) with an impulse Trans-lunar Injection (ΔV_{TLI}), usually at perigee, to increase the apogee to 384400 km (mean distance between Earth and the Moon). After reaching near Moon, another impulse (Lunar Orbit Insertion, ΔV_{LOI}) is given, usually at periselenium, so that the spacecraft is captured by the Moon. The time of flight for direct transfer varies from 2-5 days and total ΔV from a 300 km circular EPO varies from 3.5 to 4 km/s. This method was used from 1960s to 1980s including the Luna and Apollo missions, and recently by Lunar Prospector and Lunar Reconnaissance Orbiter. This is most proven approach for several applications and can provide relatively simple and fast transfer process and lowest overall risk and cost.

Both the TLI and LOI burns can be divided into several smaller burns to minimize gravity losses and is known as the phasing loop transfer. This technique was used by Clementine, SELENE, Chandrayaan-1 and Chang’E-1. This approach can provide a chance to verify the operating condition, status of the orbiter and correct any anomalies before the orbiter arrives at the Moon. In general the time of flight varies from 2-3 weeks and it involves more operational complexities. The initial direct and phasing loop trajectories are designed using the Hohmann transfer or patched conic technique, which are based on two-body dynamics. Later the trajectory is refined taking into consideration other perturbing factors like the third body perturbation, atmosphere, solar radiation pressure etc.

Weak Stability Boundary (WSB) transfer takes the orbiter to the region of Lagrange points of Earth-Sun system to arrive at the Moon with low relative velocity, thus reducing ΔV_{LOI} at Moon. A small manoeuvre in WSB regions can lead to significant change in the trajectory. This approach usually requires a complex mission design requirement and very precise targeting and control of flight parameters (Biesbroek and Janin, 2000). Since these transfers require less fuel (saving upto 150 m/s compared to Hohmann transfer), they are also called low energy transfers. The

time of flight varies from 60-100 days. Japanese Hiten used WSB transfer method to reach Moon (Belbruno, 2007).

The spiral approach requires longest time of flight compared to other transfer methods. ESA's SMART-1 used its low-thrust hall thrusters to expand its EPO to lunar orbit over a period of 16 months. In the construction of WSB and spiral trajectories the perturbation of Sun has to be included along with Earth and Moon and so 2-body dynamics is no more applicable. These trajectories are designed using the invariant manifold structures related to periodic orbits in the Restricted Three-Body Problem (R3BP).

The objective of this chapter is to bring out the developments in the area of WSB transfers and its application to find low energy transfer trajectories. We begin with the developments in the area of circular restricted three-body problem (R3BP) related to capture dynamics, use of R3BP in finding invariant manifolds in phase space, weak stability boundary transfers, methods to find an optimal trajectory and the use of manifold theory to determine low energy transfers. Some of the missions which plan to use/ have used WSB transfers are also highlighted.

2.2. Review of WSB

2.2.1. Restricted Three-Body Problem

Restricted Three-Body Problem (R3BP) is the problem to describe the motion of an infinitesimally small particle P_3 which is moving under the gravitational influence of two massive bodies P_1 (more massive primary) and P_2 (smaller primary). The two massive bodies are moving in a circular orbit about their centre of masses. It is the simplest non-integrable system. Unlike the patched conic approach, simulations in the restricted three-body problem (R3BP) consider the influence of two massive bodies on the spacecraft at all time. Egorov (1958) has presented lunar and circumlunar trajectories in the R3BP and problems like circumnavigation of the Moon with a return to Earth at a flat entry angle, using the Moon's gravity assist to

reach other planets, possibility of the lunar capture etc. He concluded that capture of projectile launched from Earth by Moon on the first circuit of the trajectory was not possible. This was based on the analysis in the R3BP. But later it has been established that when Sun's gravity is considered ballistic capture is possible.

In the three-body problem, Conley-McGehee tubes, the invariant manifolds of the periodic orbits play an important role in understanding the transfer mechanism in the solar system (Koon et al., 2007). Hunter (1967) studied the stability conditions and satellite lifetime before escape in the framework of elliptic R3BP. Conley (1968) describe the local dynamics near saddle-center equilibrium points and the construction of a lunar trajectory in the planar R3BP. From his works it is known that both the stable and unstable manifolds of periodic orbits around L_1 and L_2 are two-dimensional. He shows that the local invariant hyperbolic manifolds emanate from the Lyapunov orbits. He conjectured that a low energy transfer between Earth and Moon might exist which leads to capture by Moon. McGehee (1969) building on the work of Conley studied homoclinic transfer trajectories that takes the spacecraft off a periodic orbit and then returns it back onto that same orbit at a later time. Heppenheimer (1978) brought out the idea of using these orbits for satellites for material transportation from Moon for space colonization. Huang and Innanen (1983) numerically explore the stability and capture regions of retrograde Jovian satellites. They also obtained conditions for temporary capture of retrograde jovicentric satellites in the framework of R3BP and elliptic R3BP. Brunini (1996) investigate stability and capture regions in phase space for direct and retrograde satellites and find possible candidates to be temporary Jovian satellites. Llibre et al. (1985) showed global extension of invariant hyperbolic manifolds about the smaller primary and showed that they transversally intersect. This meant that complicated hyperbolic networks exist about the smaller primary which can be used to design low energy transfers. Murison (1989) used a surface of section analysis of a selected region of the $C-x_0$ plane to show that the finite capture time areas correspond to motion in chaotic regions while the permanent capture areas are regions where the motion is trapped in

quasi-periodic islands surrounding elliptical fixed points. He claims that most, if not all, escape/capture orbits are chaotic and boundary of such regions are fractal.

WSB transfers from Earth to Moon are constructed by using WSB of Sun-Earth to alter the spacecraft's velocity as it enters WSB of Earth-Moon so that it gets ballistically captured by Moon. WSB transfer introduces complexities to mission design compared to direct transfer. In order to design a WSB transfer trajectory, standard astrodynamics tools like two-body problem cannot be used without modification as the trajectory does not follow conic sections. When modelled in R3BP, the energy or the Jacobi constant of the trajectory changes due to thrusting. As a result the design of such trajectories is usually performed using optimization tools. Since the discovery of such chaotic regions in the three-body problem, lot of research has been done in this area to utilize these regions to design low energy interplanetary trajectories.

WSB is transition region in the phase space where the gravitational interactions between Earth, Sun and Moon tend to balance (Belbruno and Miller, 1993). They describe WSB as “a generalization of Lagrange points and a complicated region surrounding the Moon”; Belbruno (2004) describes it as “a region in phase space supporting a special type of chaotic motion for special choices of elliptic initial conditions with respect to m_2 ”; Belbruno (2004) also define it as “in the R3BP, WSB is a boundary set in the phase space between stable and unstable motion relative to the second primary. Keplerian orbits about the second primary, perturbed by the first primary are stable if after a prescribed number of revolutions they preserve the character of bounded motion. Otherwise they are unstable”; Yagasaki (2004) describes it as “a transition region between the gravitational capture and escape from the Moon in the phase space”.

2.2.1.1 Analytical definition of Capture and WSB is given by Belbruno (2004)

Let us consider elliptic restricted three-body problem.

Definition 2.1: The *two-body Kepler energy* of P_3 with respect to P_2 in P_2 -centered inertial coordinate is given by

$$E_2(X, \dot{X}) = \frac{1}{2} |\dot{X}|^2 - \frac{\mu}{r_{23}}, \quad (2.1)$$

Where, $r_{23} = |X|$, $0 \leq \mu < \frac{1}{2}$.

Definition 2.2: P_3 is *ballistically captured* at P_2 at time $t = t_1$ if

$$E_2(\varphi(t_1)) \leq 0$$

For a solution $\varphi(t) = (X(t), \dot{X}(t))$ of the elliptic restricted problem relative to P_2 , $r_{23}(\varphi(t)) > 0$.

In particular, we consider the planar circular restricted problem and determine the set $\bar{J}^{-1}(C)$ where $\tilde{E}_2(x, \dot{x}) \leq 0$ and $x = (x_1, x_2)$ are barycentric rotating coordinates. In addition, those points are considered where $\dot{r}_{23} = 0$, ie, local periapsis or apoapsis points. Set

$$\Sigma = \{x, \dot{x} | \tilde{E}_2 \leq 0\}, \quad \sigma = \{x, \dot{x} | \dot{r}_{23} = 0\}.$$

Then

$$W = \bar{J}^{-1}(C) \cap \Sigma \cap \sigma \quad (2.2)$$

defines a special set where ballistic capture occurs in the restricted problem. W is called the *weak stability boundary*. The motion of P_3 near W is sensitive.

Here we are interested to find the trajectories that go to ballistic capture. The trajectory starts near to the primary P_1 , goes to a point in W near P_2 . This type of trajectory is called a ballistic capture transfer and it has the property that it arrives at a periapsis point near P_2 with substantially lower Kepler energy E_2 than the classical Hohmann transfer trajectories.

Let $\varphi(t)$ be a smooth solution to the elliptic restricted problem for $t_1 \leq t \leq t_2$; t_2 is finite.

Definition 2.3: If $E_2(\varphi(t_2)) \leq 0$ then $\varphi(t)$ is called a *ballistic capture transfer* from $t = t_1$ to $t = t_2$, relative to P_2 .

Definition 2.4: If $E_2(\varphi(t_1)) \leq 0$ and $E_2(\varphi(t_2)) > 0$ then $\varphi(t)$ is called a ballistic ejection transfer from $t = t_1$ to $t = t_2$, which defines *ballistic ejection (or escape)* from P_2 .

Definition 2.5: Let $\varphi(t)$ be a ballistic capture transfer from $t=t_1$ to $t=t_2$. If $E_2(\varphi(t)) \leq 0$ for $t_2 \leq t \leq t_3$, $t_2 < t_3 < \infty$, and $E_2(\varphi(t)) > 0$ for $t = t_3$, then $\varphi(t)$ has *temporary ballistic capture* for $t_2 \leq t \leq t_3$. If $t_3 = \infty$, then $\varphi(t)$ has *permanent ballistic capture* for $t_2 \leq t < \infty$.

Hohmann transfer is referred to as high energy since the hyperbolic excess velocity $V_\infty (=V_M - V_F$, where V_M is the magnitude of velocity of Moon about Earth and V_F is the magnitude of velocity of P_3 on the transfer trajectory at lunar periapsis. Also, $E_2 = (1/2) V_\infty^2$) is significantly high, and a ballistic capture transfer is called low energy since the V_∞ is eliminated. This is the fundamental difference between these two types of transfers.

2.2.1.2 Numerical Algorithmic definition of WSB is given by Belbruno (2004)

Consider a radial line l from P_2 (Fig. 2.1) in a P_2 -centered rotating coordinate system X_1, X_2 . We follow trajectories $\varphi(t)$ of P_3 starting on l , which satisfy the following requirements.

- The initial velocity vector of the trajectory for P_3 is normal to the line l , pointing in the direct (posigrade) or retrograde directions.
- The initial two-body Kepler energy E_2 of P_3 with respect to P_2 is negative or 0.
- The eccentricity $e_2 \in [0,1]$ of the initial two-body Keplerian motion is fixed along l . The initial velocity magnitude

$V_2 = (\dot{X}_1^2 + \dot{X}_2^2)^{\frac{1}{2}} = (\mu(1 + e_2)/r_{23})^{\frac{1}{2}}, 0 < \mu \leq 1/2$. It varies along l . The term r_{23} is subtracted from the inertial velocity since it is a rotating system.

Thus P_3 starts its motion on an osculating ellipse which we assume is at its periapsis. Hence,

$$E_2 = \frac{\mu}{2} \left(\frac{e_2 - 1}{r_{23}} \right) \leq 0.$$

The motion of P_3 is stable about P_2 if

- (i) after leaving l it makes a full cycle about P_2 without going around P_1 and returns to a point $b \in l$, where $E_2 \leq 0$.

The motion of P_3 is unstable if either

- (ii) it performs a full cycle about P_2 without going about P_1 ($\theta_1 \neq 0$, where θ_1 is the polar angle with respect to P_1) and returns to a point $b \in l$, where $E_2 > 0$; or
- (iii) P_3 moves away from P_2 towards P_1 and makes a cycle about P_1 achieving $\theta_1 = 0$, or P_3 collides with P_1 . It is assumed that for $t > t_0$, once P_3 leaves l , where $\theta_2 = \theta_2(t_0) \in [0, 2\pi)$, P_3 need only cycle about P_2 until $\theta_2(t) = 2\pi$.

It is noted that (i) corresponds to ballistic capture at b with respect to P_2 and the orbit from a to b is a ballistic capture transfer which is bounded. (ii) corresponds to ballistic escape from P_2 and (iii) represents a different type of escape called primary interchange escape.

As the initial conditions vary along l satisfying (i), (ii), (iii), it is numerically found that there is a finite distance r^* on l from P_2 satisfying the following statements:

If $r_2 < r^*$, the motion is stable.

If $r_2 > r^*$, the motion is unstable.

r^* depends on only two parameters, the polar angle θ_2 which l makes with the x_1 -axis and the eccentricity e_2 of osculating Keplerian ellipse at the point a at $t=t_0$. r_2 is determined to be a well-defined function θ_2, e_2 .

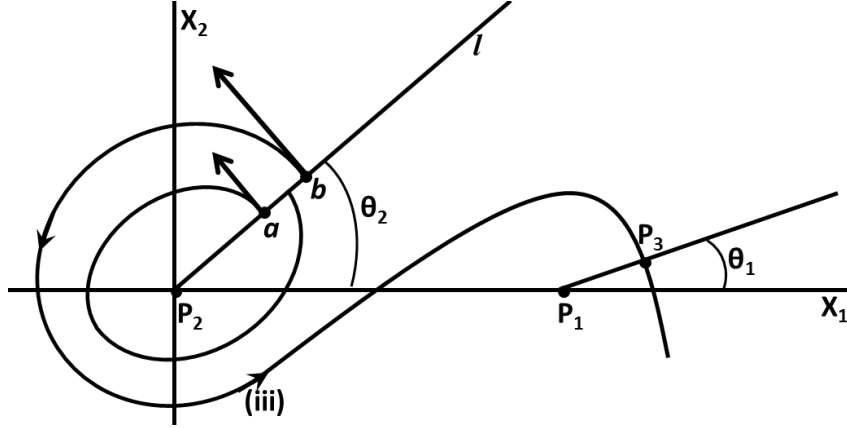


Fig. 2.1: Stable, unstable motion and primary interchange escape (Belbruno, 2004)

Define

$$W = \{r^*(\theta_2, e_2) \in \mathbf{R}^1 | \theta_2 \in [0, 2\pi], e_2 \in [0, 1]\}. \quad (2.3)$$

W is a two-dimensional stability transition region of position and velocity space, which we call the weak stability boundary. W has two components. One corresponds to retrograde motion about P_2 and the other to direct motion about P_2 after propagation from l .

2.2.1.3 Definition of WSB given by García-Gómez (2007)

In the algorithmic definition given by Belbruno (2004), García and Gómez (2007) point out that the requirements on the initial conditions fix the modulus of the velocity and its direction, but not the sense. So, for a fixed position on $l(\theta)$, there are two different initial velocities, fulfilling the four restrictions, which can produce orbits with different stability behaviour. Also, García and Gómez (2007) point out that along $l(\theta)$ there are several transitions from stability to instability. The set of stable points recalls a Cantor set. Also some maximum time interval must be fixed for the numerical integration.

García and Gómez (2007) give the initial conditions along radial segment $l(\theta)$ that must be integrated to determine the stable/unstable regions around P_2 .

Initial conditions with positive velocity (osculating retrograde motions around P_2)

$$x = -1 + \mu + r_2 \cos \theta, y = r_2 \sin \theta, \dot{x} = r_2 \sin \theta - v \sin \theta, \dot{y} = -r_2 \cos \theta + v \cos \theta. \quad (2.4)$$

Initial conditions with negative velocity (osculating direct motions about P_2)

$$x = -1 + \mu + r_2 \cos \theta, y = r_2 \sin \theta, \dot{x} = r_2 \sin \theta + v \sin \theta, \dot{y} = -r_2 \cos \theta - v \cos \theta. \quad (2.5)$$

Where v is the modulus of initial sidereal velocity P_3 given by

$$v^2 = \mu \left(\frac{2}{r_2} - \frac{1}{a} \right) = \frac{\mu(1+e)}{r_2}. \quad (2.6)$$

For fixed value of eccentricity e and the angle θ , all the possible values of the distance r^* along l are searched for which there is a change of the stability property of the orbit. For a finite number of points (up to a certain precision) $r_1^* = 0, r_2^*, \dots, r_{2n}^*$ such that $r_2 \in [r_1^*, r_2^*] \cup [r_3^*, r_4^*] \cup \dots \cup [r_{2n-1}^*, r_{2n}^*]$ then motion is stable otherwise unstable. The number of points r_i^* as well as their values depend on e, θ and the precision of the computation. Thus, WSB is defined as

$$\bar{W} = \{[r_{2k-1}^*(\theta, e), r_{2k}^*(\theta, e)], k = 1, \dots, n; \theta \in [0, 2\pi], e \in [0, 1)\}. \quad (2.7)$$

2.2.2. WSB Trajectory Design

The research done in the area of WSB transfers can be classified into three parts namely, the manifold theory, optimization methods and mission design. Belbruno (1987) discovered this new type of transfer from Earth to Moon using ballistic lunar capture (ie, no ΔV_{LOI}), which was demonstrated by Japanese spacecraft, Hiten in 1991. When a spacecraft undergoes ballistic capture at Moon, it goes into an unstable orbit around Moon automatically without any ΔV to slow it down near Moon. The spacecraft remains in this orbit for finite time and then escapes. In this weak capture state it is in the transitional boundary between capture

and escape. This orbit can be stabilized by imparting small impulse ΔV . The mechanism of such capture is studied by Belbruno (2004). He has mapped out the region in the phase space (position-velocity space) where weak capture can occur about the Moon. This region is called weak stability boundary. The initial orbit conditions depend on the location of the Sun relative to the Earth and the Moon (Miller, 2003). Belbruno (1990) used numerical simulations to demonstrate that the spacecraft undergoes resonance transition via weak capture. They use Poincare surface of section to visualize WSB regions. Belbruno and Marsden (1997) have showed that resonance hopping in comets occur when comets flyby Jupiter in WSB region. Topputo et al. (2008) illustrate that resonance transition mechanism is related to weak capture. They numerically demonstrate that the orbits that undergo resonance transition pass through the WSB boundaries. They incorporate solar perturbation to study ballistic escape. Belbruno et al. (2008b) use special normalized resonance Poincare surfaces to visualise WSB and its role in resonance transitions. They use correlation dimension to analyse different kinds of orbits and find that orbits close to resonance exhibit mixed regular-chaotic behaviour.

Belbruno and Miller (1993) have shown the existence of WSB numerically. They compare WSB transfers with Hohmann, bipolarabolic and bielliptic transfers. They have shown that WSB transfers require 18%, 14% and 37% lesser ΔV compared to Hohmann, bipolarabolic and bielliptic transfers, respectively. Belbruno (2007) has shown the existence of very low energy orbits around Moon, which can orbit Moon for extended periods and change their inclination using 12 times lesser ΔV compared to conventional method. The WSB theory is used for the trajectory design of Hiten (Belbruno and Miller, 1990; Uesugi, 1996) and Lunar GAS (Belbruno, 1987), Lunar Observer Mission (Belbruno and Miller, 1993), Blue Moon Mission (Belbruno et al., 1997), SMART-1 (Schoenmaekers et al., 2001), ARTEMIS (Folta et al, 2011) and GRAIL (Chung, et al 2010). Belbruno (2005) gives the concept for design of a low energy lunar transportation system for servicing lunar base. The system consists of Crew Exploration Vehicle and a robotic Tanker Craft.

The later uses WSB transfer to reach Moon and supply necessary fuel to the Crew Vehicle.

Miller and Belbruno (1991) gives the methodology for design of a WSB trajectory so-called Belbruno-Miller (B-M) trajectory that receives gravity assist from Moon on its way to Sun-Earth Lagrange point about 1.5 million km from Earth. In that region, the gravitational acceleration of Earth-Moon system and Sun tend to balance when combined with the inertial acceleration of spacecraft. A small manoeuvre in this region returns the spacecraft for ballistic capture by Moon. Krish (1991) has carried out injection period analysis for a particular B-M trajectory. It is found that the injection period can be increased to 4 and 11 days, respectively, with maximum allowable ΔV of 100 m/s and 150 m/s. It is observed that a nominal B-M trajectory can save 150 m/s over the Hohmann transfer.

Belbruno and Carrico (2000) introduce a forward targeting method to design WSB transfers from Earth to Moon and analyze launch windows in full force model using the software package STK/Astrogator.

Yamakawa (1992); Yamakawa et al. (1992); Yamakawa et al. (1993) have provided a systematic method of construction and wide variety of examples of ballistic lunar capture trajectories. They classify these trajectories into two categories namely, 1) earth side approach to the moon through geocentric orbit with initially small semi-major axis and 2) anti-earth side approach through geocentric orbit of large semi-major axis. They have identified perilune conditions which take advantage of solar gravity to reduce C3 wrt moon at perilune. They investigate the influence of solar gravity on geocentric orbit from angular momentum point of view and show that spacecraft (s/c) location in 2nd or 4th quadrant in sun-earth fixed frame increases local perigee distance. They also find that the total flight time of earth-moon transfer can be reduced by the use of lunar swing-by as it reduces the local eccentricity and hence raise initial perigee of geocentric orbit. Using the above information they give a systematic method of orbit design which makes use of gravitational capture by

Moon and solar gravity to raise perigee of initial EPO. Working on the same lines Dutt et al. (2016), have represented the capture trajectories, obtained by back-propagation of highly elliptical lunar orbits, on the phase space with colour code on time of capture. So looking at the phase space diagrams short flight duration trajectories can be differentiated from longer flight duration trajectories. Also the distribution of trajectories with different capture durations in the phase space can be clearly visualized. Similarly, highly eccentric geocentric orbits for which the perigee increases from LEO to Earth-Moon distance are also represented on the phase space with colour code on time of one revolution. Once the geocentric orbit and lunar capture orbits are identified the two are patched using Fixed Time of Arrival method and optimal patching points are found using Genetic Algorithm to obtain a WSB transfer trajectory from Earth to Moon.

Ivashkin (2002); Ivashkin (2003); Ivashkin (2004) developed a method to construct transfers between Earth and Moon using the Sun's gravitational influence. Bollt and Meiss (1995) constructed a trajectory using a series of four very small manoeuvres, to capture by Moon using far less energy than conventional direct transfers. Schroer and Ott (1997) reduced the time of such transfers from 2.05 years to 0.8 years, by targeting specific three-body orbits near the Earth. The total cost remained approximately the same.

The algorithm to compute WSB as given by Belbruno (2004) starts from an orbit around M_2 (Moon) and integrate it backward in time after giving a ΔV until it reaches the WSB region which is measured by the two-body energy of P with respect to M_2 . The other part of the trajectory starts from an orbit around M_1 (Earth) with a ΔV , which is integrated forward in time. Both the integrations are varied by some optimization technique so that the final positions of both the trajectories match and also reduce the total ΔV . Hence the solution is a trajectory traced by P initially near M_1 which reaches M_2 and gets captured there with minimum ΔV . In this case, only one orbit around M_2 is considered before P reaches the WSB. Instead of one cycle, García and Gómez (2007) generalized this region by considering the capture of P by

M_2 after it has performed n cycles around it. Hence they define an n^{th} weak stability boundary. They define generalized WSB as the union of these sets for $n=1,2,3,\dots$. They give a rough estimate of the stable/unstable regions around M_2 . They compute the stable and unstable manifolds associated to orbits around the collinear Lagrangian points and establish connection between these manifolds and the stable/unstable regions.

Howell et al. (1994) studied on construction of trajectories from low EPO to Halo orbits in Sun-Earth three-body problem. Nakamiya et al. (2010) analyse escape and capture trajectories to and from Halo orbits and apply it to the design of Earth-Mars round-trip transportation system. They observe that the ΔV required for round-trip transfer between low-Earth orbit and low-Mars orbit via spaceports on Earth and Mars Halo orbits is slightly larger than that of direct round-trip transfer. But evaluation in terms of required spacecraft wet mass for Earth-Mars transportation system revealed that it can be reduced by one-half compared with direct transfer if the propellant for return is left at the spaceports at Earth and Mars halo orbits on the way to low Mars orbit. Such an option to use stored fuel at spaceports is not available during direct round-trip transfers.

Circi and Teofilatto (2001) determine the spacecraft-Earth-Moon-Sun configuration that enable WSB transfers and demonstrate the role of Sun in increasing the spacecraft perigee and allowing lunar capture. It is demonstrated that Sun provides the spacecraft with minimum energy necessary to reach the Moon. The conditions generating WSB transfers in ‘quasi ballistic capture’ is estimated by analytical method. The generalizations of Tisserand-Laplace definition of sphere of influence into exterior and interior spheres of influence is accounted for the study of capture dynamics using analytical and numerical methods. Griesemer et al. (2011) have developed an algorithm for targeting a ballistic lunar capture transfer. The algorithm uses a particular member of a family of periodic orbits, documented by Markellos (1974) as family *f16*, as an initial guess for an Earth-Moon transfer.

Topputo (2013) has surveyed all the families of two-impulse Earth to Moon transfers in the framework of restricted four-body problem. These transfers include Hohmann, Sweetser's theoretical minimum, and those investigated by Yamakawa, Belbruno, Yagasaki, Pernicka, Mingotti etc. Parker and Anderson (2013) have surveyed two-burn transfers to 100 km polar orbit around Moon. These transfers include 3-6 days direct transfer, transfers including Earth phasing orbits and/or lunar flyby and 3-4 month low energy transfers. Parker (2010) investigates annual and monthly variations in low energy ballistic transfers from Earth to Lunar Halo Orbits. Variations are attributed to Earth's and Moon's non-circular and non-coplanar orbits. They have found that some families of transfers exist only in certain months of a year due to their sensitivity to geometric shifts. Anderson and Parker (2011a,b) have studied lunar landing trajectories at different elevation angles using invariant manifolds both in planar and 3D R3BP problem.

Strizzi et al. (2001) simulated and analysed Earth to Mars transfers using Lissajous orbit. They demonstrated that a braking manoeuvre at low altitude Mars periapsis prior to LOI can save significant fuel. They have used a loose control technique for station keeping. Castillo et al (2003) have described numerical method to find WSB transfers to inner planets and outer planets. For inner planets, ie, Mercury, Venus and Mars trajectory design is discussed for Bepi Colombo, Venus Express and Mars Express missions, respectively. They claim that WSB transfers to inner planets does not decrease the total ΔV required for the capture, but provides greater flexibility when selecting the geometry of the target orbit. They show that for outer planets, when natural moons are available, GA combined with WSB can be used. The combination of both methods provides opportunity to explore the giant planets (eg Jupiter and Saturn) and their moons. Kulkarni and Mortari (2005) demonstrate that Earth to distant planet can be reached using hopping between Halo orbits and it could save 35% fuel compared to gravity assist. Nakamiya et al. (2008) describe the use of Halo/Lyapunov periodic orbits to reduce propellant requirement to reach distant planet. Topputo and Belbruno (2009) have computed and visualized the

WSB regions for the Sun-Jupiter system. Topputo and Belbruno (2015) have given a new concept for the design of WSB trajectory to Mars. They target a distant point (few million km from Mars) which finally leads to a capture orbit. They claim that 25% ΔV_{MOI} can be saved with penalty on flight duration which can be 1.5 to 2 years when compared with conventional direct transfer.

2.2.3. Dynamical System Theory

Koon et al. (2000) describe the theory of Lagrange point dynamics of three-body system, the use of stable and unstable manifold tube to transport to and from the capture region and their application in mission design. They have suggested the division of four-body problem into two restricted three-body problems (R3BP) for the design of low energy transfers. Topputo et al. (2004) have used surface sections to identify intersections between two manifold tubes from two R3BP. They have assigned a merit function to each intersection and used systematic search to find optimal starting and arriving trajectories. Once an appropriate first guess is obtained, it is refined using sequential quadratic programming (SQP) method. This algorithm is used for design of low-energy interplanetary transfer trajectories.

Villac and Scheeres (2004) have presented a simple corrector algorithm to compute hyperbolic invariant manifolds associated to periodic and quasi-periodic orbits about the libration points L_1 and L_2 , which are significant for low energy trajectory design. Gómez and Masdemont (2000) describe heteroclinic transfer trajectories to transfer between three dimensional libration point orbits. Parker and Chua (1989); Wiggins (1994); Gómez et al. (2004) and many more authors describe invariant manifolds which can be used to construct homoclinic and heteroclinic transfer trajectories.

Gómez et al. (2004) explain geometrically the phenomenon of natural routes among the planets and/or their satellites with the help of invariant manifold structures of the collinear libration points in R3BP. Such invariant manifold tubes can be used to construct spacecraft trajectories between the two primaries. They apply this

technique to construct a 3D Petit Grand Tour of the Jovian moon system. This technique has an advantage of more visibility compared to Voyager-type flybys where the flybys last for only few seconds. In this technique the spacecraft can be made to orbit about a moon in a temporary capture orbit for desired revolutions, then it can be made to escape that moon and perform a small manoeuvre to get ballistically captured by a nearby moon for some revolutions. Also the ΔV in this case is much less compared to those required for joining two-body motion segments.

Neto and Prado (1998) study the effect of various parameters like mass ratio, distance between the spacecraft and secondary body at the time of manoeuvre (r_p), the energy C3 of spacecraft at that moment, direction of velocity at that point and departure angle (α) on time required for capture. The results show that time of capture can be reduced without reduction in energy savings by proper selection of initial conditions. Melo et al. (2007) have studied stable and escape-capture trajectories in R3BP (Earth-Moon-Particle) and four-body (Sun-Earth-Moon-particle) problem. They have mapped out regions in the phase space where these trajectories can be found.

An important development by Topputo et al. (2005) is worth mentioning. They demonstrate that a capture trajectory to Moon can be obtained via L_1 in the framework of Earth-Moon R3BP neglecting the presence of Sun. Romagnoli and Circi (2009) studied the geometry and performance of low energy transfers to Moon in the framework of three-body and four-body models. They have considered various low energy transfer orbits by varying the periselenium altitude and eccentricity of the initial osculating orbit of spacecraft. They find that equatorial captures with low pericenter altitude leads to minimum ΔV . Another important observation is that the lunar orbit eccentricity and the presence of Sun does not affect the WSB geometry much, both in the planar and in the 3D case. Castellà and Jorba (2000); Prado (2005); Jorba (2000) used bicircular problem to study low energy transfers. Yagasaki (2004 a,b) compute optimal low energy Earth-to-Moon transfers with moderate flight

duration by solving nonlinear boundary value problem in PR3BP. Circi and Teofilatto (2006) use WSB for design of economical lunar satellite constellation.

Fantino et al. (2010) consider four combinations of the two collinear libration points namely, $L_i^{SE} - L_j^{EM}$ ($i, j = 1, 2$) connections for determination of low energy transfers. In the above notation, subscript denotes the collinear libration point, L_1 or L_2 and superscript denotes the R3BP system under consideration, namely, Sun-Earth (SE) or Earth-Moon (EM) system. They find that $L_1^{SE} - L_2^{EM}$ and $L_2^{SE} - L_2^{EM}$ connections can provide low or zero cost transfers. This capability to provide low cost (ΔV at connection) transfers depends on the energy of libration point orbits (LPOs) to be connected. The cost is higher for lower energy LPOs. The unstable points of WSB region effectively confine to the points of invariant manifold trajectories which are characterized by orthogonality between radial and velocity vectors relative to smaller primary. They also find that the temporary capture is more efficient when the Jacobi constant of the invariant manifold is larger and the size (amplitude) of the progenitor LPO is smaller.

Generally, WSB transfers are less expensive compared to the conventional Hohmann transfer but suffer from long flight durations. In order to reduce the transfer time, it is necessary to hop from one orbit to another using the invariant manifold. There are very many possibilities of switching between orbits to attain the destination. Several researchers have contributed in the use of optimization methods to find trajectories connecting two or more arcs like Luo et al. (2006); Luo et al. (2007); Yokoyama and Suzuki (2005); Radice and Olmo (2006); Lizia et al. (2005). There are also studies concerning optimization of transfer trajectories using low thrust engines and the combination of impulsive and low thrust engines like Kluever (1997) and Mingotti et al. (2003).

Alessi et al. (2009a) have simulated rescue orbits, trajectories that depart from the surface of Moon and reach a LPO around the L_1 or L_2 points of the Earth-Moon system, in the framework of R3BP. They analyze the trajectories that can leave

the Moon's surface that is the accessible regions on the Moon, the velocity and the angle of arrival (angle between the velocity vector and the Moon's surface normal vector) and the time required for the transfer. They identify regions on Moon's surface from which departure is possible and regions where departure is almost orthogonal (departure velocity vector is perpendicular to Moon's surface). Longer transfer duration non-direct rescue orbits are available from much larger regions on Moon compared to direct rescue orbits. Alessi et al. (2009b) have explored LPO to LEO transfers and found that the minimum cost connection occurs when the LPO around L_1 increases in size and at maximum distance between Earth and arrival point on the manifold. They refine these trajectories in realistic model and conclude that the cost of manoeuvres in R3BP do not change much.

Vetrisano et al. (2012) present the concept of capture corridor which consists of all the lunar weak capture trajectories in the neighbourhood of the nominal one in the state space. This will help to ensure capture in presence of uncertainties due to orbit determination process and in the control of thrust vector. They have analysed three sequential filtering techniques for orbit determination process and have found that the unscented Kalman filter meets the accuracy requirements at an acceptable computational cost. The strategies developed are applied for the European Student Moon Orbiter.

2.2.4. Optimization for computation of WSB trajectories

Ockels and Biesbroek (1999); Biesbroek et al. (1999) and Biesbroek and Ancarola (2003) have studied the use of genetic algorithm to construct WSB trajectories from GTO to Moon. The parameters chosen to be optimized are time spent in GTO or phasing orbit, ΔV at perigee of GTO, magnitude, azimuth and declination of ΔV at WSB region. The fitness function is negative of total ΔV . A small population size (10) was sufficient for interplanetary trajectory optimization problems eg. using multiple swing-by but for WSB higher population size (100) gave

better results. GA was able to find WSB transfers to Moon for each day in a year saving 218-265 m/s ΔV with respect to the conventional direct transfer.

Moore (2009) utilize invariant manifolds of planar R3BP to find initial guess trajectories from Earth to Moon which is optimized using the optimal control algorithm DMOC (Discrete Mechanics and Optimal Control) by two different approaches. First approach is based on patching invariant manifolds of the Sun-Earth and Earth-Moon 3body systems to create a trajectory which is then modified to fit 4 body dynamics. Second approach is based on finding out intersections of trajectories that originate at the endpoints on the manifolds near the Earth and Moon. Moore finds that DMOC optimization trajectories to minimize ΔV obtained by these two methods generate very different trajectories. Yamakawa (1992) uses modified Newton's algorithm with controls on velocity and orientation of perigee and perilune, total time of flight, sun phase angle, epochs at both ends of intermediate trajectory segments to minimize total ΔV .

Lantoine (2009) use the multiple shooting technique for the design of missions to inter-moon transfers of Jovian system. Pre-computed unstable resonant orbits serve as initial guess for the highly nonlinear optimization problem along with Tisserand-Poincaré (TP) graph. Assadian and Pourtakdoust (2010) use non-dominated sorting genetic algorithm with crowding distance sorting (NSGA-II) for multi-objective optimization of trajectories from EPO around Earth to a circular orbit around Moon in the framework of 3D restricted four-body problem (R4BP). Apart from ΔV at TPI and LOI another mid-course manoeuvre is permitted to patch the Earth escape path to Moon's ballistic capture trajectory. Arrival date at Moon, mid-course manoeuvre time and some of the orbital elements of the ballistic capture orbit around Moon are parameters used to minimize total ΔV and flight time.

Peng et al. (2010) use an improved differential evolution algorithm with self-adaptive parameter control for the design of Earth-Moon low energy transfer to find the patch point of the unstable and stable manifold of the Lyapunov orbit around Sun-

Earth L_2 . They find this optimization technique more effective compared to three other evolutionary algorithms namely, genetic algorithm, particle swarm optimization and standard differential evolution. Peng et al. (2011) use adaptive uniform design differential evolution (AUDE) with self-adaptive parameter control method to find low energy Earth-Moon transfers. Coffee et al. (2011) describe a two-stage approach to construct low energy transfers between arbitrary unstable periodic orbits to reduce fuel requirements. They use an adaptive approach to global optimization to identify position-space intersections of invariant manifolds. Grover and Andersson (2012) optimize GTO-to-Moon mission by appropriately timed ΔV s which are obtained by shooting and Gauss-Pseudospectral collocation method for different phases of the mission.

2.3. Notable Missions/Planned Missions

The Japanese Hiten mission used both a lunar swing-by and a WSB trajectory to reach the Moon with favourable conditions for capture into a highly elliptic lunar orbit in 6 months (Belbruno and Miller, 1990; Uesugi, 1996).

Kawaguchi et al. (1995) describe the use of solar and lunar gravity assist to reduce the propellant required for LUNAR-A mission to Moon and PLANET-B (Nozomi) mission to Mars. The LUNAR-A mission (presently cancelled) planned in 1997 utilizes ballistic capture at Moon. The expected C3 gain is $0.8 \text{ km}^2/\text{s}^2$ or 5-9% in spacecraft mass assuming a specific impulse of 300-500s compared to Hohmann-type transfer. For the PLANET-B mission that was planned in 1998, they found that triple lunar gravity assist can reduce C3 by $4.5 \text{ km}^2/\text{s}^2$. Among three solutions thus obtained they selected one based on the launch window constraints. The expected C3 gain was around $2 \text{ km}^2/\text{s}^2$.

Petit Grand Tour of the moons of Jupiter is already discussed in previous section.

Sweetser et al. (1997) discuss a number of trajectory design techniques for Europa Orbiter Mission. The spacecraft shall reach Jupiter by the end of the decade and plan for a follow-up mission to Europa. After it arrives at Jupiter, it will undergo two Ganymede flyby G0 and G1 to reduce its incoming hyperbolic velocity. After reducing arrival V_∞ , a phase called endgame begins, which requires certain arrival conditions for the final flyby of the tour. The endgame is designed by JPL (Johannesen and D'Amario, 1999) to further reduce ΔV_{POI} using combination of Europa flybys. Heaton et al. (2002) start investigating the E0 trajectory after G1. They analyse sequences of Jovian satellites flyby to reduce arrival V_∞ at Europa. They explore and evaluate enormous number of possible tours using a graphical method based on Tisserand's criterion to reduce arrival V_∞ (from 3.3 km/s to 2 km/s) and total radiation exposure (by 70%).

Jehn et al. (2004) describe the trajectory of BepiColombo mission to Mercury which is a joint exploration mission by ESA and JAXA. Two spacecrafts will be launched jointly in 2015 and they are destined to reach Mercury in 2021 utilizing several gravity assists and SEP (Solar Electric Propulsion) ion engine thrust arcs. Since the thrust level of SEP is very low for a capture from hyperbolic approach, various options of Mercury Orbit Insertion (MeOI) through Gravitational Capture are found by varying the capture time and speed of the spacecraft, right before MOI. The trajectory which provides the best recovery options in case of a failed orbit insertion is selected for the 2012 baseline. The spacecraft on this trajectory arrives with very low excess velocity and from a direction where the gravity of Sun and Mercury have similar effects on the orbit. In case of failure in orbit insertion, the spacecraft will make five revolutions around Mercury before escaping again. It is observed that at the second, fifth and sixth perihelion, the altitude, inclination and orientation of the line of apsides for this trajectory is not very far from the nominal values. With small manoeuvres (less than 10 m/s) close to the previous apoherms, new orbit insertion possibilities arise with nearly same orbital parameters. Campagnola and Lo (2007) find that the manifolds of symmetric quasi-periodic orbits

around Mercury play a key role as symmetry properties provide several recovery opportunities to the mission. Jehn et al (2008) describe the navigation strategy for BepiColombo during the final phase of WSB capture by Mercury.

Ross et al. (2003) find trajectory for the Multi-Moon Orbiter (MMO) in which the spacecraft would orbit three of Jupiter's moons namely, Callisto, Ganymede and Europa one after the other using very little fuel. They found a tour trajectory with ΔV of the order of 22 m/s (vs 1500 m/s using conventional methods) and will spend about 4 years in the inter-moon phase. Finally ΔV of about 450 m/s is required to put the spacecraft into a 100 km orbit about Europa with an inclination of 45° . Ross et al. (2004) use patched three-body approximation method to compare the trade-off between flight time and ΔV for the MMO. They tried to reduce the flight duration to find another feasible tour trajectory which takes 227 days of flight duration for ΔV of 211 m/s.

Folta et al. (2016) describe Adaptive Trajectory Design (ATD) developed by NASA GSFC and Prude University and General Mission Analysis Tool (GMAT) for design of complex trajectories in multi-body systems. They demonstrate the use of these design softwares for the Lunar IceCube CubeSat mission and WFIRST.

2.4. Low Thrust Trajectories

Low thrust trajectories (LTT) use low thrust propulsion (LTP) systems which utilize propellant more efficiently like electric propellant, solar sail etc. and hence they can significantly enhance payload capability or enable high- ΔV missions. LTT are different from ballistic trajectories because the spacecraft is propelled for long periods and sometimes almost continuously by low-thrust engines. So it experiences the gravitational attraction of celestial bodies and other perturbations along with the change in energy due to thrusting. Lo and Parker (2005) show that the unstable simple periodic orbits can be chained together using their invariant manifolds to generate "chains" to build LTT for space exploration. Similar technique was used for the design of Genesis mission (Howell et al., 1997) and Lunar Sample

Return Mission (Lo and Chung, 2002). The incorporation of knowledge of invariant manifolds of unstable orbits within optimization tool and a good initial guess are important for reducing the time required for an optimization routine to search for an optimal LTT. Lo et al. (2004) compared LTT with the invariant manifolds at same energy level. In order to reduce the time of flight it is important to switch from one manifold to another by application of small manoeuvres. But ΔV causes change in energy and hence the Jacobi constant. Anderson and Lo (2004) and Anderson and Lo (2009) analyse the Planar Europa Orbiter (PEO) trajectory and conclude that in order to switch from one manifold to another, an impulsive manoeuvre is required at the point where the manifolds intersect in configuration space but not in phase space. They also find that even with change in the Jacobi constant, PEO travels along the manifolds. Hence they have shown that the underlying dynamics of multiple gravity assist is provided by the invariant manifold theory. Mingotti et al. (2009) formulate a systematic method for the design of low-energy transfers to Moon using high specific impulse low-thrust engines (eg. ion engines). They derive the initial guess with no velocity discontinuity at the patching point in the bicircular four-body problem. The search is reduced to the search of a single point on a suitable surface of section. Optimization is carried out in controlled four-body dynamics using a direct multiple shooting strategy. They find this method efficient in finding low energy transfers that require lesser propellant compared to standard impulsive low energy transfers.

Gurfil and Kasdin (2002) applied Deterministic Crowding Genetic Algorithm to characterize and design of out-of-plane trajectories in Sun-Earth system. They have addressed to the constraints imposed by interplanetary dust (IPD) for space-borne observation missions. They found a low-energy trajectory with maximum normal displacement of 0.223 AU and maximum reduction of 67% IPD. The second optimal trajectory had a maximum normal displacement of 0.374 AU above the ecliptic and reduction of 97% IPD. Dachwald (2004) demonstrate the use of evolutionary neurocontrollers to find near optimal LTT without an initial guess and without the requirement to embed the knowledge of invariant manifolds in the

optimization code named InTrance (Intelligent Trajectory optimization using neurocontroller evolution). The performance of InTrance is assessed for interplanetary missions. It was able to reduce the transfer time of a reference trajectory to near-Earth asteroid by 74%. It was also used for analysis of Mars mission using a spacecraft with nuclear electric propulsion system. Vasile et al. (2005) present a novel global optimization approach which has characteristics of evolutionary algorithms with systematic search. They use this algorithm to obtain roundtrip to Mars, either direct or via Venus, considering long and short stays on Mars and free return trajectories over a wide range of possible launch dates. They use the algorithm to investigate electric propulsion options and possibility of low cost capture at Mars via Mars' Lagrangian points. Yam et al. (2009) use differential evolution and simulated annealing with adaptive neighbourhood to find optimal LTT for Earth-Mars rendezvous problem. The solution obtained when used as an initial guess for a local optimizer yield high convergence rates.

2.5. Conclusion

Weak Stability Boundary (WSB) Transfers has proved revolutionary in reducing the fuel requirements for lunar missions, but suffer from major drawback of longer flight durations. A review of the developments in the area of WSB transfers, use of the invariant manifold theory and optimization techniques to design low energy and low thrust trajectories are presented. Some notable missions and planned missions that have used/proposed to use the WSB theory for trajectory design are listed. The richness of this area is evident from the works of several researchers since the last decade. Still, this area provides opportunities for further research which can be classified into three parts namely, the manifold theory, optimization methods and mission design.

In the next chapter we study planar fly-by trajectories to Moon in the framework of restricted three-body problem.

CHAPTER 3

ANALYSIS OF PLANAR FLY-BY TRAJECTORIES TO MOON

3.1. Introduction

The conventional method to obtain an initial lunar trajectory is by using the patched conic technique in the two-body problem. In the initial phase, the gravitational influence of Moon is neglected and in the final phase when the spacecraft is within the sphere of influence of the Moon, the gravitational influence of Earth is neglected. After the initial trajectory is finalized it is improved by numerical integration of the full-force equations of motion which mainly takes into account the asphericity of Earth, solar and lunar gravity, atmospheric drag and solar radiation pressure. The time of flight for such trajectories varies from 3-6 days (Battin, 1999). In order to consider the gravitational attraction due to Earth and the Moon during the entire trajectory, the three-body problem (Earth-Moon-spacecraft) is used here. The spacecraft is of negligible mass and so its influence on the motion of the primaries, (namely the Earth and the Moon, in this case) can be neglected. This is the restricted three body problem (R3BP). Detailed equations of motion for R3BP are available in Appendix. This also gives only an initial estimate because of assumptions like the circular motion of the primaries and neglecting Sun's perturbation, atmospheric drag etc., and so the trajectory has to be improved using the full-force models.

As a first step toward orbiter mission, in this chapter we study planar fly-by trajectories to Moon. In order to understand the dynamics of fly-by trajectories and their distribution in the phase plane, a sample of initial conditions close to Earth are propagated for 1000 days, an upper bound for practical purposes. The initial conditions are of the form $(x_0, 0, 0, y_0)$ and $(-\mu, y_0, \dot{x}_0, 0)$. During propagation if the minimum distance of the spacecraft from the surface of Moon is less than 2000 km, then that trajectory is recorded. Poincaré surface of section is used to identify the

existence of periodic and quasi-periodic orbits in these regions. This method is different from others because here the initial conditions are propagated forward in time for 1000 days irrespective of whether they reach near Moon or not. This enables us to identify the regions containing transfer trajectories to Moon in the phase space with respect to transfer time (within 1000 days) which is not available in previous works.

3.2. Methodology

In R3BP, the energy E of the orbit corresponds to the energy integral or Jacobi constant C from (A.19)-(A.20).

$$E = \frac{-C}{2} = \frac{1}{2}(\dot{x}^2 + \dot{y}^2) - \frac{1}{2}(x^2 + y^2) - \left(\frac{m_1}{r_1} + \frac{m_2}{r_2} \right). \quad (3.1)$$

Putting $\dot{x}^2 + \dot{y}^2 = 0$ for a given value of C , the above equation defines the zero velocity curves, and can be interpreted as the borders that limit the regions of this plane that are free or forbidden for the particle to move in. A decrease in the value of C , will increase the region in which the particle can move. According to the value of C of a particle its motion in the phase space can be divided into three categories (Szebehely, 1967):

- a) $C \geq C(L_1) = 3.18834$: the particle's orbit will always be around one of the primaries.
- b) $C(L_2) \leq C < C(L_1)$, the particle will be able to move around the two primaries, because the passage through L_1 is open for $C < C(L_1) = 3.18834$.
- c) $C < C(L_2) = 3.17216$, the particle will be able to move around the two primaries and might escape from the Earth–Moon system through L_2 , since the passage through L_2 is open for $C < C(L_2)$.

Our goal is to utilize this property to find sets of trajectories that travel from the Earth and reach Moon. These paths define natural routes that can be used in low-energy Earth–Moon transfers. Poincaré surface of sections (PSS) can be used to get a

qualitative picture of the phase space in the regions containing these trajectories. In a PSS periodic and quasi-periodic orbits appear as closed loops or islands and width of these islands are a measure of the stability of the corresponding periodic orbit lying at the center of the island. This technique has been used previously in many studies (Henon 1965 a,b; Jefferys, 1971; Winter, 2000; Dutt and Sharma, 2010; Dutt and Sharma, 2011; Safiya Beevi and Sharma, 2011)

A number of initial conditions (IC) near Earth (from about 200 km to 25,000 km from Earth's surface) are integrated in the framework of R3BP for a period of 1000 days (assumed to be an upper bound for practical purposes). The IC of these trajectories in the synodic coordinate system have the following form,

- (i) $(x, y, \dot{x}, \dot{y}) = (x_0, 0, 0, \dot{y}_0)$
- (ii) $(x, y, \dot{x}, \dot{y}) = (-\mu, y_0, \dot{x}_0, 0)$

We consider the values of the Jacobi constant (C) from 2 to $C(L_1)$. Propagation of IC by integrating equations of motion (Appendix A.15-A.18) is carried out to analyze the trajectories to Moon in R3BP. Integration of equations can be carried out with any standard numerical integration technique. The selection of integration technique does not affect the analyses. The idea is to bring out the concepts and categorization of the planar fly-by trajectories in Earth-Moon system under R3BP. Very similar results are obtained with fourth order Runge-Kutta method (Abramowitz and Stegun, 1972) and fourth order variable step-size Runge-Kutta-Gill method (Abramowitz and Stegun, 1972). Though the results are similar, variable step size integrator performed better in terms of convergence, number of function evaluations and execution time. Here, we provide results with fourth order variable step-size Runge-Kutta-Gill method.

In order to determine the values of x_0 and \dot{y}_0 for the set (i) of IC, we consider firstly another Cartesian coordinate system with origin fixed in the Earth centre of mass (Geocentric system), such that at $t = 0$, the x -axis of this system coincides with x -axis of the synodic system. Then, perigee distance, RP is varied

from 6600 km to 2,56,600 km with a step size of 500 km. Thus, $x_0 = \frac{RP}{D} - \mu$, where D is 384400 km, the distance between Earth and Moon. Given C , the value of y_0 is calculated from Eq. (3.1). This means that in this case at time $t=0$ a particle located at a distance x_0 from the Earth, on the line joining Earth and Moon and with a given energy $(-C/2)$. This IC is propagated for 1000 days by integrating Eqs (A.15)-(A.16) in Appendix using variable step-size Runge-Kutta-Gill method. Similar procedure is adopted for the set (ii) of initial conditions. In this case at time $t=0$, a particle is located at a distance $y_0 = \frac{RP}{D}$, from the Earth, on the line perpendicular to the line joining Earth-Moon, and has energy $(-C/2)$. Given C and $x = -\mu$, the value of x_0 is determined from Eq. (3.1). This IC is also propagated for 1000 days. During this integration time if the distance of the particle from the surface of Moon becomes less than 2000 km (or 3738 km from center of Moon) it is considered close enough and the corresponding ICs are recorded. Similar procedure is carried out for all the ICs along the negative axis as well. Thus, in such cases, for the set (i), $x_0 = -\frac{RP}{D} - \mu, y_0 = 0$ and for set (ii), $x_0 = -\mu, y_0 = -\frac{RP}{D}$.

3.3. Results

First we consider the set (i) of ICs with x_0 lying between the Earth and Moon. Figs. 3.1 (a) and 3.1 (b) gives the fly-by time in the initial condition space of C versus $x(=x_0)$. The time of flight (TOF) is represented with different colour codes. Sample trajectories with TOF less than 90 days and periodic orbits (PO) are also shown in the surrounding figures. In the figures containing the trajectories, solid blue line denotes the trajectory in synodic system, black dashed line denotes in non-rotating co-ordinate system and red dotted line shows the path of Moon during the flight duration. The white regions in the plot represent periodic orbits or fly-by trajectories whose nearest distance from the center of Moon is greater than 3738 km. Poincaré surface of sections (PSS) confirm the presence of periodic orbits (PO) in these regions. Some sample PSS along with the PO contained in them are shown in

Figs. 3.2 (a) - 3.2 (b). The triangular white region with C lying between 2 to 2.3 and x ranging from 0.45 to 0.65 denotes escape trajectories.

As seen in Fig. 3.1 (b) the fly-by trajectories with $\text{TOF} \leq 20$ days appear as a curve in the phase space. These fly-by trajectories take about 14 to 16 days TOF. A sample trajectory is also shown. The fly-by trajectories with $20 \text{ days} < \text{TOF} \leq 45$ days can be seen as a curve and also as cluster in the phase space. These trajectories visit Moon twice or thrice before coming close by 3738 km from the center of Moon. The periodic orbits also occupy certain regions in the phase space.

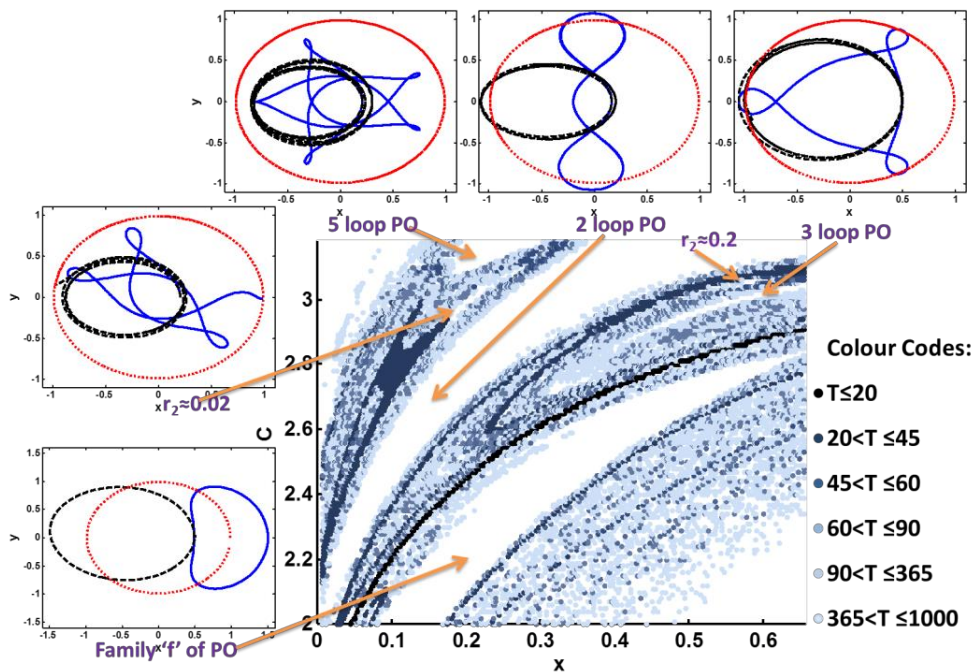


Fig.- 3.1(a): Initial condition space along with the periodic orbits contained in the white regions.

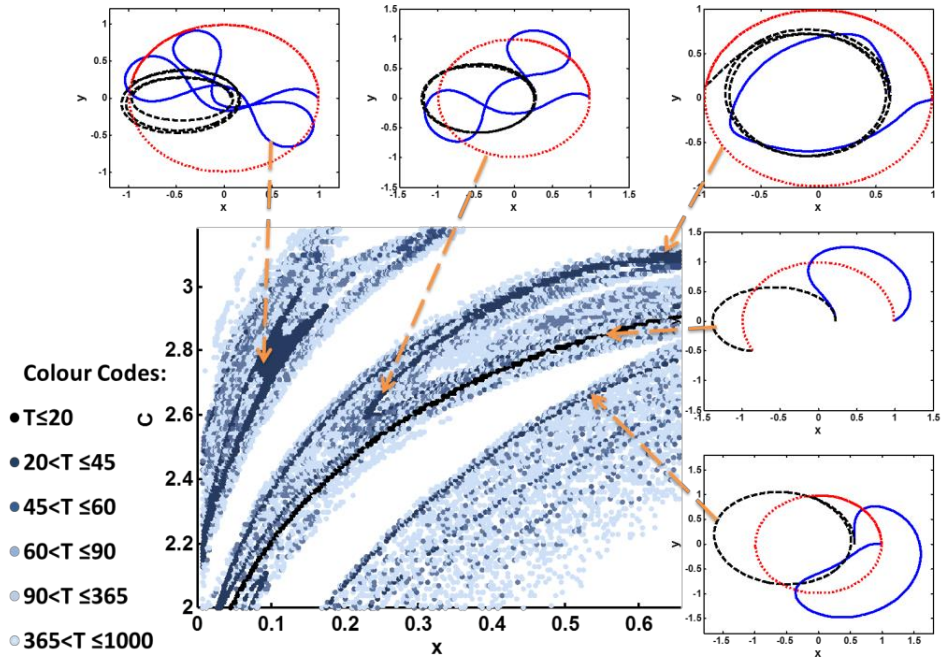


Fig.-3.1(b): Initial condition space along with the fly-by trajectories with TOF ≤ 90 days

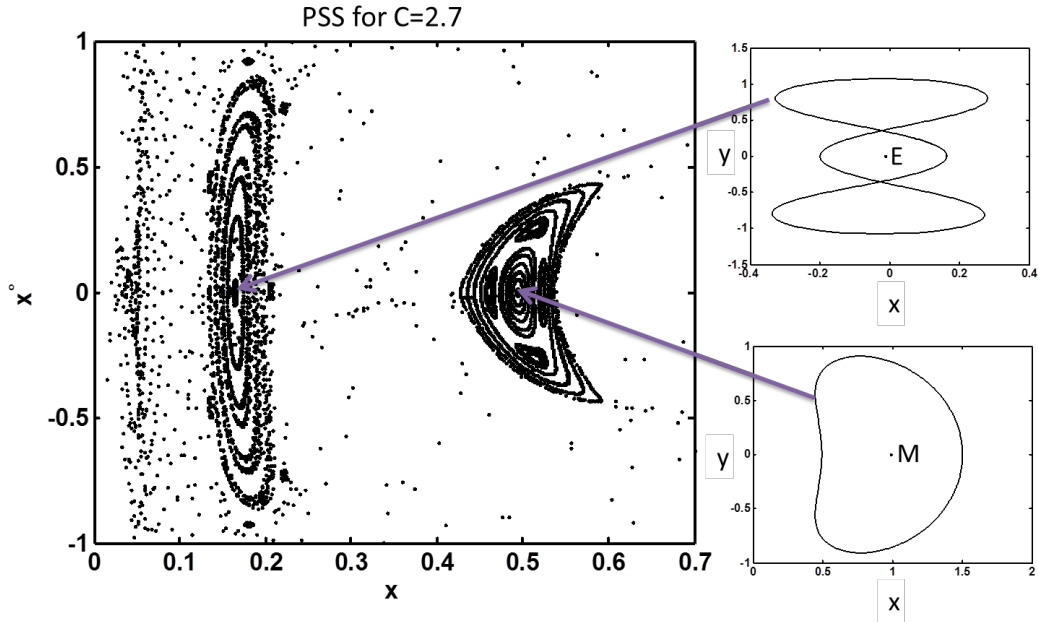


Fig. 3.2(a): Poincaré surface of section for $C=2.7$ and corresponding periodic orbits

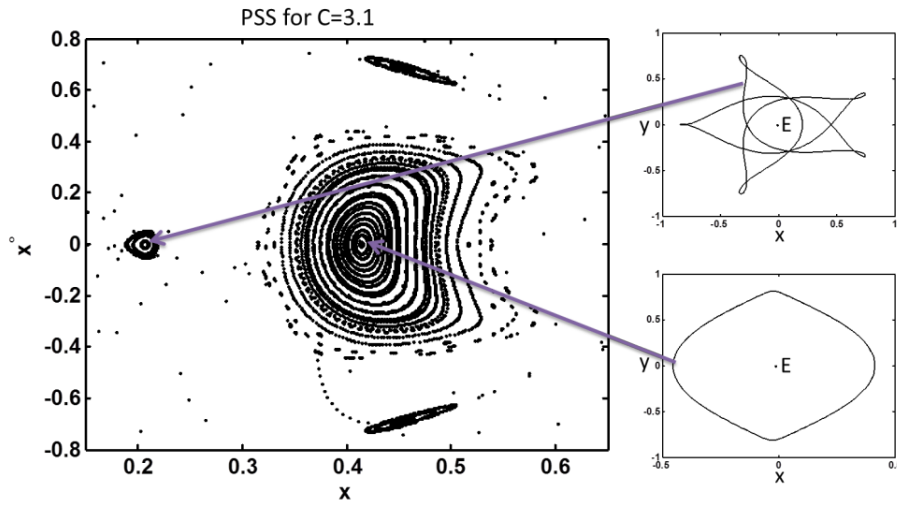


Fig. 3.2(b): Poincaré surface of section for $C=3.1$ and corresponding periodic orbits

A typical trajectory starting near Earth and reaching Moon in 37 days is shown in Fig. 3.3. After reaching Moon it moves around Moon in elliptical orbit whose apoapsis keeps decreasing, till it becomes 408 km from the center of Moon. In this problem the primaries are considered to be point mass and so such a close approach is obtained. Study is also carried out with set (i) of initial conditions with x_0 lying between Earth and Lagrange point L_3 , but in this case trajectories going towards Moon are not found.

Similar analysis is carried out with set (ii) of initial conditions. The positive values of y_0 do not yield satisfactory results in this case. The trajectories obtained by varying the negative values of y_0 with respect to C are plotted with different colour codes in Fig. 3.4 depending upon the TOF. As in the previous case, the white regions indicate the presence of PO or fly-by (whose distance from Moon is greater than 3738 km). Unlike for set (i) ICs, in this case the presence of PO could not be confirmed by PSS.

As seen in Fig. 3.4(b), the fly-by trajectories with $\text{TOF} \leq 5$ days and $5 \text{ days} < \text{TOF} \leq 15$ days appear as bands in the phase space. These fly-by trajectories take lesser flight duration compared to first type. The trajectories with TOF lying between

15 to 40 days was further divided into two groups, namely TOF from 15 to 30 days and TOF from 30 to 40 days, and various trajectories were found and plotted in Figs. 3.5(a) and 3.5(b). Figure 3.6 gives a typical trajectory that travels from near Earth to Moon in 17 days. It moves around the Moon in elliptical orbit whose apoapsis decreases till 421 km from the center of Moon.

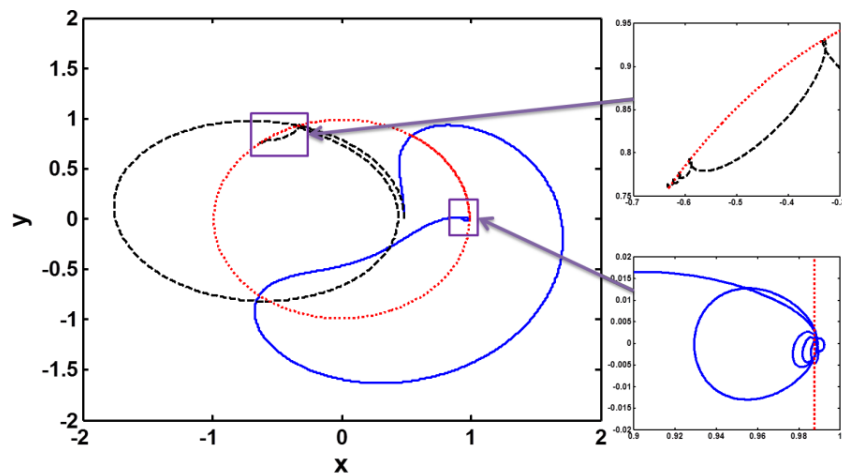


Fig. 3.3: A typical trajectory with $C=2.6$, $x=0.48368684$, TOF=37 days, $r_2=408$ km

Figs. 3.1 and 3.4 indicate that the trajectories reaching Moon and the periodic orbits appear in certain regions of the phase space and follow some kind of pattern. They are not scattered randomly in the phase space. For example in Fig. 3.1, the trajectories to Moon with flight duration of about 14 to 16 days can be easily identified as a curve appearing in the phase space. Similarly, in Fig. 3.4, the trajectories with TOF ≤ 5 days occupy a definite region of the phase space. Similar conclusion can be drawn for periodic and quasi-periodic orbits also. The step size (500 km for distance and 0.01 for Jacobi constant) can be taken as an error bar on the results. Moreover, the step size on distance was reduced to 10 km for some cases like for $C = 2.5, 2.6, 2.7, 2.8, 2.9$ and 3.0 and compared with those generated with step size of 500 km. The results agree in the sense that the trajectories with similar TOF and PO are still clustered together in the same regions of the phase space.

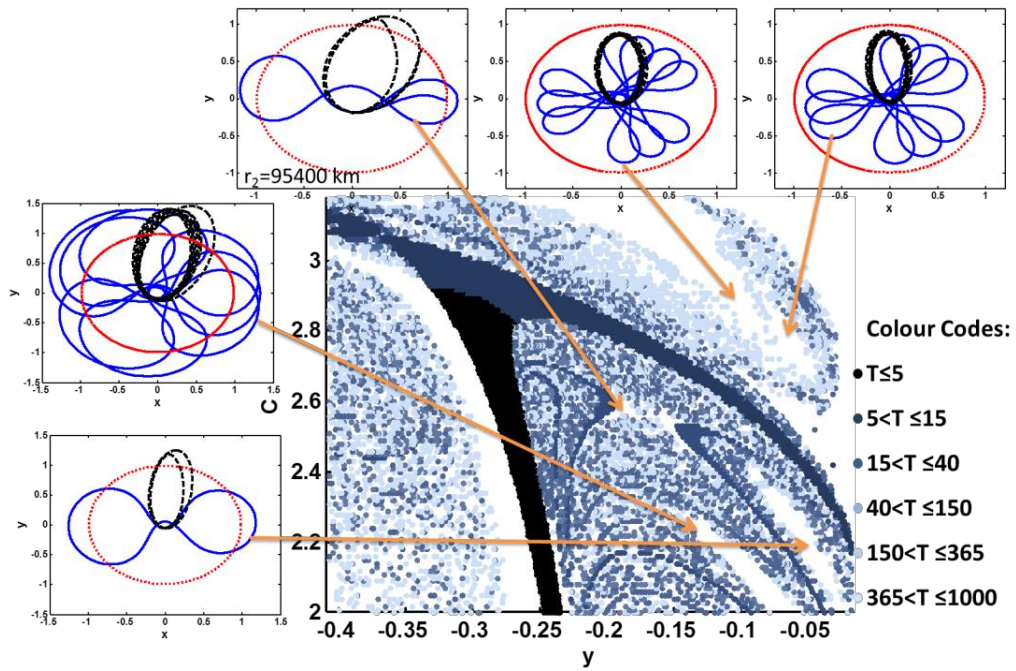


Fig. 3.4(a): Initial condition space for set (ii) ICs along with PO contained in the white regions

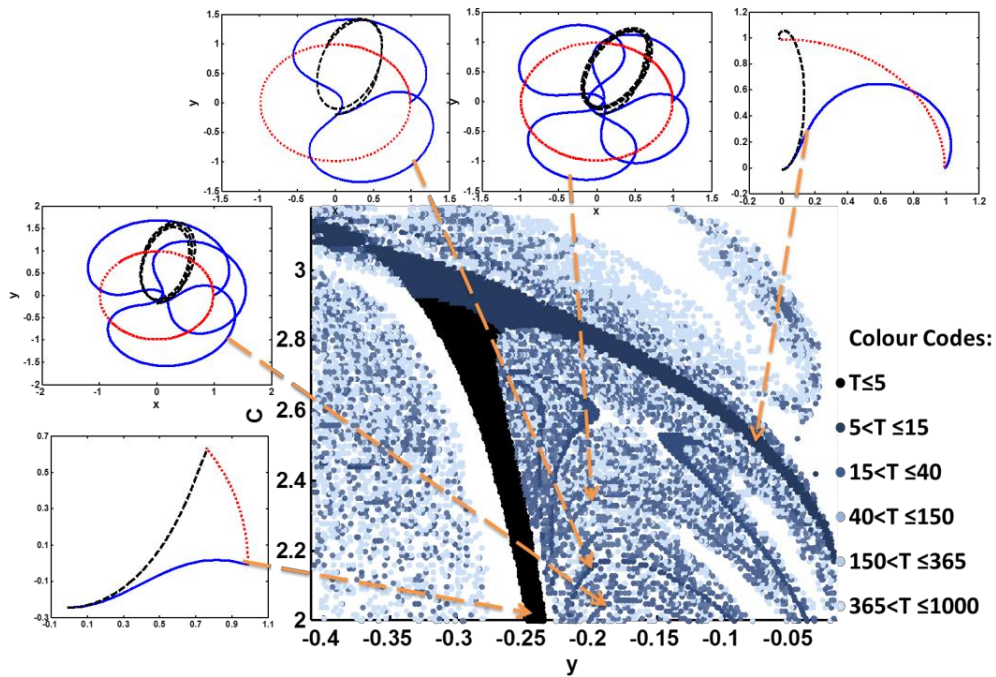


Fig. 3.4(b): Initial condition space for set (ii) along with some fly-by trajectories

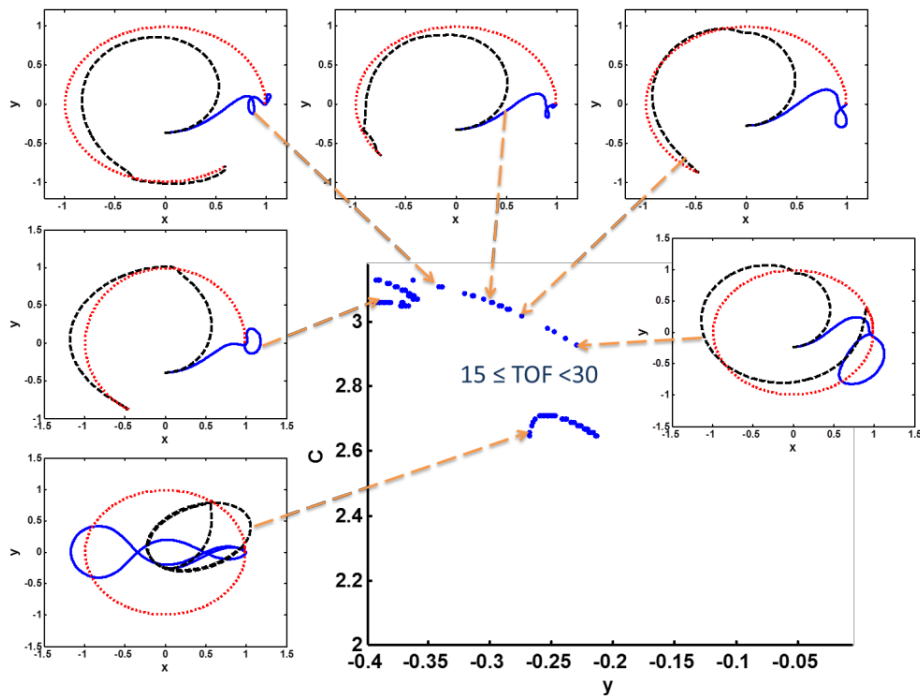


Fig. 3.5(a): Fly-by trajectories for IC of set (ii) whose TOF lies between 15 to 30 days

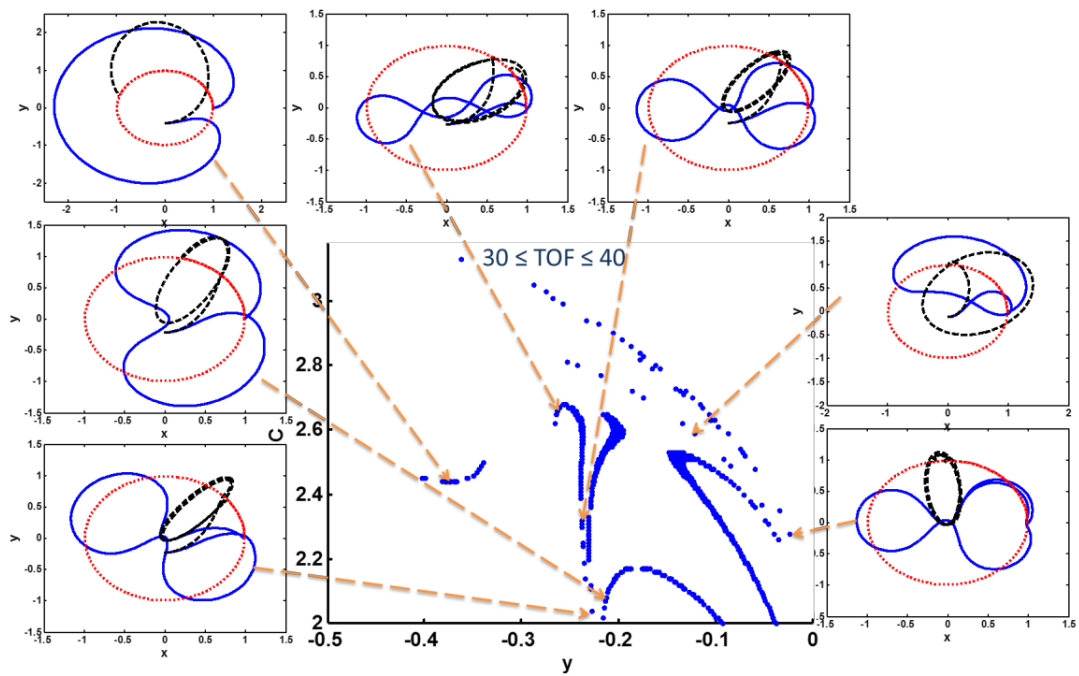


Fig. 3.5(b): Fly-by trajectories for set (ii) of IC whose TOF lies between 30 to 40 days.

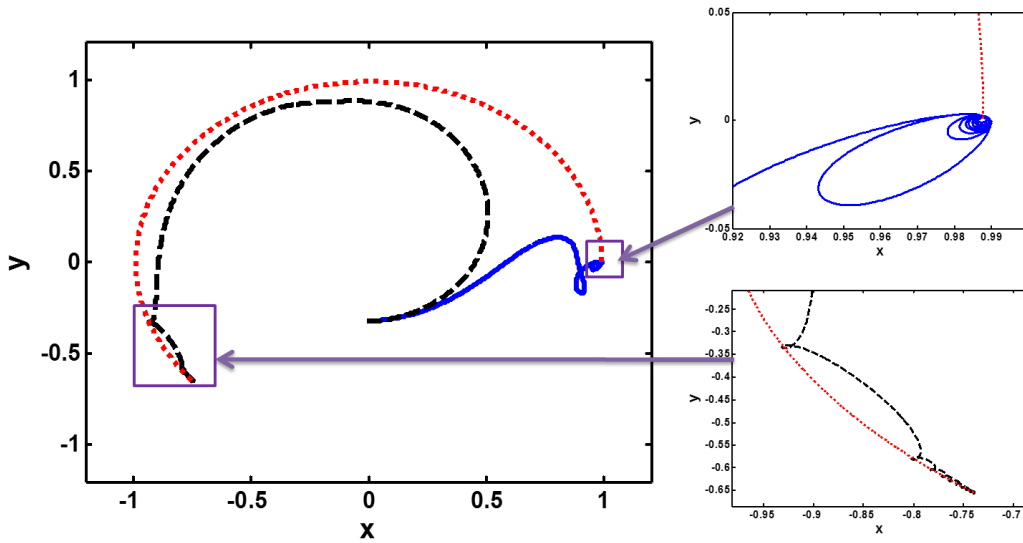


Fig. 3.6: A typical trajectory of set (ii) IC with $C=3.09$, $y= -0.32154006$, $\text{TOF}=16.8$ days, $r_2=421$ km

3.4. Conclusion

In order to understand the distribution of fly-by trajectories from Earth to Moon in the phase space, a number of trajectories with initial conditions of the form $(x_0, 0, 0, \dot{y}_0)$ and $(-\mu, y_0, \dot{x}_0, 0)$ near Earth (from about 200 km to 25,000 km from Earth's surface) and Jacobi constant 2 to $C(L_1) = 3.18834$ are propagated for 1000 days in the framework of restricted three-body problem. If the distance between spacecraft and center of the Moon is less than or equal to 3738 km, that initial condition and flight duration are recorded. Such trajectories are represented in plots of x_0 or y_0 and Jacobi constant with colour code on time of flight.

It is observed that the trajectories with similar flight duration appear in clusters or groups in the phase space, with error bar of step size on distance and Jacobi constant. Many of these trajectories reach near Moon where a small ΔV can put the spacecraft in an orbit around the Moon. For example for the initial condition of first type the fly-by trajectories to Moon with flight duration of about 14 to 16 days can be easily identified as a curve and those with flight duration between 20 and 45

days as curves and clusters appearing in the phase space. Similarly, for the second type of initial conditions the trajectories with flight duration ≤ 5 days and 5-15 days appear as a band on the phase space. The trajectories with flight duration 15-40 days appear as curves on the phase space. It is also observed that the initial conditions of second type give planar fly-by trajectories to Moon with lesser flight duration compared to first type.

Some regions in the phase-space were identified where the trajectories do not reach close to the Moon to the desired extent. Poincaré surface of section revealed the presence of periodic and quasi-periodic orbits in those regions. The periodic and quasi-periodic orbits also occupy certain regions in the phase space.

The results presented in this chapter can be considered as first step towards the study of weak stability boundary (WSB) transfers to Moon. With the background of distribution of planar fly-by trajectories to Moon in the phase space, and identification of sample fly-by trajectories to Moon which start near Earth and make few orbits around Moon, we now proceed to the construction of WSB trajectories to Moon in the next chapter. WSB trajectories to Moon start near Earth (from an Earth Parking Orbit) and reach Moon with sufficient velocity to get automatically captured by Moon.

CHAPTER 4

DYNAMICS OF WEAK STABILITY BOUNDARY TRANSFER TRAJECTORIES TO MOON

4.1. Introduction

Yamakawa (1992) describes Gravitational Capture at Moon as “Although local C_3 with respect to Moon is positive outside the sphere of influence, finally it becomes negative at perilune”. The perilunes located in first and third quadrant in selenocentric Earth-Moon fixed frame can be achieved by gravitational capture from a geocentric orbit. Solar gravity helps to enlarge the perigee from LEO distance (200-2000 km) to Earth-Moon distance and to attain Moon from large geocentric orbit with semi-major axis over 5,00,000 km. Spacecraft located in second and fourth quadrant in Sun-Earth fixed frame yields increase in local perigee distance. Lunar swing-by reduces local eccentricity (and helps in perigee raise) by which total flight time for Earth-Moon transfer can be reduced. It also gives flexibility in orbit design by controlling initial semi-major axis and swing-by distance.

In this chapter, lunar capture trajectories are obtained by back-propagation in the framework of restricted three-body (Earth-Moon-spacecraft) problem and are represented in phase-space as a function of capture time. Highly elliptical geocentric orbits are investigated in Sun-Earth-spacecraft system and those for which the perigee increases to Earth-Moon distance are also represented in phase space with “colour code on time of capture”. By “colour code on time of capture” we mean that different colours have been assigned to different ranges of time of capture (number of days the trajectory from an orbit around moon is back propagated so that its C_3 wrt moon becomes positive), so that looking at the figure short flight duration trajectories can be differentiated from longer flight duration trajectories. Moreover the distribution of trajectories with different capture durations in the phase space can be clearly visualized. The two trajectory segments are joined using Fixed Time of Arrival Targeting (FTAT) method.

Genetic Algorithm is used to find patching points to reduce ΔV . The role of initial phase angle for perigee enlargement is highlighted. Also lunar swing-by on the way to apogee is studied.

This study will be helpful for mission planners to design a WSB trajectory of their choice of arrival point and flight duration. Due to colour code on time of capture in the phase space diagrams, an approximation of total flight duration can be made without actually constructing the complete trajectory. This method is different from other methods available in literature because it provides feasible options for arrival (to lunar capture orbit) and departure (from highly elliptical geocentric orbit) conditions for the construction of a WSB trajectory from Earth to Moon. Given departure and arrival conditions GA is used to find patching points on these trajectories so that the patching ΔV is minimized. Moreover due to the detailed study of arrival and departure conditions, the algorithm to design WSB trajectory, presented here, is designed in such a way that the dimension of search space is reduced to just two.

4.2. Equations of Motion

Lunar capture trajectories are obtained in Restricted Three-Body Problem (R3BP) by back propagation of initial conditions near Moon. The equations of motion of R3BP are given in Appendix A. Fixed time of arrival targeting as given in Appendix D, is implemented to patch two trajectories, namely, one forward propagated from Earth and other capture trajectory obtained by back-propagation. Genetic algorithm (GA) is implemented to find patching points on the two trajectories. During forward propagation from Earth, the role of Sun to raise perigee altitude is investigated in Bicircular Restricted-Three Body Problem. The equations of motion are given in Appendix C. Also fly-by Moon on the way to WSB Earth to reduce time of flight is evaluated.

The equations of motion are integrated using Runge-Kutta-Fehlberg (7,8) or RKF(7,8) scheme. RKF(7,8) is embedded Runge-Kutta method of order $O(h^7)$ with error estimator of order $O(h^8)$ (Fehlberg, 1969; Hairer et al, 1993; Dumitras and Elena, 1997; Albrecht, 1996). The following function was numerically

integrated with different initial step sizes and error tolerance values using double precision variable.

$$\int_0^1 \frac{1}{1+x^2} = [\tan^{-1}x]_0^1 = \frac{\pi}{4}$$

Fig. 4.1 gives the variation in error (with compared with analytical value) due to initial step size for different error tolerance levels. It is noted that step size equal to and greater than 1.0 the magnitude of error remains the same because the step size is automatically adjusted to 1.0 (difference between upper and lower bound of integration). For step size less than 1.0, the error is of the order of 10^{-6} , which is sufficient for our studies. Fig. 4.2 shows how the step size was changed by the integrator for a given initial step size and number of iterations involved for various initial step sizes. For an initial step size of 10^{-4} , the integrator took six steps to complete the integration and step size was increasing at every step. For initial step size of 0.5, the integration was complete in two steps of 0.5 step size each. For initial step size of 1.0 the integration was complete in one step itself.

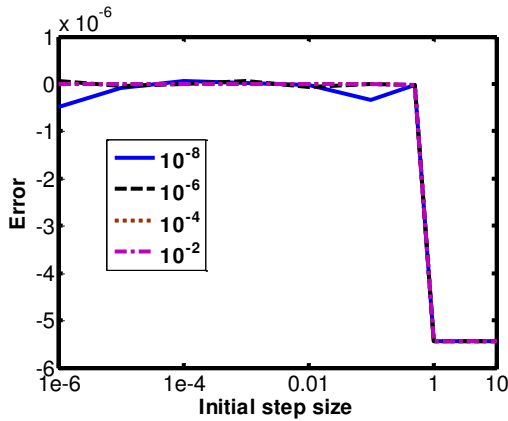


Fig. 4.1: Variation in error due to initial step size for different tolerance values

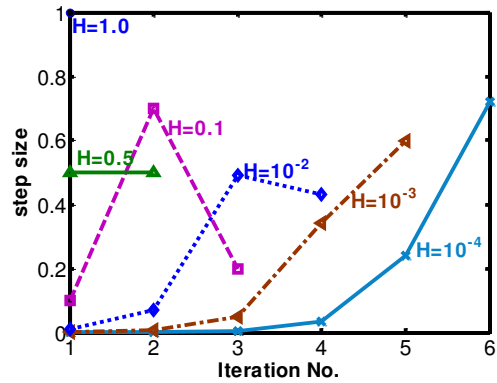


Fig. 4.2: Variation of step-size within the RKF integrator for a given initial step size (H)

The position and velocity of a particle in orbit around smaller primary m_2 are given by García and Gómez (2007). The initial conditions with positive velocity (osculating retrograde motions about m_2) and those with negative velocity (osculating direct motions about m_2) given in equations (2.4-2.6) in

Chapter 2. In Section 4.3 these equations are back-propagated to find lunar capture trajectories.

In order to understand the role of Sun to enlarge perigee altitude, initial conditions near Earth are propagated forward in time in the bicircular R3BP. The two body orbital elements in planar case associated to the orbit of m_3 around m_1 , are given by the following map (Belbruno, 2008)

$$(a, e, \omega, \varphi) \rightarrow (x, y, \dot{x}, \dot{y}) \quad (4.1)$$

Here a is the semi-major axis, e is the eccentricity, ω (referred as AOP later in the text/figures) is the angle between x -axis and line of apsis and φ is the angle between line of apsis and radial line in m_1 centered co-ordinate system. At $t=t_0$, when the rotating and the inertial Earth-centered frames are parallel, we can write

$$x = r \cos(\omega + \varphi) - \mu, \quad (4.2)$$

$$y = r \sin(\omega + \varphi), \quad (4.3)$$

$$\dot{x} = \dot{r} \cos(\omega + \varphi) - r \dot{\varphi} \sin(\omega + \varphi) + r \sin(\omega + \varphi), \quad (4.4)$$

$$\dot{y} = \dot{r} \sin(\omega + \varphi) + r \dot{\varphi} \cos(\omega + \varphi) - r \cos(\omega + \varphi), \quad (4.5)$$

where

$$r = \frac{a(1 - e^2)}{1 + e \cos \varphi}, \quad (4.6)$$

$$\dot{\varphi} = \frac{\sqrt{a(1 - e^2)(1 - \mu)}}{r^2}, \quad (4.7)$$

$$\dot{r} = \frac{ae(1 - e^2)\dot{\varphi} \sin \varphi}{(1 + e \cos \varphi)^2}. \quad (4.8)$$

4.2.1 Conditions for Easy Capture at Moon

Consider Earth-Moon-Spacecraft three-body problem. A ballistic capture trajectory from Earth to Moon is obtained in the following way. A spacecraft in highly elliptical orbit around Moon is back propagated with respect to time, till its C3 with respect to Moon becomes positive. From eq. (B.17) we get the following boundary conditions:

$$\frac{dC3_M}{dt} = 0 \Leftrightarrow \left(\frac{dr_M}{dt} = 0 \right), \left(\varphi_M = 0, \cos\chi_M = \pm \frac{1}{\sqrt{3}} \right), \left(\chi_M = 0, \cos\varphi_M = \pm \frac{1}{\sqrt{3}} \right) \quad (4.9)$$

The above back propagated trajectory is patched with a forward propagated highly elliptical orbit around Earth. The initial orbit around Earth should satisfy eq. (B.22) in Sun-Earth system, so that after one orbit its perigee distance increases to the Earth-Moon distance. So the boundary conditions for such an orbit is given by

$$\frac{dh_E}{dt} = 0 \Leftrightarrow (\varphi_E = \pm n\pi), (r_E + 2\cos\varphi_E = 0), \text{ where } n = 0, 1, 2, \dots \quad (4.10)$$

In the above equations, subscript M stands for Moon and E for Earth. Thus, combining (4.9) and (4.10) we get the following boundary conditions:

- (1) $\frac{dr_M}{dt} = 0$ and $\varphi_E = \pm n\pi$
 - (2) $\frac{dr_M}{dt} = 0$ and $r_E + 2\cos\varphi_E = 0$
 - (3) $\varphi_M = 0, \cos\chi_M = \pm \frac{1}{\sqrt{3}}$ and $\varphi_E = \pm n\pi$
 - (4) $\varphi_M = 0, \cos\chi_M = \pm \frac{1}{\sqrt{3}}$ and $r_E + 2\cos\varphi_E = 0$
 - (5) $\chi_M = 0, \cos\varphi_M = \pm \frac{1}{\sqrt{3}}$ and $r_E + 2\cos\varphi_E = 0$
 - (6) $\chi_M = 0, \cos\varphi_M = \pm \frac{1}{\sqrt{3}}$ and $\varphi_E = \pm n\pi$
- (4.11)

4.3. Dynamics of WSB Trajectories

4.3.1 Lunar Capture Trajectories:

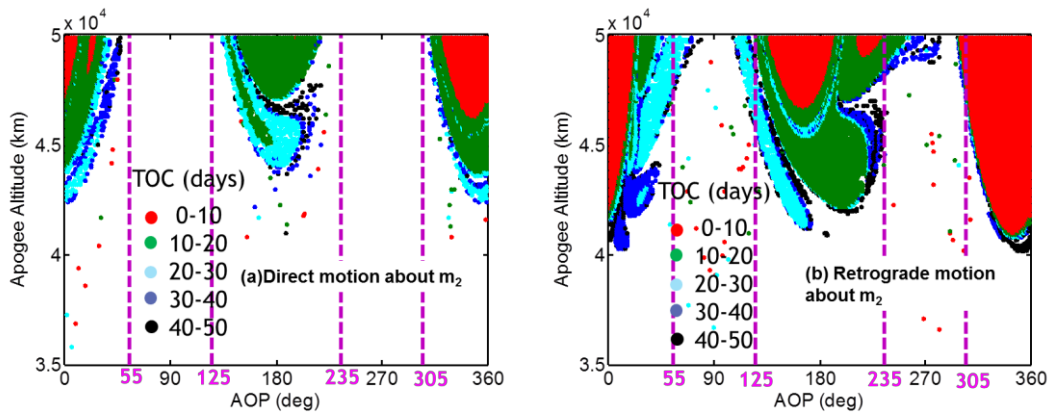


Fig. 4.3: Lunar capture trajectories obtained by back propagation for 50 days. The initial conditions which lead to a capture trajectory are plotted in the phase space with colour code on time of capture. (a) Direct motion about m_2 , (b) Retrograde motion about m_2 .

The model used here is Restricted Three Body Problem (R3BP) - Earth-Moon-spacecraft, to back propagate initial conditions obtained from equations (2.4)-(2.6). The equations of motion are provided in Appendix (A.15)-(A.18). Perilune is fixed at 100 km and apolune is varied from 100 km to 50,000 km. The argument of perilune (ω) is varied from 0° to 360° . Perilune of 100 km is selected as it gives the most useful mapping orbit around Moon. Most of lunar missions including Chandrayaan-1 have been placed in 100 km circular orbit around Moon. Apolune is varied till 50,000 so that the eccentricity of the 100 km \times 50,000 km orbit is 0.93 which is approximately where ballistic capture occurs. Once captured the orbit apolune can slowly be decreased to get a circular orbit. Time of capture, ie, the time of back-propagation till C3 wrt Moon becomes positive, is recorded in each case. Fig. 4.3 (a) and (b) shows the phase space representation of lunar capture trajectories with colour code on time of capture. Similar trend is observed with perilune 500 km. With the help of these phase space diagrams, one can select an appropriate arrival point with respect to desired time of flight. The trend observed for direct motion is well within AOP range of -55° to 55° and 125° to 235° as predicted by Yamakawa (1992), Proposition 3.3. In case of retrograde motion for higher apolune altitudes the above mentioned trend is violated to some extent. This may be due to truncation of Taylor's series during the derivation of Proposition 3.3.

4.3.2 Enlargement of perigee from LEO to Earth-Moon distance:

Using the equations (4.1)-(4.8), Earth Parking Orbits (EPO) with perigee altitude 200 km, apogee altitude varying from 1 to 1.5 million km (distance of L_1 point from Earth in Sun-Earth System) and argument of perigee varying from 0° to 360° are obtained and propagated in bi-circular restricted three-body problem - Sun-Earth-Moon-spacecraft, for one revolution using equations given in Appendix C (C.1-C.2). The perigee altitude is fixed at 200 km as most launch vehicles inject their payload in Geostationary Transfer Orbits (GTO) with perigee at about 200 km.

The orbits for which the perigee altitude increased from 200 km to $384400 \text{ km} \pm 50000 \text{ km}$ were represented in the phase space in Fig. 4.4, with

colour code on time of flight, along with some orbits. ± 50000 km is taken so that the trajectory is within the sphere of influence of Moon. The initial lunar phase angle (θ_{M0}) is 0° . In the phase space diagram two peaks are visible in the 2nd and 4th quadrant. This supports the result by Yamakawa (1992) that spacecraft location in 2nd and 4th quadrant in Sun-Earth fixed frame yields increase in local perigee distance. This diagram is also useful for mission designers as one can identify appropriate departure condition wrt time of flight.

There is a slight variation in the phase space diagram when the initial phase of Moon changes. Fig. 4.5 compares the phase space representation of EPO whose perigee rose from 200 km to about 384400 km for initial phase angle 0° and 90° . This tells us that the choice of initial lunar phase angle is important for WSB trajectory design. Fig. 4.4 indicates the EPO which encounter Moon when the spacecraft returns to the perigee. All the EPO for which the distance between Moon and spacecraft at perigee is less than 50,000 km are plotted.

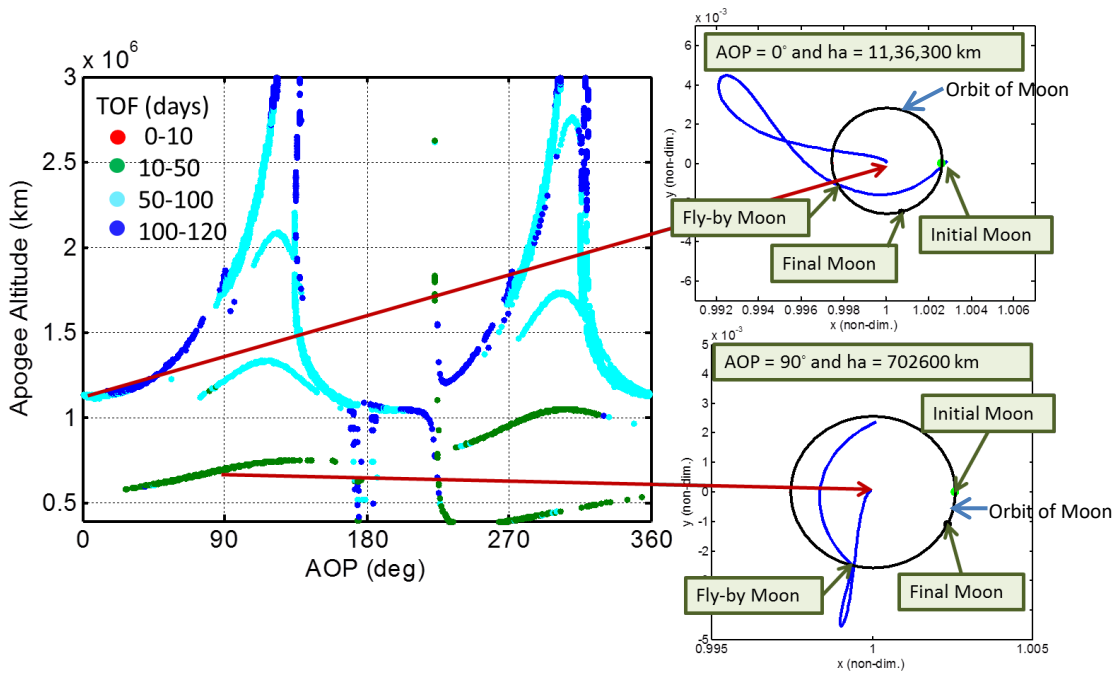


Fig. 4.4: EPO whose perigee rose from 200 km to about 384400 km propagated in bi-circular R3BP (Initial lunar phase angle is 0°) with colour code on time of flight

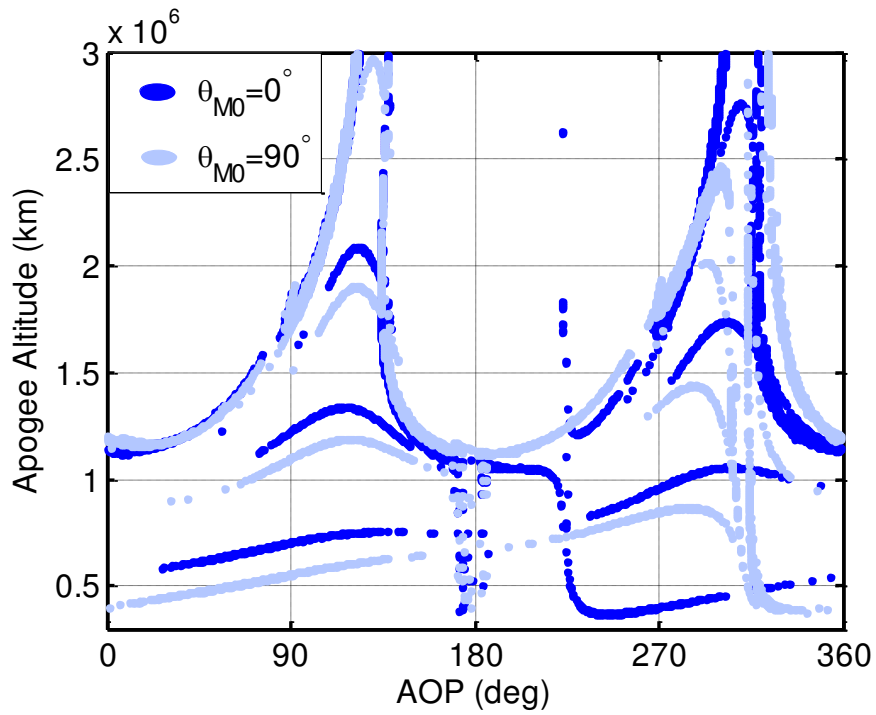


Fig. 4.5: Comparison of phase space re presentation of EPO whose perigee rose from 200 km to 384400 km for initial lunar phase angle (θ_{M0}) 0° and 90° .

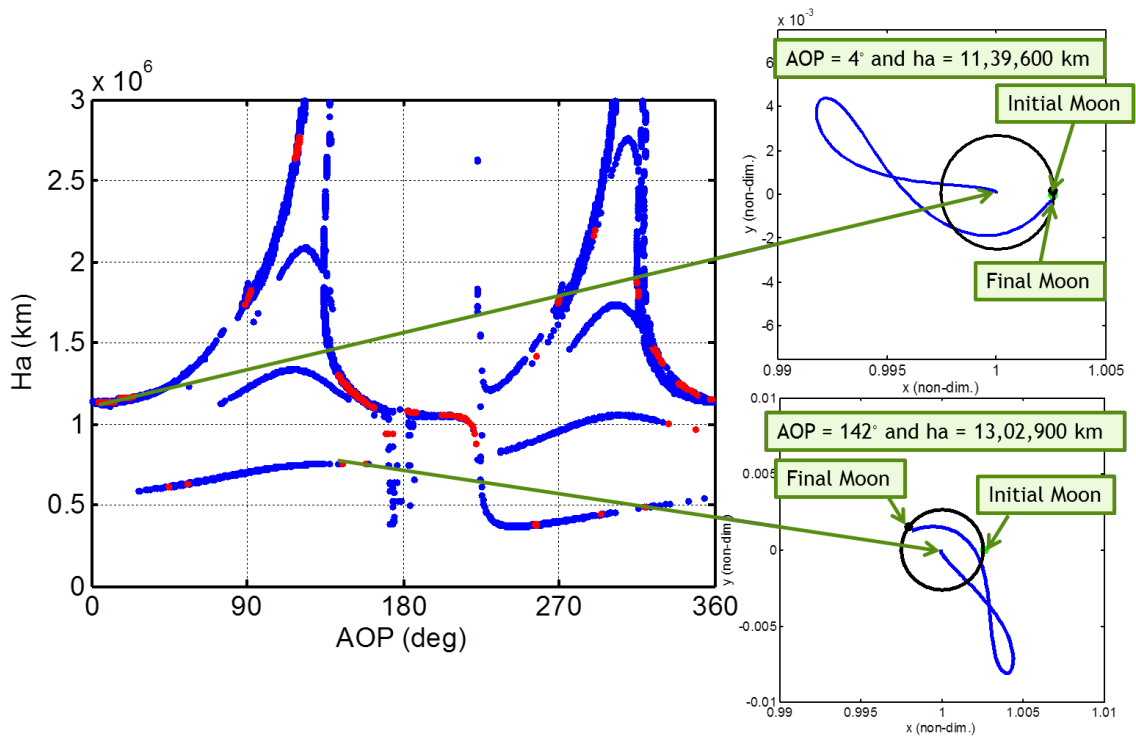


Fig. 4.6: EPO which encounter Moon on return to perigee

4.3.3. Fly-by Moon on the way to apogee

The initial lunar phase angle is adjusted so that fly-by occurs on the way to apogee. Fig. 4.7 shows the phase space representation of the EPO, with perigee fixed at 200 km, apogee varying from 0.4 to 3 million km and AOP varying from 0° to 360° in each case, which have a fly-by on the way to apogee and their perigee increases from 200 km to $384400 \text{ km} \pm 50000 \text{ km}$. It is observed that the opportunities have increased and flight duration has decreased in many cases compared to Figs. 4.4-4.6. Fig. 4.8 gives the dependence of time of flight on the angular position of Moon during flyby on the way to apogee.

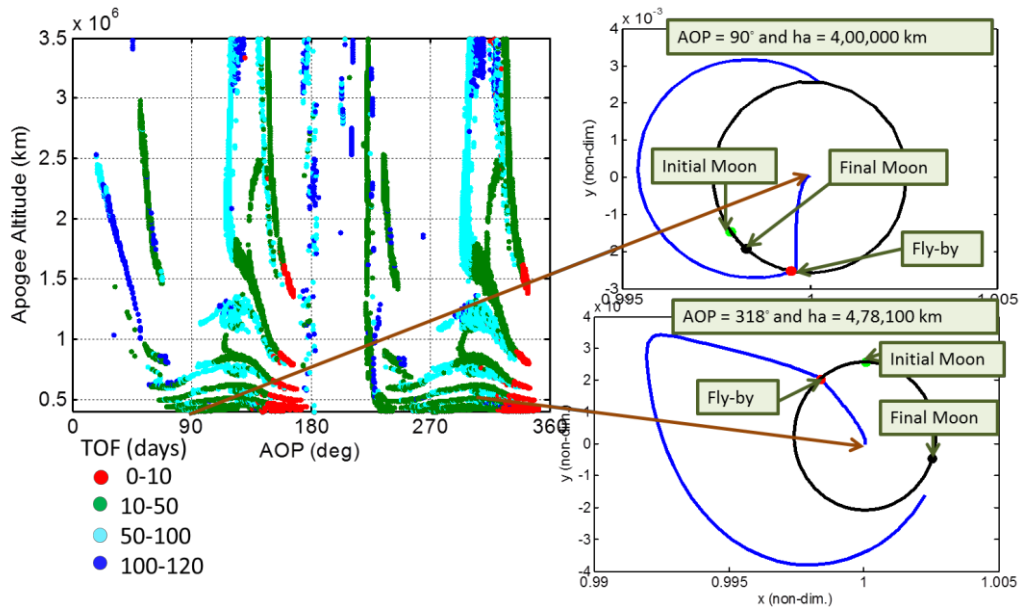


Fig. 4.7: Fly-by Moon on the way to apogee with colour code on time of flight

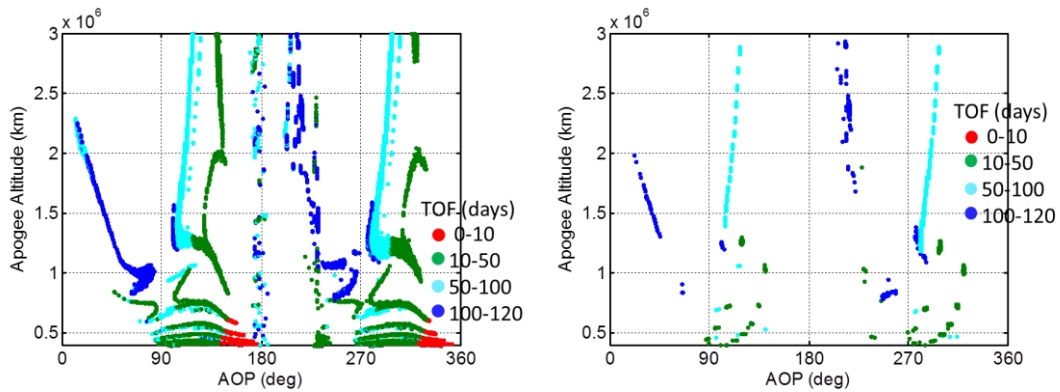


Fig. 4.8(a): Fly-by Moon ($\theta_{M0}-1 \text{ deg}$)

Fig. 4.8(b): Fly-by Moon ($\theta_{M0}-1 \text{ deg}$) and arrive Moon at first perigee passage

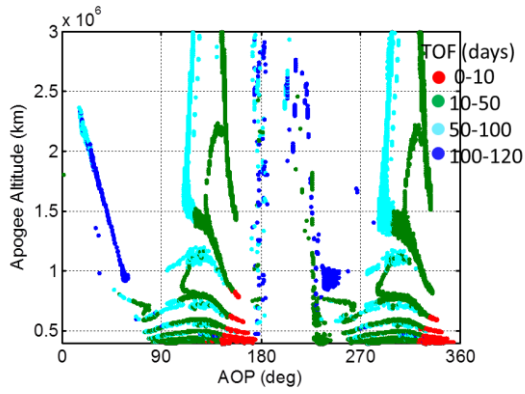


Fig. 4.6c: Fly-by Moon ($\theta_{M0}=-0.5\text{deg}$)

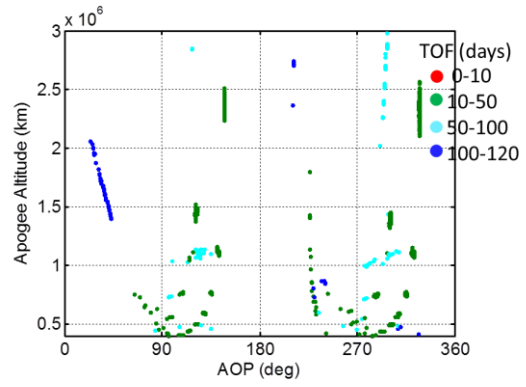


Fig. 4.6d: Fly-by Moon ($\theta_{M0}=-0.5\text{deg}$) and arrive Moon at first perigee passage

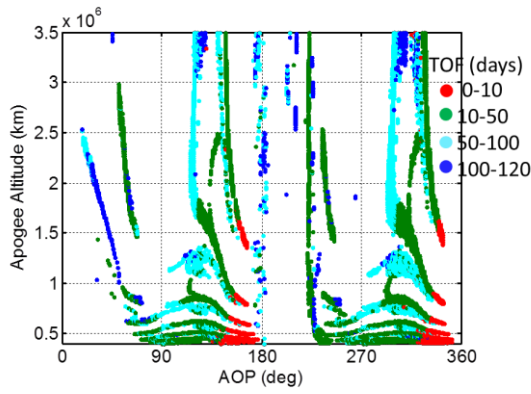


Fig. 4.6e: Fly-by Moon (θ_{M0})

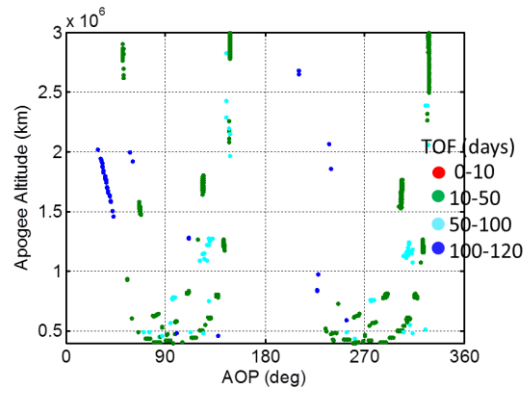


Fig. 4.6f: Fly-by Moon (θ_{M0}) and arrive Moon at first perigee passage

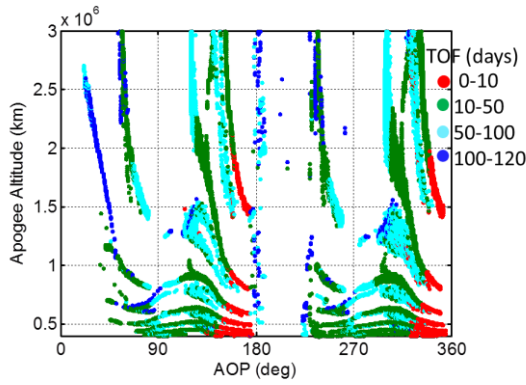


Fig. 4.6g: Fly-by Moon ($\theta_{M0}+0.5\text{deg}$)

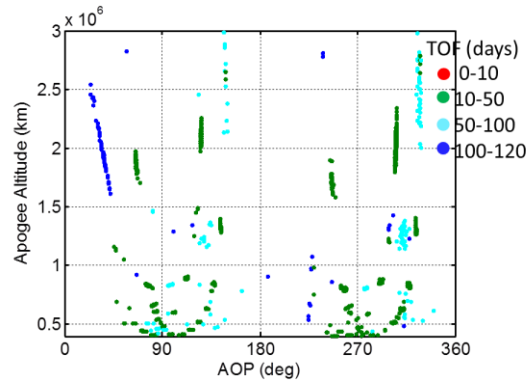


Fig. 4.6h: Fly-by Moon ($\theta_{M0}+0.5\text{deg}$) and arrive Moon at first perigee passage

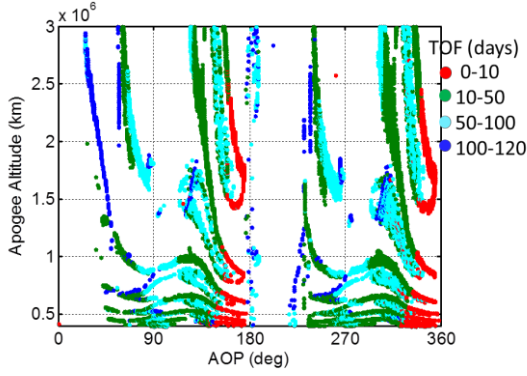


Fig. 4.6i: Fly-by Moon ($\theta_{M0}+1\text{deg}$)

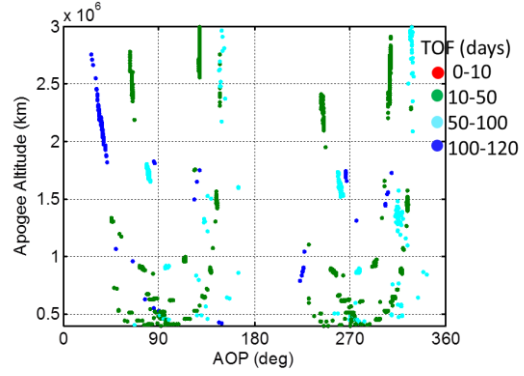


Fig. 4.6j: Fly-by Moon ($\theta_{M0}+1\text{deg}$) and arrive Moon at first perigee passage

Fig. 4.6: Dependence of time of flight on the angular position of Moon during flyby on the way to apogee

4.4. Construction of WSB Trajectory

The phase space diagrams provided in Section 4.3 helps in locating feasible departure (high eccentricity geocentric orbit) and arrival (lunar capture orbit) conditions. Once the departure and arrival orbits are identified they are patched using Fixed Time of Arrival Targeting (FTAT) algorithm provided in Appendix D.

As an example, Fig. 4.9 gives Earth-centered orbit that fly-by Moon. The initial conditions are: perigee altitude is 200 km, eccentricity is 0.976, AOP and true anomaly are 0° . These initial conditions are propagated forward in time till a lunar fly-by is obtained. It takes about 68.7 days to reach near Moon. A point A is selected on this trajectory, which will be the patching point for FTAT. Another set of initial conditions near Moon are propagated backward in time till it reaches about 10^5 km away from Moon or its energy wrt Moon becomes positive. One such trajectory is shown in Fig. 4.10.

The initial conditions (ICs) for this trajectory is perilune is 100 km, eccentricity is 0.917 and AOP=0°. It requires approximately 39 days to escape from Moon. A point B is selected on this trajectory for patching with the previous one. At present these points A and B are selected judiciously and are not optimized for minimum patching ΔV .

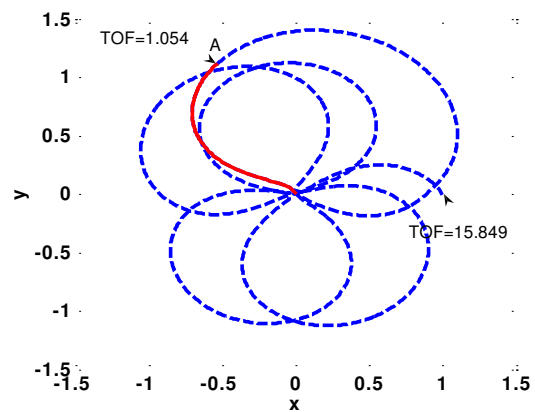


Fig. 4.9: An Earth centered orbit

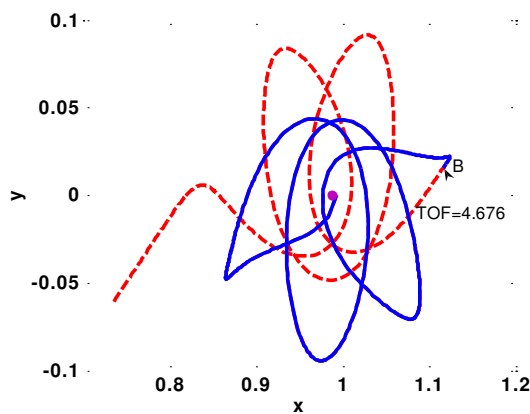


Fig. 4.10: Lunar Capture orbit

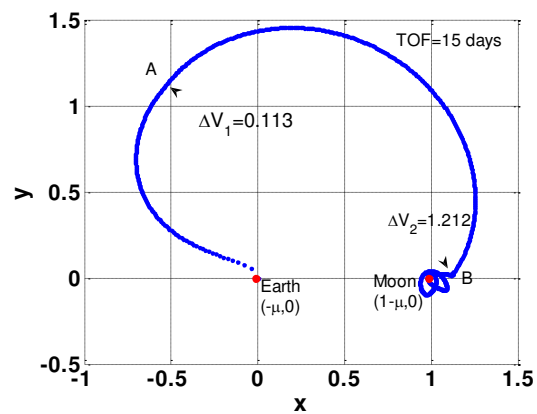


Fig. 4.11: Patching Earth centered orbit with Lunar capture orbit using FTAT

The points A and B are patched using FTAT. The resultant trajectory is a ballistic capture trajectory at Moon as shown in Fig. 4.11, and so theoretically no impulse is required for orbit insertion. Real-valued Genetic Algorithm (GA) is implemented to find patching points to minimize patching ΔV requirements (Deb 1995, Deb 2001). GA provides sufficiently good solutions inspite of highly nonlinear dynamics involved in the system.

Variables:

1. Time t_1 is the propagation time from IC near Earth to the patching point A.
2. Time t_2 is the back propagation time from IC near Moon to the patching point B.

Objective is to minimize ΔV (sum of ΔV required at both patching points A and B). The fitness function is

$$f = \frac{1}{(1 + \Delta V)}$$

Characteristics/Parameters of GA:

1. No. of individuals in a population = 50
2. No. of generations over which solution evolves = 50
3. Crossover probability = 0.85
4. Elitism, retaining the best individual in a generation unchanged in the next generations, is used.
5. Mutation rate is dynamically adjusted.
6. Roulette wheel selection is used for crossover.

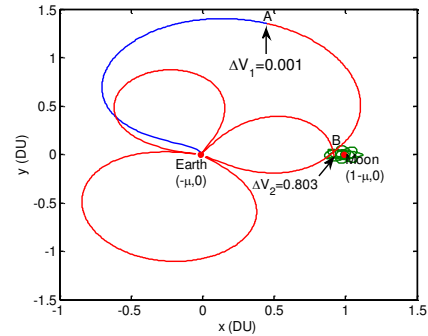


Fig. 4.12: Patching points A and B obtained by GA

In the previous example GA was used to find patching points A and B to reduce ΔV . Fig. 4.12 gives the optimized trajectory.

The algorithm for construction of WSB trajectories using the dynamics is as follows:

1. Select a suitable arrival condition based on the orbit and capture duration from Fig. 4.3.
2. Select a suitable departure orbit based on orbit, transfer time and requirement of lunar fly-by from Figs. 4.4-4.8.
3. The above two segments are joined using FTAT (inner loop). The patching points on the two segments are searched using GA (outer loop).

Any optimization algorithm can be used instead of GA. As a case study, Pattern Search (PS) (Abramson, 2002; Audet and Dennis, 2003) and Nelder-Mead Simplex algorithm (Lagarias et al, 1998) were implemented and tested for 6 test cases along with GA. In all these cases, the initial orbit around Earth is fixed with perigee altitude 200 km, eccentricity 0.976 and AOP and true anomaly are 0° . The perilune altitude is fixed as 100 km. For the first three cases initial lunar orbit has

AOP 0° and eccentricities are 0.917, 0.928 and 0.938, respectively. For next three cases, AOP of initial lunar orbit is 180° and eccentricities are 0.921, 0.931 and 0.941, respectively. Table 4.1 gives the results obtained for these 6 cases using three optimization techniques. It is observed that GA gives lower total ΔV for all the cases compared to other two methods, while no. of function evaluations are lesser for PS compared to other two algorithms.

Table 4.1: Comparison between optimization methods – Pattern Search, Nelder-Mead Simplex algorithm and genetic algorithm

Method	Case No.	t₁ (days)	t₂ (days)	Total ΔV (km/s)	No. function evaluations
Pattern Search	1	8.97	16.95	0.906	132
	2	18.33	20.83	1.109	217
	3	19.57	42.39	1.233	115
	4	6.81	28.89	0.572	224
	5	12.34	0.43	0.874	210
	6	13.13	16.85	0.689	120
Nelder Mead Simplex Method	1	3.86	16.93	0.925	402
	2	4.57	17.40	1.066	401
	3	3.79	14.27	1.214	233
	4	4.26	18.65	1.315	195
	5	4.29	18.92	1.212	219
	6	4.44	17.57	1.032	400
Genetic Algorithm	1	0.20	8.33	0.825	2600
	2	26.15	8.13	0.120	2600
	3	3.30	44.99	0.394	2600
	4	43.97	16.52	0.418	2600
	5	34.90	5.13	0.132	2600
	6	35.16	19.46	0.075	2600

Topputo et al. (2004) have presented a method using invariant manifold theory to compute transfers from Earth to Moon. They start from an Earth Parking Orbit and compute trajectory arcs that target a point on W_{LI}^S using Lambert's three-body problem. A first manoeuvre places the spacecraft into a translunar trajectory starting from an Earth Parking Orbit (LEO/GTO); second manoeuvre injects the spacecraft on the capture trajectory on W_{LI}^S . The total cost of transfer is sum of two manoeuvres. In an example, they consider two departure orbits, 200 km circular LEO and 200 km X 35840 km GTO. The given trajectory arrives Moon in an unstable orbit around Moon with mean altitude of 21600 km. The same example has been worked out with the present method using GA optimization (Table 4.2). In the present analysis we consider an EPO with perigee altitude 200 km, eccentricity 0.833 and AOP and true anomaly are 0° . The capture orbit around Moon is 21600 km X 42338 km and AOP 0° . One of the solutions obtained by present method with GA gives ΔV of the order of 296.5 m/s and time of flight is 100 days. In order to start from 200 km circular LEO to EPO (200 km X 65947 km), ΔV is 2.755 km/s. So total ΔV is 3.052 km/s. If we start from GTO (200 km X 35840 km) to EPO (200 km X 65947 km), ΔV is 300 m/s and so the total ΔV is 596.5 m/s.

Table 4.2: Comparison between Hohmann transfer, Invariant manifold theory (Topputo et al 2004) and present method using GA.

Method	ΔV (m/s)		Flight duration (days)
	LEO	GTO	
Hohmann transfer (Topputo et al 2004)	3344	1177	6.5
Invariant manifold (Topputo et al 2004)	3081	914	49
	3085	918	119
	3091	924	47
Present Method using GA optimization	3052	597	100

4.5. Conclusions

A Weak Stability Boundary (WSB) trajectory to Moon is designed in two stages. First, a highly elliptical geocentric (HEG) orbit is propagated forward in time so that its perigee increases to Earth-Moon distance. Second, a highly elliptical selenocentric orbit (Lunar capture orbit) is propagated backward in time till it starts moving towards Earth. The two trajectories are patched using Fixed Time of Arrival Targeting method to obtain a WSB transfer trajectory. It is observed that the lunar capture trajectories obtained by back-propagation is grouped in the phase space with respect to time of flight. It is also observed that initial phase angle plays an important role in getting captured at Moon. HEG orbits are studied in Sun-Earth-Moon-spacecraft bi-circular R3BP. Trajectories which encounter Moon at 1st perigee passage are represented in the phase space. Typical trajectories are also shown. Fly-by moon on the way to apogee helps to reduce time of flight. Initial lunar phase angle is adjusted to obtain fly-by. Those trajectories which arrive at Moon are also represented in phase space. Dependence of time of flight on angular position of Moon during fly-by is also investigated. Genetic Algorithm is used to find patching points between HEG and lunar capture orbit. This study will be helpful for mission designers. The phase space diagrams with colour code on time of capture enables selection of departure and arrival orbits and an approximation of total flight duration can be made without actually constructing the complete trajectory.

In this chapter, we understand the dynamics of highly elliptical geocentric orbits and lunar capture trajectories (LCT) used for the construction of WSB trajectories to Moon in the framework of R3BP and bi-circular R3BP. In the next chapter we use these properties of HEG orbits and LCT to construct WSB trajectories to Moon in full-force model.

CHAPTER 5

DESIGN OF WSB TRAJECTORY TO MOON USING FORWARD PROPAGATION

5.1. Introduction

Forward propagation algorithm to find WSB trajectories to Moon in high fidelity force model is presented in this chapter. The forward-backward propagation algorithms to find WSB trajectories face major problem of launch vehicle constraint satisfaction. Forward-backward propagated trajectories may lead to a patching point, too expensive for a launch vehicle to satisfy its maximum payload constraints (mainly AOP and inclination). This drawback is eliminated here, as the algorithm starts from the required EPO. This algorithm is valid for both circular and elliptical parking orbit. Also given a departure date and EPO conditions, a number of WSB arrival orbits can be found using the given algorithm with marginal difference in impulse requirements. The one suiting our requirement can be selected. Another advantage of this algorithm is that we find the WSB trajectories in high fidelity force model which can be used for real missions.

5.2. Methodology

A numerical algorithm is developed to obtain WSB trajectories to Moon using forward propagation. The force model used for propagation includes high order gravity model for central body (Earth and Moon in this case) and third body perturbation. When the spacecraft is under the influence of Earth, 8×8 WGS84 gravity model is used along with Sun and Moon as third body effects. When the spacecraft is near Moon, 15×15 LP15Q gravity model is used along with Earth and Sun as third body effects. The algorithm consists of two loop optimization (Fig. 5.1).

The control variables for outer loop are departure epoch (LD), Right Ascension of Ascending Node (Ω) and Argument of Perigee (ω) of the EPO and ΔV_1 to increase the apogee of EPO to about 1.5 million kilometre. In case of maximum payload constraint on ω by the launch vehicle, ω can be fixed. Time spent in phasing orbit can be used as control variable instead of ω . The outer loop ensures that the perigee of highly elliptical orbit is near Moon, so that in the inner loop a ballistic capture can be obtained. The inner loop, based on

the arrival conditions at apogee of high elliptical orbit, a small manoeuvre, ΔV_2 at apogee is varied, so that the trajectory reaches Moon and gets ballistically captured there. The sum of impulse requirements ΔV_1 , ΔV_2 and ΔV_3 (impulse required for reducing capture orbit at Moon to desired mapping orbit at Moon) forms the objective function. Suitable weights are assigned to ensure that on the way back to Moon, perigee of high elliptical orbit is increased to Earth-Moon distance, Moon is near the arrival point and C3 of the spacecraft with respect to Moon becomes negative within specified time duration.

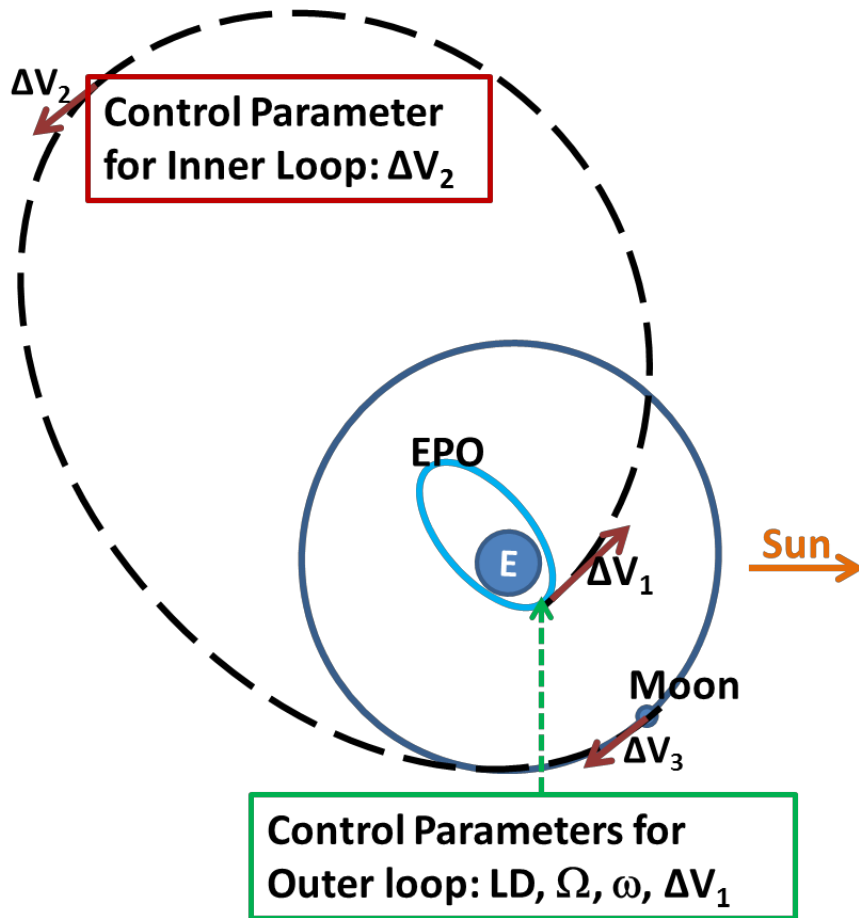


Fig. 5.1: Control parameters for trajectory optimization – WSB Moon

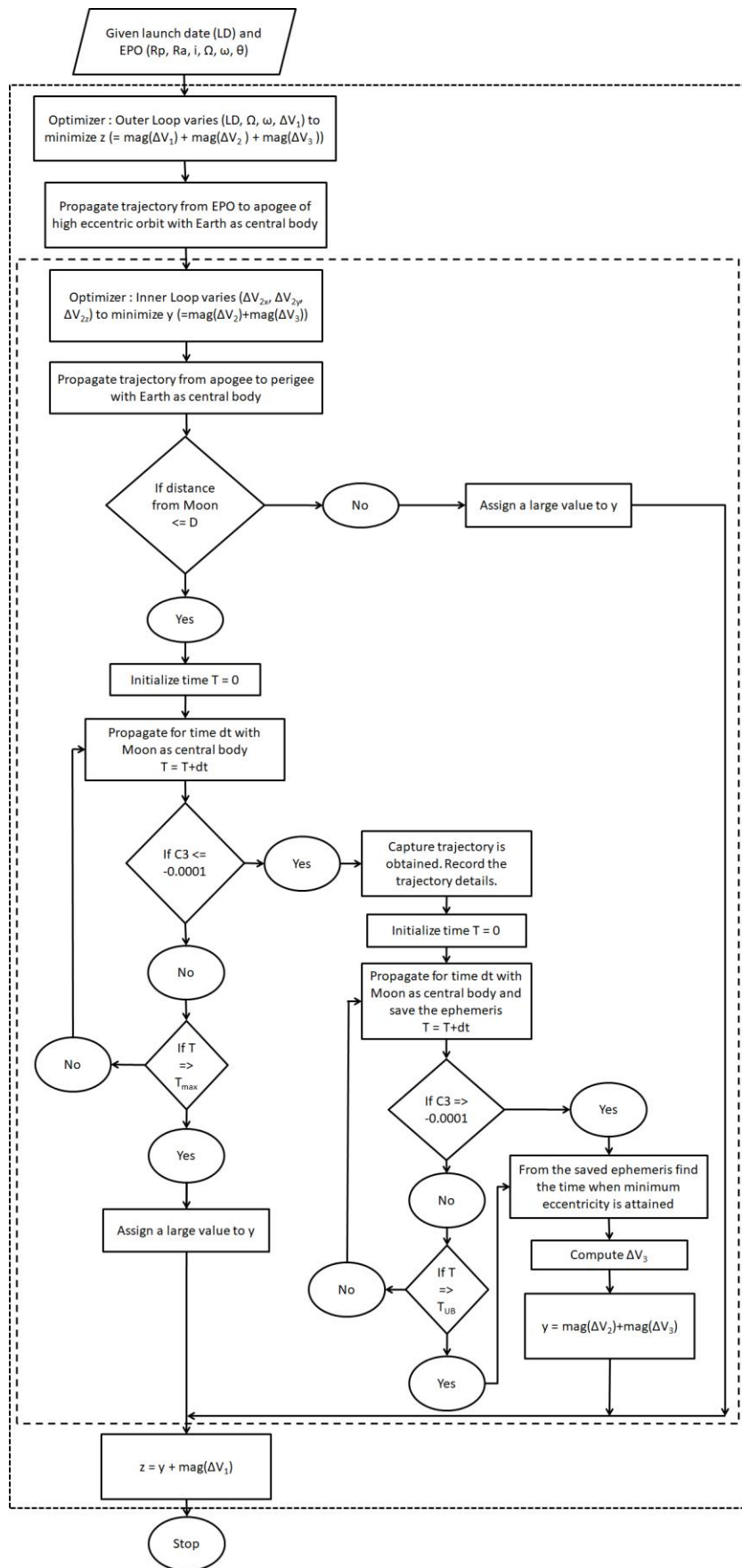


Fig. 5.2: Flowchart of the process for computation of WSB trajectory to Moon

The algorithm consists of following steps:

1. Given the above trajectory, the control variables LD , Ω , ω and ΔV_1 are varied by the outer loop to obtain different arrival conditions at apogee.
2. The inner loop varies ΔV_2 at apogee to obtain the capture orbit within specified time interval (here, 100 days maximum time limit is considered) from arrival at perilune. A capture orbit is identified whenever $C3$ with respect to Moon crosses $-0.0001 \text{ km}^2/\text{s}^2$ or eccentricity crosses 0.999 decreasing.
3. After attaining a capture orbit at Moon, the orbit is further propagated for specified duration (here, 50 days maximum time limit is considered) or till eccentricity crosses 1.0 increasing, whichever ever happens first. This propagation is used to identify the minimum eccentricity attained by the capture orbit. From that minimum eccentricity orbit, another impulse ΔV_3 is given to reduce the capture orbit to desired mapping orbit (here, 100 km circular orbit is considered).
4. The total ΔV ($=\Delta V_1 + \Delta V_2 + \Delta V_3$) is minimized.

Flowchart of the full process is depicted in Fig. 5.2. Any optimization algorithm can be used for inner and outer loops. Based on experience in the study of WSB trajectories, genetic algorithm is used for both inner and outer loops.

5.3. Results

A number of test cases were evaluated using the above algorithm. This algorithm is valid for both circular and elliptical EPO. For the test cases considered here we have used an EPO of 250 km X 23,000 km with 18° inclination, which is same as Chandrayaan-1 Mission. The mapping orbit at Moon is taken to be 100 km circular, which is also same as Chandrayaan-1 Mission.

5.3.1 Analysis of WSB transfers to Moon

A number of test cases are evaluated using the present algorithm. Some launch dates during the year 2017 are considered for these test cases. Some important parameters during the journey from EPO to Moon for direct transfer and WSB transfer are listed in Table 5.1. Ω and ω correspond to right ascension of ascending node and argument of perigee of EPO. For direct transfers to Moon, the launch date is kept same as the examples considered for WSB transfers and flight duration is 5 days. ΔV_{TLI} (trans-lunar insertion) is the impulse given at

perigee of EPO to initiate the journey towards Moon. For direct transfer trajectory initially the spacecraft is captured into a higher orbit with the help of ΔV_{MOI} (Moon orbit insertion) manoeuvre. Later this arrival orbit is reduced to 100 km circular orbit at Moon. For WSB trajectories, time of flight is the number of days starting from launch date till minimum eccentricity orbit is attained at Moon; ΔV_1 corresponds to the impulse required from EPO to a highly elliptical orbit with apogee altitude of the order of 1.5×10^6 km; arrival perilune altitude, arrival velocity magnitude and arrival C3 are respectively, the perilune altitude, velocity magnitude and C3 of the spacecraft with respect to Moon when its C3 with respect to Moon becomes negative; ΔV_2 is the velocity impulse applied at apogee of highly elliptical orbit so that a capture orbit is obtained on its way back to Moon; perilune and apolune altitudes, inclination, velocity, C3 energy with respect to Moon correspond to the minimum eccentricity orbit at Moon; ΔV_3 is the impulse required to come down to 100 km circular orbit from the minimum eccentricity orbit at Moon.

Tables 5.2 and 5.3 give the details of example trajectories obtained from the algorithm. It is observed that about 22% ΔV_{LOI} (Lunar Orbit Insertion manoeuvre to establish 100 km circular orbit at Moon) can be saved using WSB trajectory compared to the conventional 5 days direct transfer trajectory to Moon. An important characteristic of the present algorithm is that it waits for the capture orbit to attain minimum eccentricity, and then reduces the capture orbit to desired mapping orbit. By doing so, one can save about 700 m/s impulse to get 100 km circular orbit at Moon. Figures 5.3-5.12 give the three- and two-dimensional plots of WSB trajectory examples considered here.

5.3.2 Analysis of capture orbits for a particular case

All the capture orbits obtained for 3rd case (listed in Table 5.1) are analysed. The departure date for this case is 10 Dec 2017. For a conventional 5 days trajectory to Moon total ΔV will be 2.167 km/s ($\Delta V_{TLI} = 0.973$ km/s and $\Delta V_{MOI} = 1.194$ km/s) to obtain 100 km circular orbit around Moon. The minimum total ΔV WSB trajectory to Moon obtained by the presented algorithm requires total ΔV of 1.825 km/s and its flight duration is 146 days.

Fig. 5.13 gives the total ΔV histogram for the capture orbits obtained for case 3. It is observed that for maximum cases the total ΔV is between 1.825 to 1.9 km/s. Fig. 5.14 gives the $\Delta V_C (= \Delta V_2 + \Delta V_3)$ for all the capture orbits. It is observed that ΔV_C is distributed between 0.7 to 1.1 km/s. Fig. 5.15 gives the total time of flight (time from departure from EPO to apogee till minimum eccentricity orbit attainment). Figs. 5.16, 5.17 and 5.18, respectively,

give the histogram of minimum eccentricity attained by the capture orbits, perilune altitude at minimum eccentricity and inclination of capture orbit at minimum eccentricity. It is observed that various inclination orbits can be obtained using WSB irrespective of the declination of incoming excess hyperbolic velocity vector.

Fig. 5.19 gives the variation in C3 of the spacecraft with respect to Moon as a function of iteration number for specific outer and inner loops for case 3. These figures show how within a particular outer and inner loop, the C3 of spacecraft was varied by the inner loop to converge to a negative C3 value. Fig. 5.20 gives the variation in objective function value within an outer loop. These figures show how the inner loop varied its parameters (components of ΔV_2) to change the objective function value. Fig. 5.21 shows the mean variation in ΔV_2 for all the outer loops. For a given outer loop, mean of ΔV_2 is taken for all the inner loops. Fig. 5.22(a-c) shows the mean variation in all the three components of ΔV_2 for all the outer loops. Fig. 5.23 shows the minimum value of ΔV_2 among all the inner loops corresponding to an outer loop. Fig. 5.24 shows the variation in minimum value of C3 for all the outer loops. Figs 5.25 and 5.26 show how the outer loop varied AOP and RAAN, respectively, and the corresponding distance of spacecraft from Moon upon arrival at perigee. Figs. 5.27, 5.29 and 5.30, respectively, gives the perilune and apolune, semi-major axis and eccentricity and perilune and ΔV_3 profiles corresponding to the minimum eccentricity orbit. Specific colour and marker denote a particular outer loop. It is seen that in most of the cases the profiles of a particular outer loop are clustered together or their variation follows a particular fashion.

The algorithm was able to find WSB trajectories to Moon for all the cases considered in this study.

5.4. Conclusion

In this chapter, an algorithm is developed to generate ballistic capture trajectories to Moon using exterior WSB transfer. The algorithm is valid for departures from circular and elliptical Earth parking orbits (EPO). It uses forward propagation from the EPO to reach Sun-Earth Lagrange Point L_1 (or L_2) distance where a small manoeuvre is performed so that on its way back the spacecraft is captured by Moon. For a given departure date and EPO conditions, a number of capture orbits at Moon are obtained with marginal difference in impulse requirement. The backward-forward propagation algorithms available in literature face major

problem of launch vehicle's maximum payload constraint satisfaction, which is ruled out in this case. Using this algorithm, a number of test cases have been evaluated and detailed analysis of capture orbits for a particular case is presented. The algorithm was able to find WSB trajectories to Moon for all the cases considered in this study. Another strength of this algorithm is that for all the capture orbits obtained, we wait for minimum eccentricity so that the impulse required to achieve the target orbit at Moon is reduced compared to that required just after capture orbit is attained.

With this chapter we conclude our studies on the development of WSB trajectories to Moon. With this background, we now proceed to study WSB trajectories to Mars, our nearest neighbour.

Table 5.1: Test cases

Example 1:		
Event Name	Direct	WSB
Launch Date (UTC)	20 Nov 2017 01:51:56.627	19 Nov 2017 22:35:49.000
RAAN (deg)	20.055	34.042
AOP (deg)	116.704	194.751
Time of Flight (days)	5	83.671
$\Delta V_{TLI} / \Delta V_1$ (km/s)	0.971	1.033
Arrival periapsis altitude (km)	2373.294	71419.962
Arrival Velocity magnitude (km/s)	1.725	0.234
Arrival C3 (km ² /s ²)	0.589	-0.00001
$\Delta V_{MOI} / \Delta V_2$ (km/s)	0.6	0.000535
Perilune altitude (km)	1897.511	72040.419
Inclination (deg)	6.711	67.709
Velocity (km/s)	1.358	0.137
C3 Energy (km ² /s ²)	-0.770	-0.032
ΔV for 100 km circular orbit / ΔV_3 (km/s)	0.686	0.909
Total ΔV (km/s)	2.257	1.943
Example 2		
Event Name	Direct	WSB
Launch Date (UTC)	2 Dec 2017 10:43:20.000	1 Dec 2017 22:55:43.000
RAAN (deg)	34.004	8.55637
AOP (deg)	275.151	85.9434
Time of Flight (days)	5	125
$\Delta V_{TLI} / \Delta V_1$ (km/s)	0.964	1.0296
Arrival periapsis altitude (km)	1439.868	12980.379
Arrival Velocity magnitude (km/s)	1.961	0.728
Arrival C3 (km ² /s ²)	0.760	-0.079
$\Delta V_{MOI} / \Delta V_2$ (km/s)	0.87	0.017
Perilune altitude (km)	500.86	24849.860
Inclination (deg)	29.386	48.5
Velocity (km/s)	1.718	0.346
C3 Energy (km ² /s ²)	-1.431	-0.00179
ΔV for 100 km circular orbit / ΔV_3 (km/s)	0.391	1.052
Total ΔV (km/s)	2.225	2.099
Example 3		
Event Name	Direct	WSB
Launch Date (UTC)	10 Dec 2017 19:26:40.000	9 Dec 2017 23:04:58.000
RAAN (deg)	358.298	209.425
AOP (deg)	66.731	348.803
Time of Flight (days)	5	145.7
$\Delta V_{TLI} / \Delta V_1$ (km/s)	0.973	1.0528
Arrival periapsis altitude (km)	1584.838	7024.044
Arrival Velocity magnitude (km/s)	1.883	0.1007
Arrival C3 (km ² /s ²)	0.595	-0.000098
$\Delta V_{MOI} / \Delta V_2$ (km/s)	0.7	0.0

Inclination (deg)	8.950	94.959
Velocity (km/s)	1.421	0.1007
C3 Energy (km ² /s ²)	-1.218	-0.00103
ΔV for 100 km circular orbit / ΔV_3 (km/s)	0.494	0.772
Total ΔV (km/s)	2.167	1.825
Example 4		
Event Name	Direct	WSB
Launch Date (UTC)	19 Dec 2017 23:14:12.626	19 Dec 2017 23:04:58.000
RAAN (deg)	120.181	353.693
AOP (deg)	42.170	51.953
Time of Flight (days)	5	119.5
$\Delta V_{TLI} / \Delta V_1$ (km/s)	0.975	1.043
Arrival periapsis altitude (km)	500	9706.958
Arrival Velocity magnitude (km/s)	2.2648	0.270
Arrival C3 (km ² /s ²)	0.747	-0.0001
$\Delta V_{MOI} / \Delta V_2$ (km/s)	0.8	0.000278
Inclination (deg)	19.788	101.414
Velocity (km/s)	1.778	0.165
C3 Energy (km ² /s ²)	-1.876	-0.032772
ΔV for 100 km circular orbit / ΔV_3 (km/s)	0.237	0.835
Total ΔV (km/s)	2.012	1.878
Example 5		
Event Name	Direct	WSB
Launch Date (UTC)	30 Dec 2017 01:23:20.000	30 Dec 2017 00:16:14.000
RAAN (deg)	58.972	16.023
AOP (deg)	255.634	81.919
Time of Flight (days)	5	181
$\Delta V_{TLI} / \Delta V_1$ (km/s)	0.965	1.029
Arrival periapsis altitude (km)	500.055	5604.392
Arrival Velocity magnitude (km/s)	2.277	0.965
Arrival C3 (km ² /s ²)	0.803	-0.00664
$\Delta V_{MOI} / \Delta V_2$ (km/s)	0.870	0.003194
Perilune altitude (km)	80.406	26737.915
Apolune altitude (km)	1422.217	76813.600
Inclination (deg)	93.197	170.217
Velocity (km/s)	1.175	0.232
C3 Energy (km ² /s ²)	-1.970	-0.091619
ΔV for 100 km circular orbit / ΔV_3 (km/s)	0.208	0.964
Total ΔV (km/s)	2.043	1.996

Table 5.2: Details of Trajectory for the test cases – Part I

S.No.	Departure Date	Apogee altitude (km)	TOF to Apogee (days)	Time from Apogee to Perilune (days)	Perilune altitude at arrival (km)	Time duration from periapsis arrival to capture orbit (days)	Capture altitude (km)	Time span for captured orbit (days)
1	20 Nov 2017	1.32e6	35.8	42	37509.098	4.27	71419.96	4.8
2	02-Dec-2017	1.48e6	49.3	66	12980.379	0	12980.38	9.6
3	10-Dec-2017	2.09e6	48.6	88.7	7024.044	8.4	733880.65	0.26
4	19-Dec-2017	1.70e6	43.2	45	6582.782	28.3	9706.96	3.78
5	30-Dec-2017	1.34e6	39.0	44.3	5604.392	0	5604.392	102.5

Table 5.3: Details of Trajectory for the test cases – Part II

S.No.	Departure Date	ΔV_1 (km/s)	ΔV_2 (km/s)	Capture orbit characteristics at minimum eccentricity				ΔV_{total}
				Semi-major axis (km)	Ecc.	Inclination (deg)	ΔV_3 (km/s)	
1	20 Nov 2017	1.0327	0.000534	152050.272	0.514780	67.709	0.909	1.943
2	02-Dec-2017	1.0296	0.017012	2.73e6	0.990274	48.5	1.052	2.099
3	10-Dec-2017	1.0528	0.0	4.76e5	0.823161	95	0.772	1.825
4	19-Dec-2017	1.0429	0.000287	149602.5	0.135789	101.4	0.835	1.878
5	30-Dec-2017	1.0290	0.003194	53513.2	0.467882	170.2	0.964	1.996

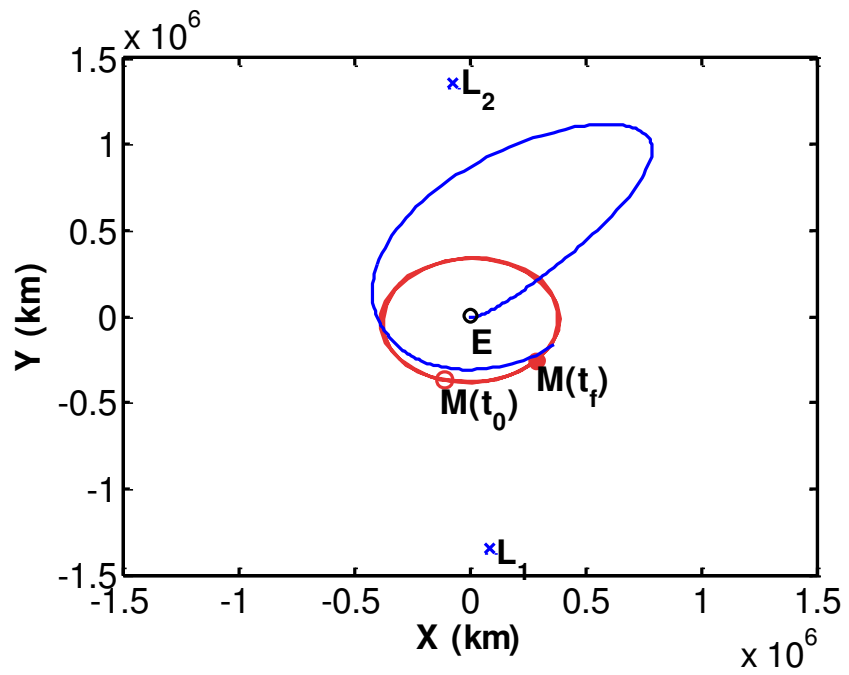


Figure 5.3: WSB trajectory to Moon for example 1 (launch date 20 Nov 2017) in 2D space.

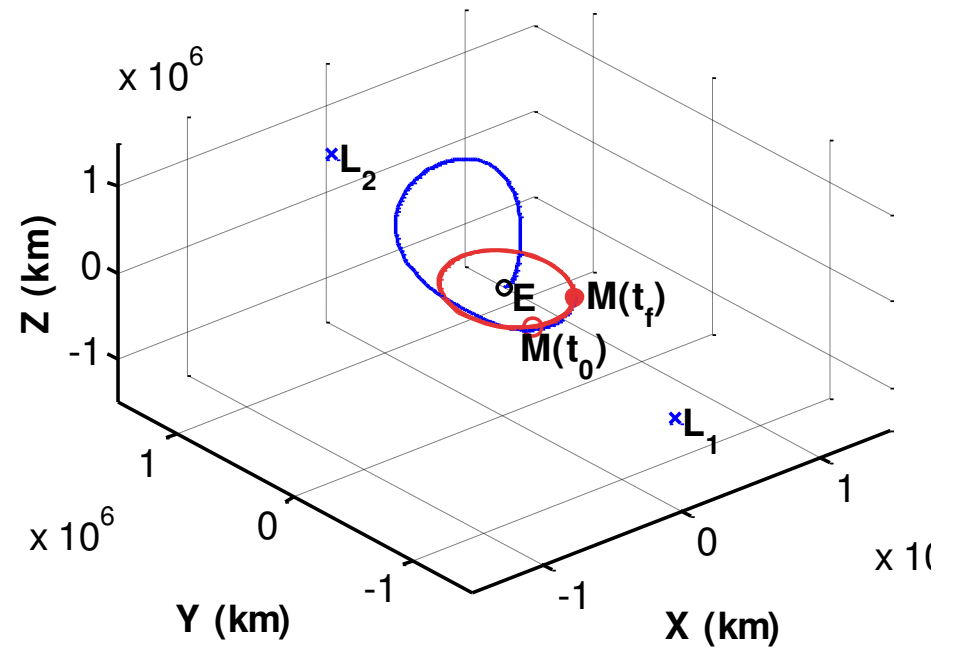


Figure 5.4: WSB trajectory to Moon for example 1 (launch date 20 Nov 2017) in 3D space.

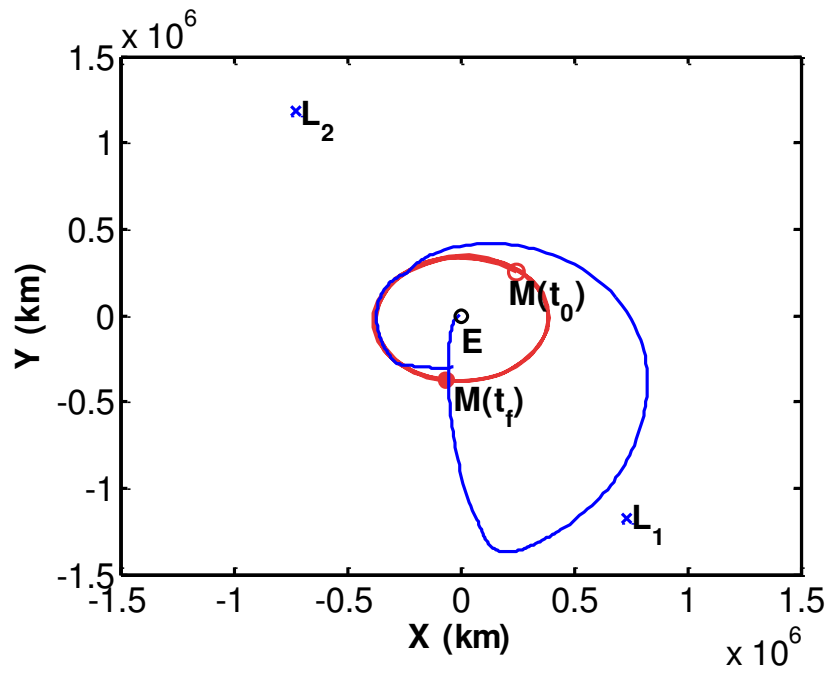


Figure 5.5: WSB trajectory to Moon for example 2 (launch date 2 Dec 2017) in 2D space.

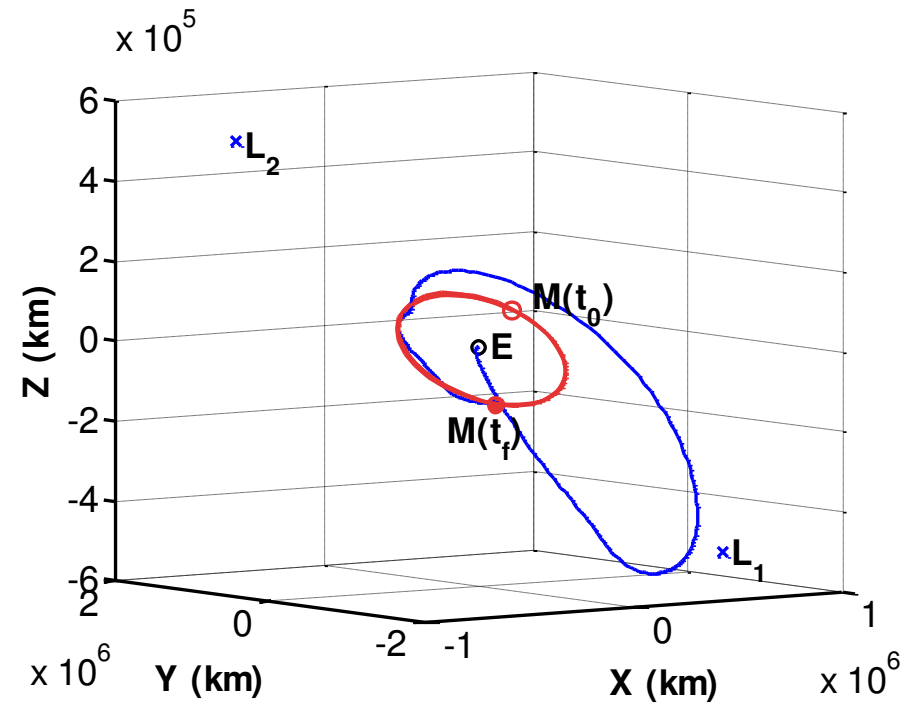


Figure 5.6: WSB trajectory to Moon for example 2 (launch date 2 Dec 2017) in 3D space.

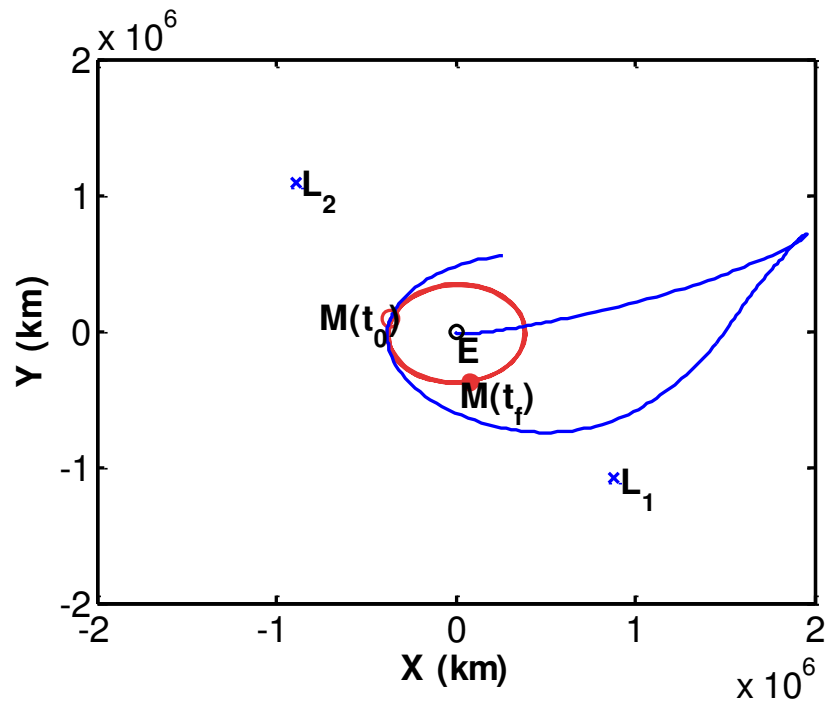


Figure 5.7: WSB trajectory to Moon for example 3 (launch date 10 Dec 2017) in 2D space.

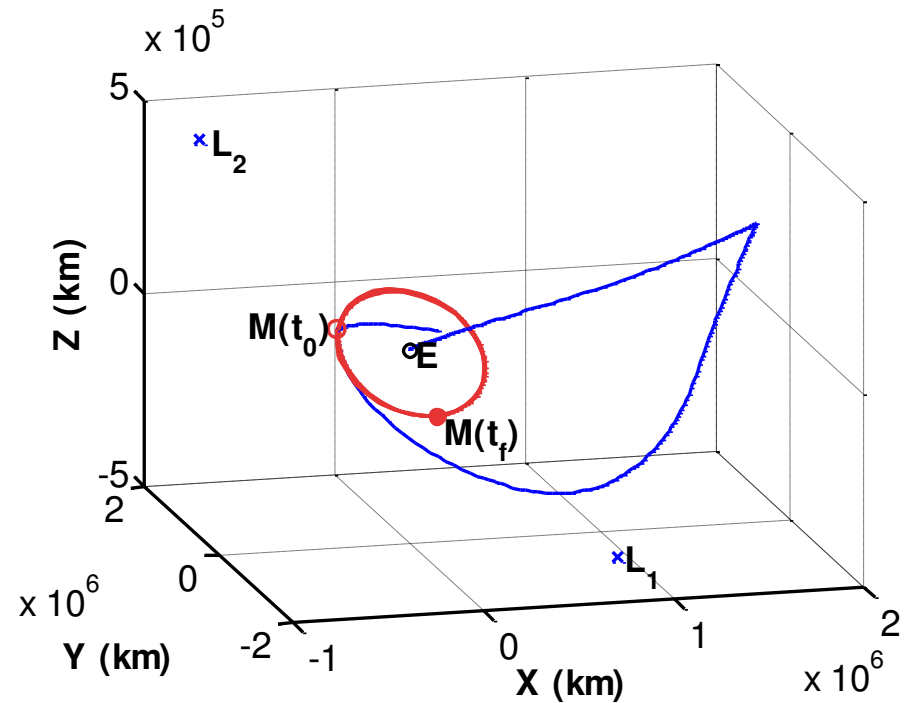


Figure 5.8: WSB trajectory to Moon for example 3 (launch date 10 Dec 2017) in 3D space.

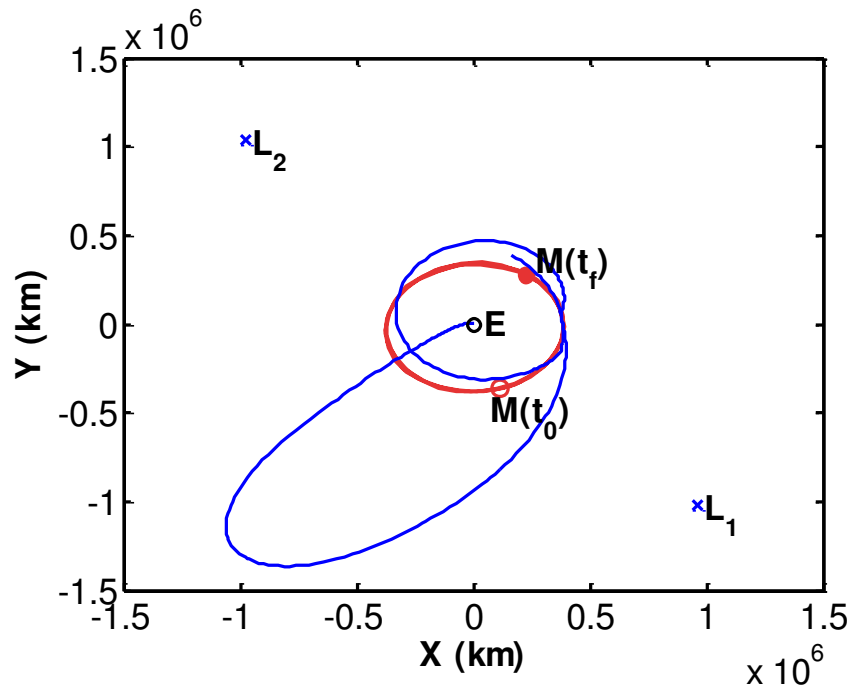


Figure 5.9: WSB trajectory to Moon for example 4 (launch date 19 Dec 2017) in 2D space.

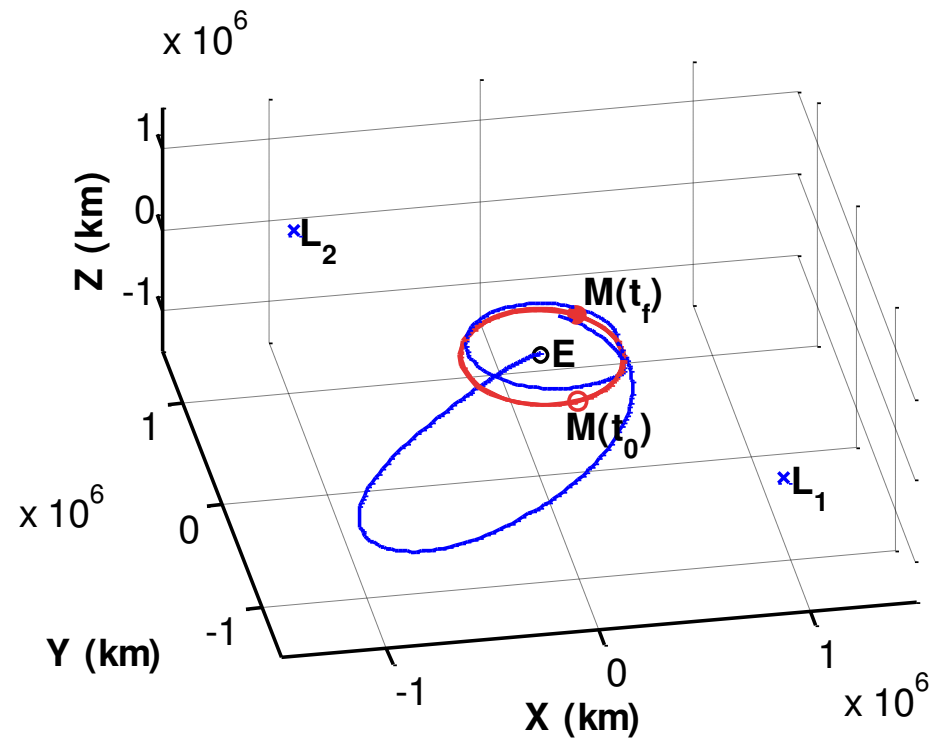


Figure 5.10: WSB trajectory to Moon for example 4 (launch date 19 Dec 2017) in 3D space.

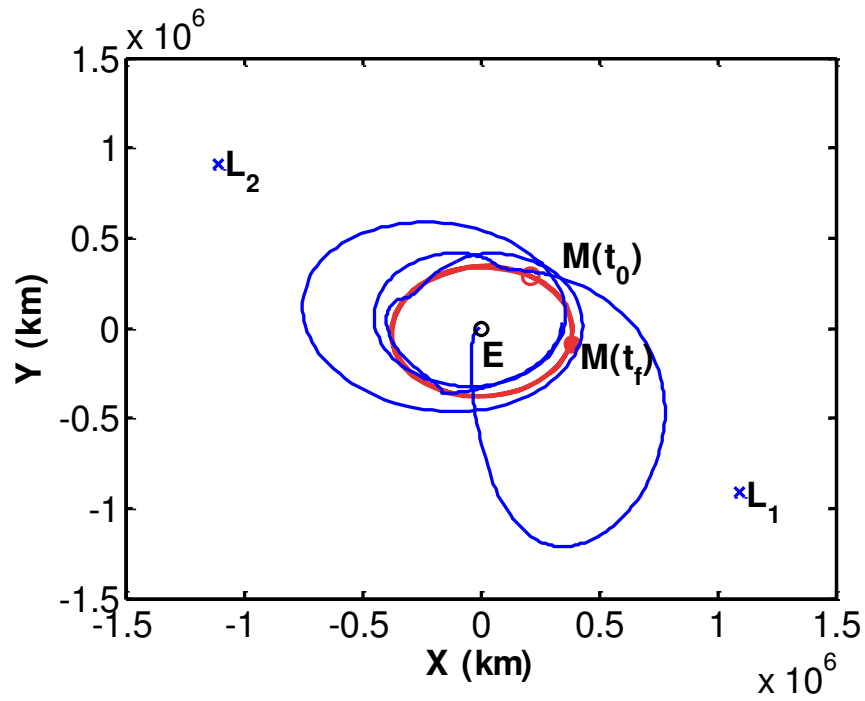


Figure 5.11: WSB trajectory to Moon for example 5 (launch date 30 Dec 2017) in 2D space.

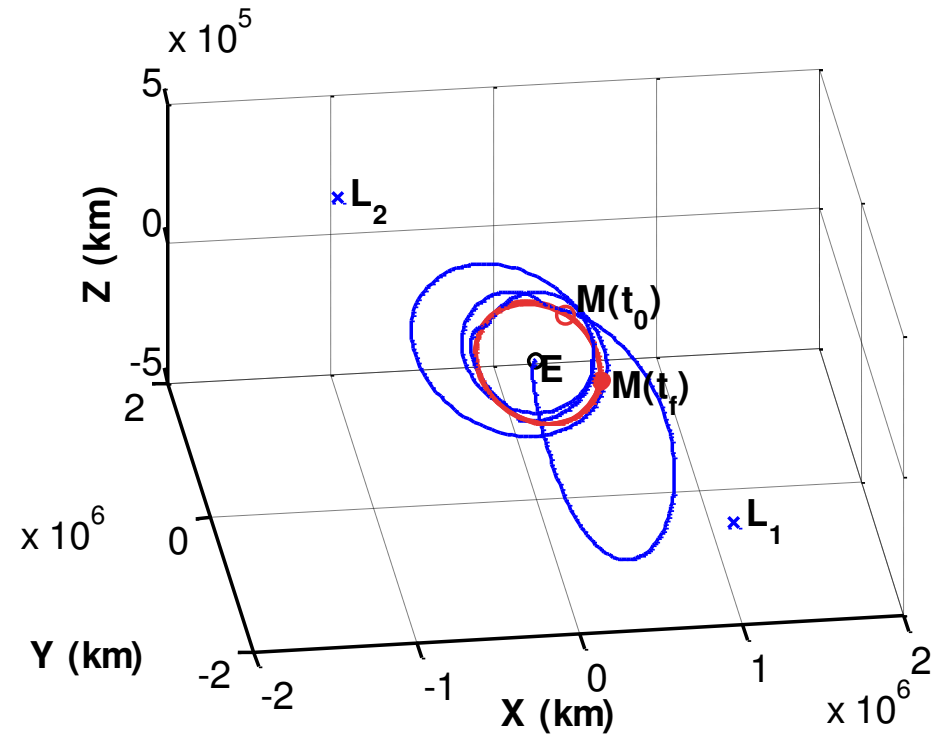


Figure 5.12: WSB trajectory to Moon for example 5 (launch date 30 Dec 2017) in 3D space.

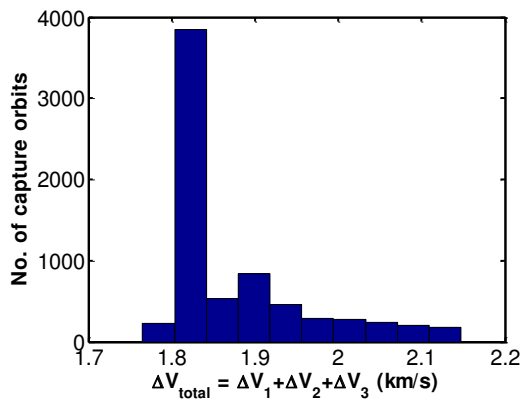


Fig. 5.13: Total ΔV histogram for capture orbits in case 3

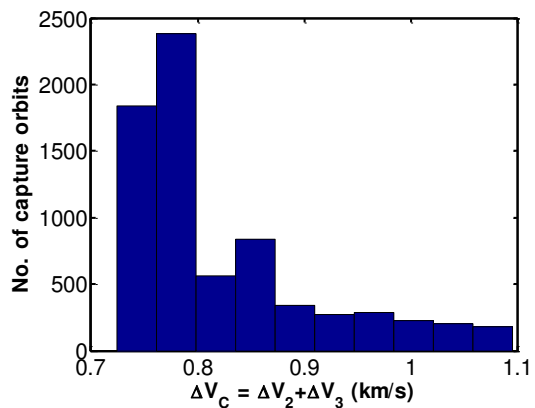


Fig. 5.14: ΔV_C histogram for capture orbits in case 3

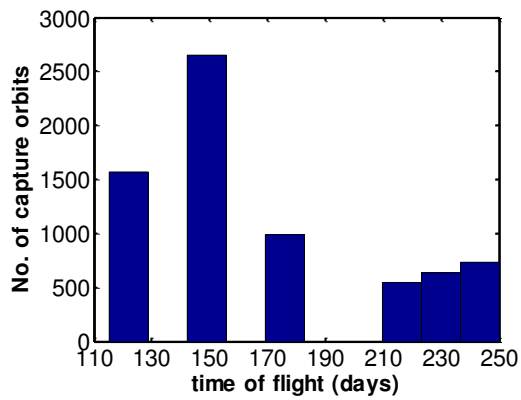


Fig. 5.15: Total time of flight histogram for capture orbits for case 3

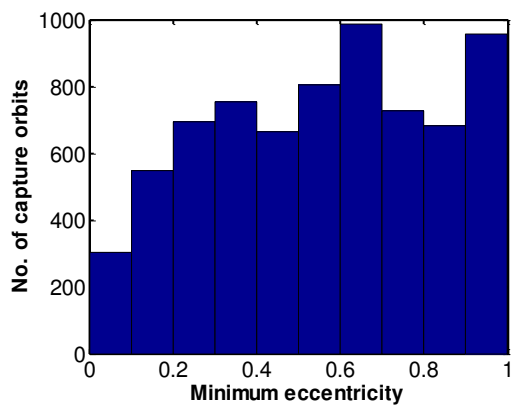


Fig. 5.16: Histogram of Min. eccentricity attained by the capture orbits for case 3

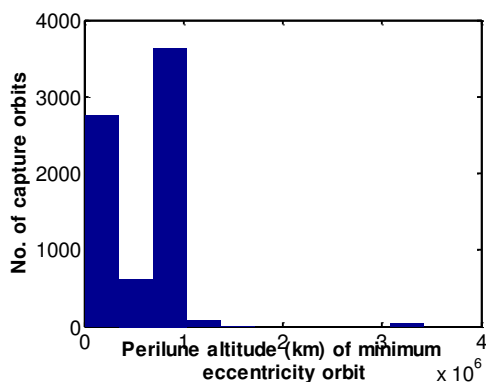


Fig. 5.17: Histogram of Perilune altitude of capture orbit at minimum eccentricity for case 3

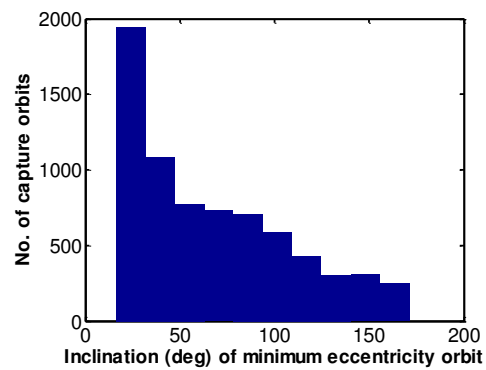


Fig. 5.18: Histogram of inclination of capture orbits at minimum eccentricity for case 3

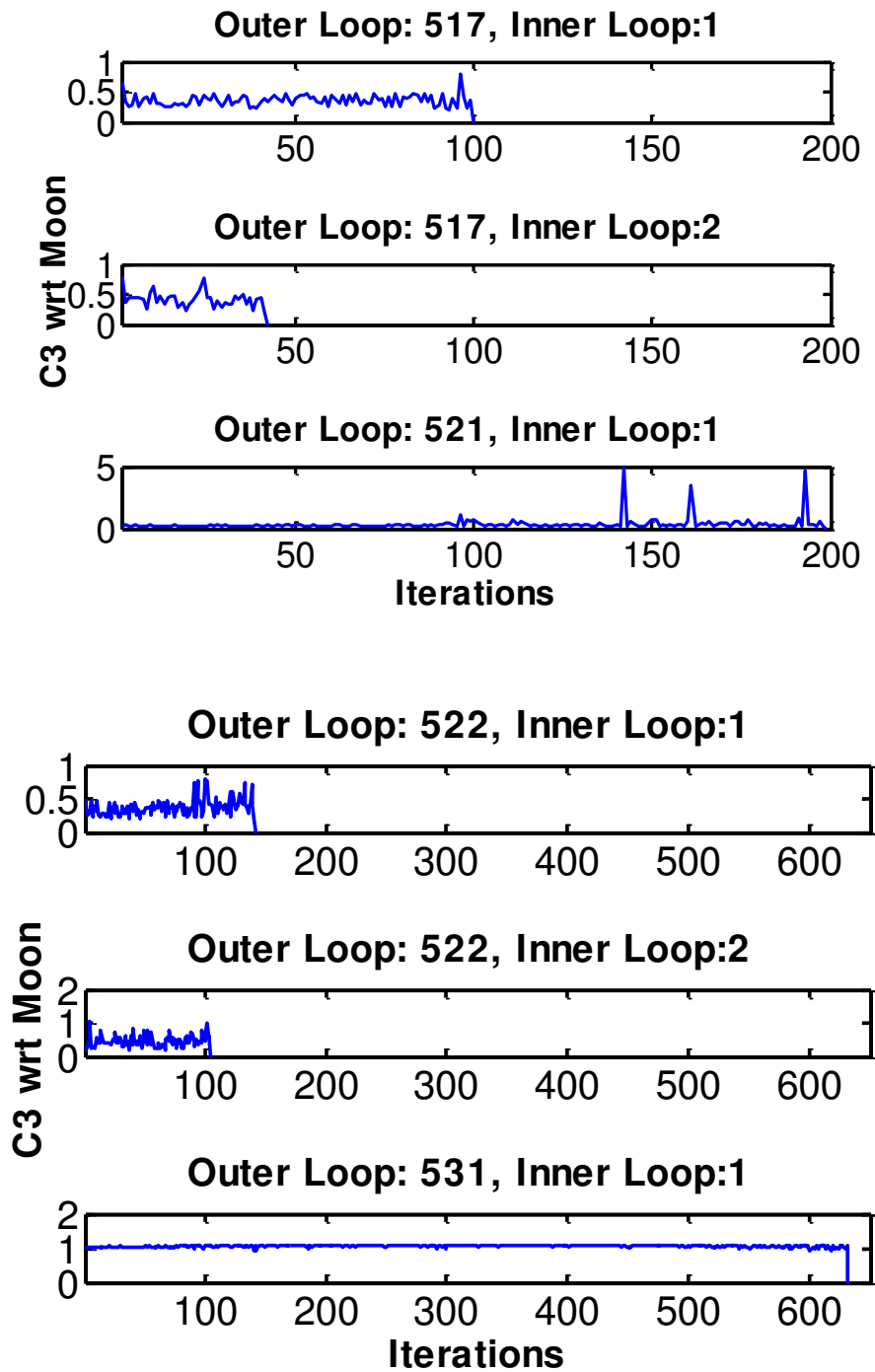
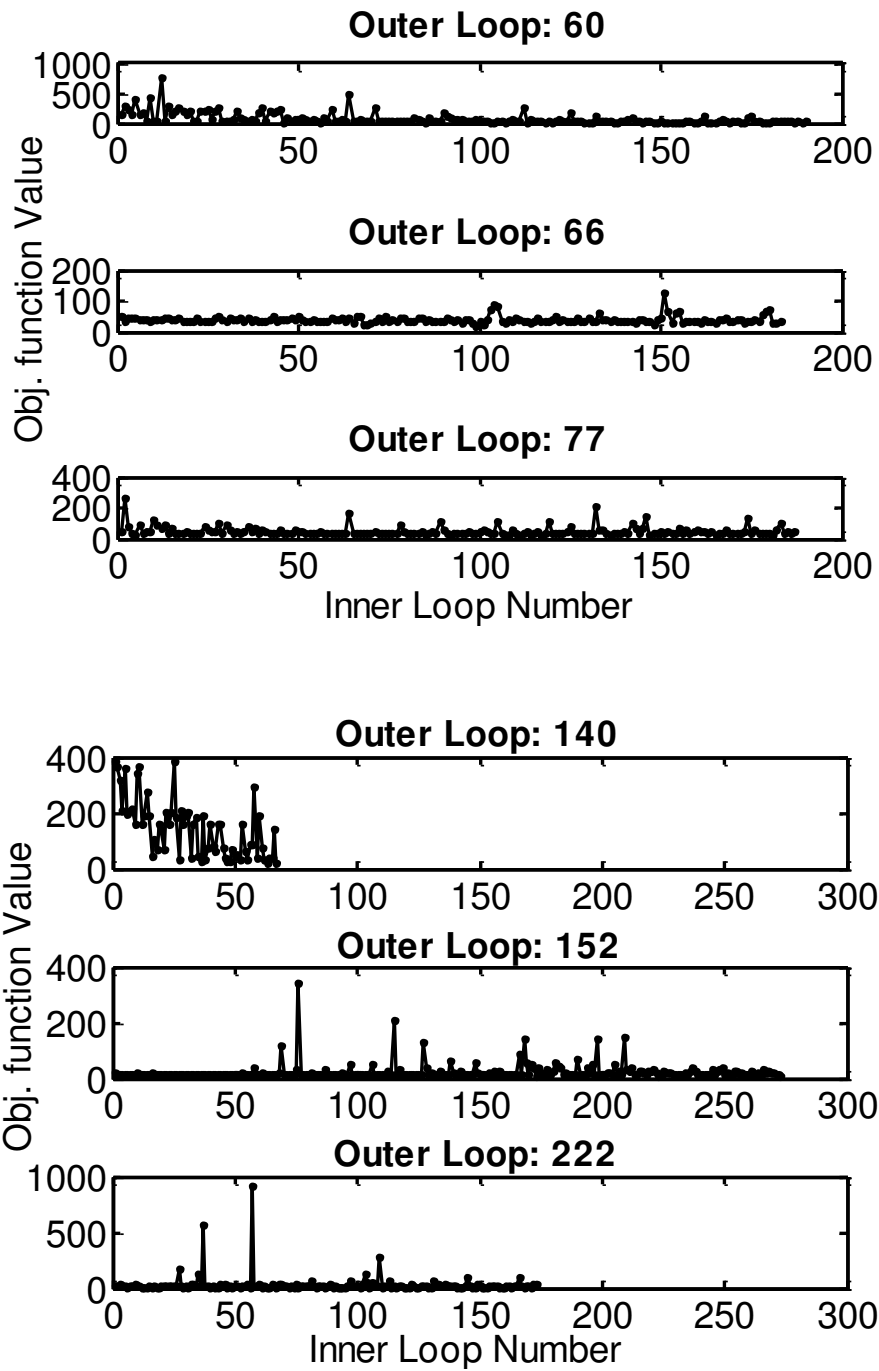


Fig. 5.19: Variation in C3 of the spacecraft with respect to Moon as a function of iteration number for some of the outer and inner loops in case 3.



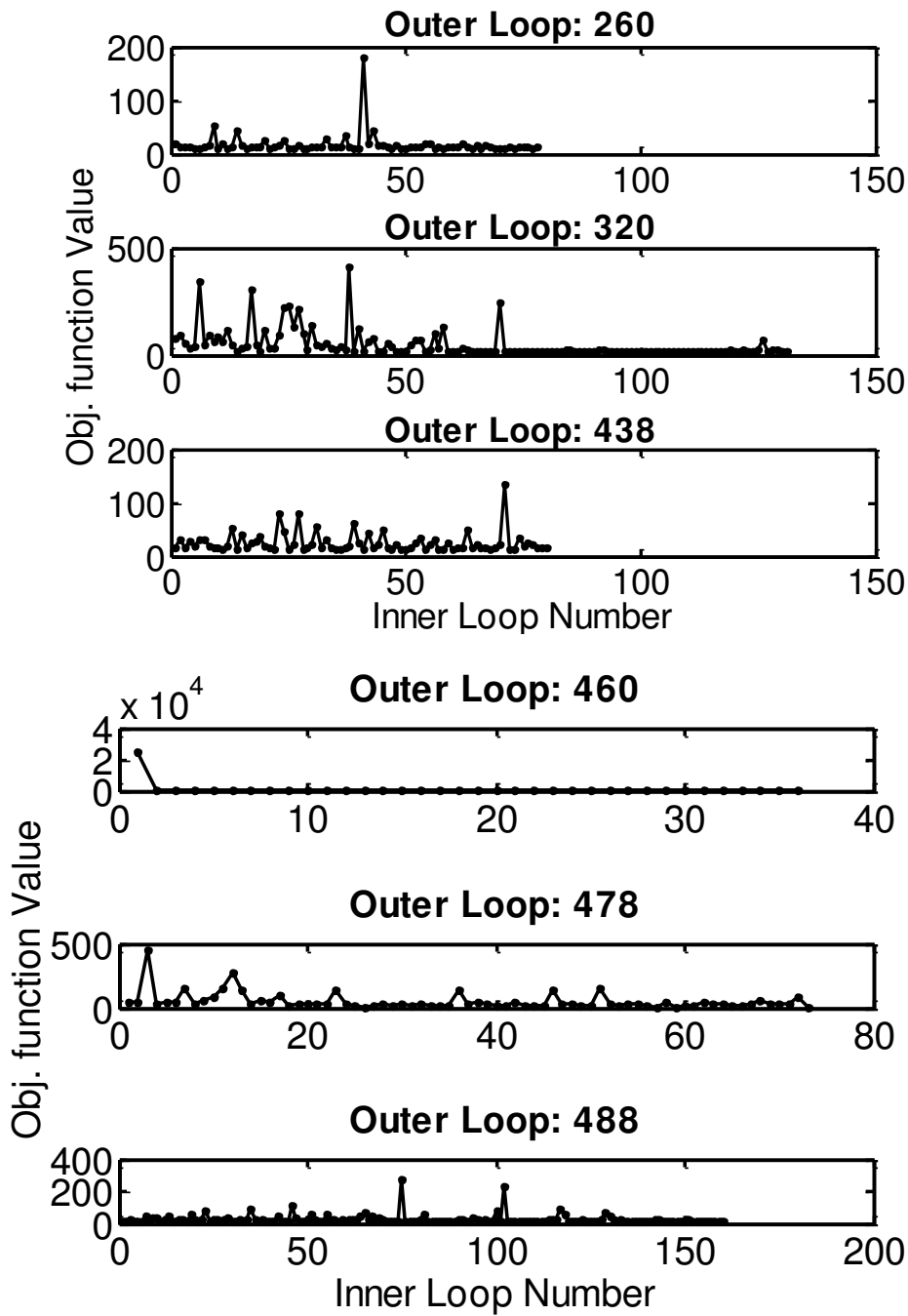


Fig. 5.20: Variation in objective function value as a function of inner loop number for some outer loops for case 3.

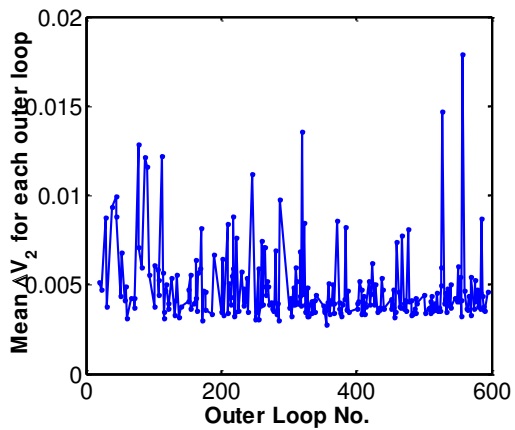


Fig. 5.21: Mean variation in ΔV_2 for all the outer loops in case 3

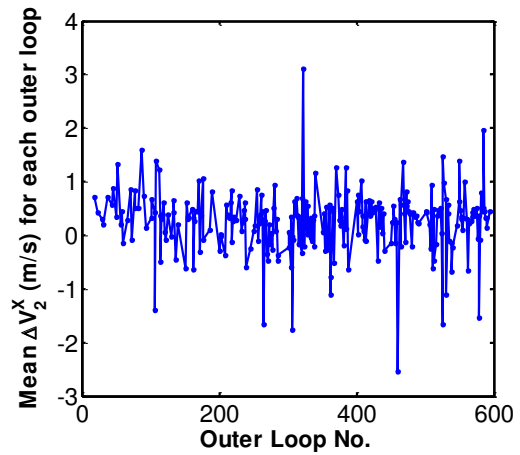


Fig. 5.22(a): Mean variation in ΔV_{2x} for all the outer loops in case 3

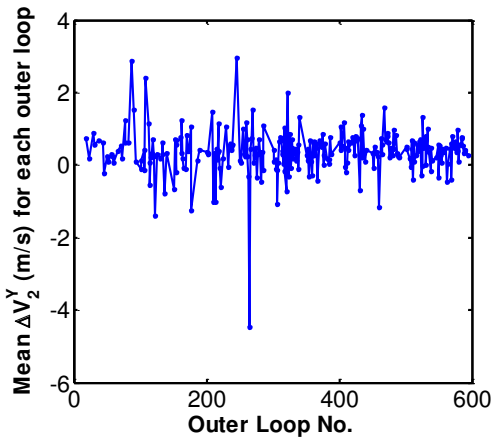


Fig. 5.22(b): Mean variation in ΔV_{2y} for all the outer loops in case 3

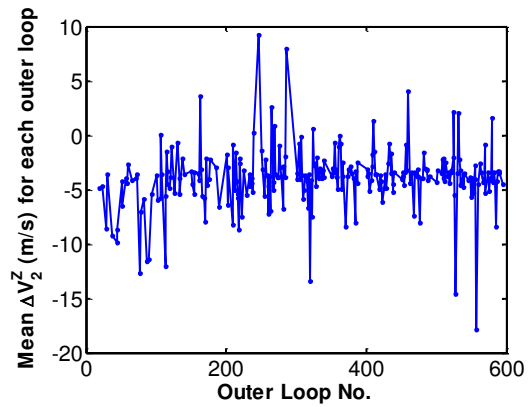


Fig. 5.22(c): Mean variation in ΔV_{2z} for all the outer loops in case 3

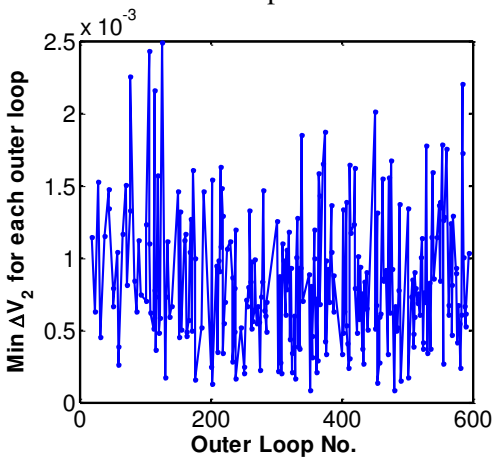


Fig. 5.23: Variation in min. ΔV_2 for all the outer loops in case 3

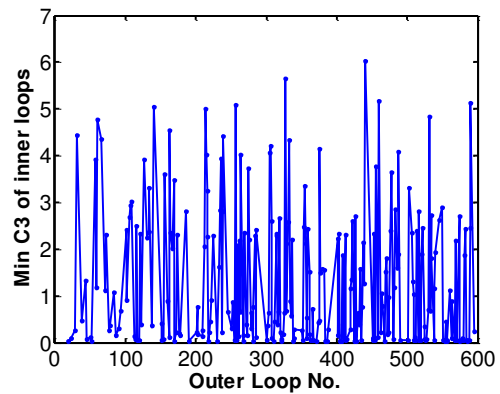


Fig. 5.24: Variation in min. C3 of spacecraft wrt Moon for all the outer loops in case 3

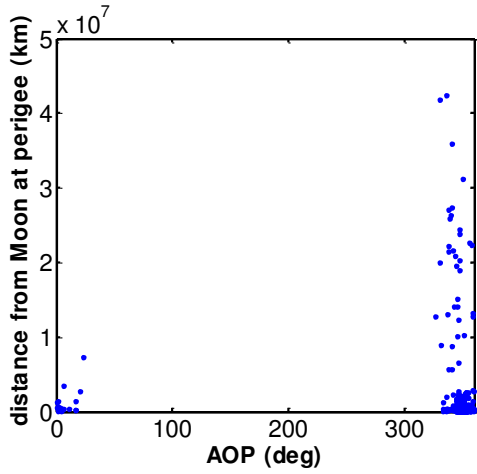


Fig. 5.25: AOP varied by the outer loops and corresponding distance from Moon

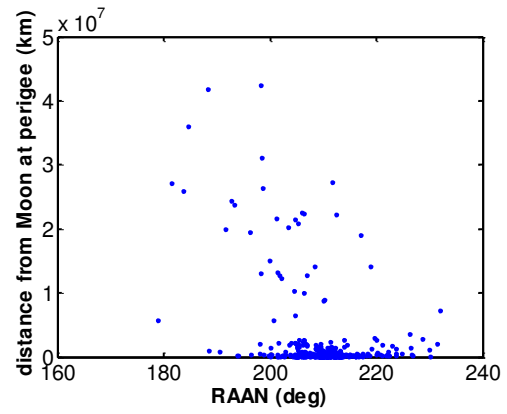


Fig. 5.26: RAAN varied by the outer loops and corresponding distance from Moon

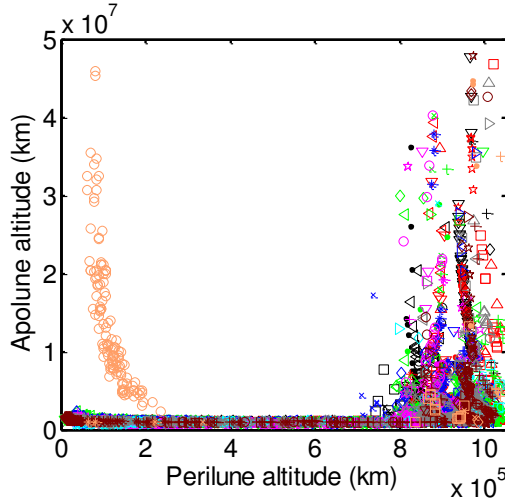


Fig. 5.27: Perilune and apolune profiles for minimum eccentricity orbit attained by various outer loops (same color and marker denotes same outer loop)

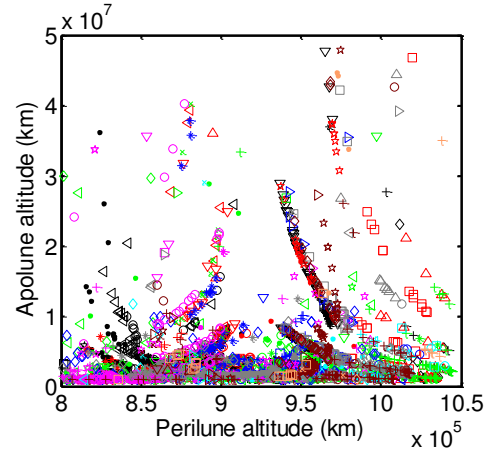


Fig. 5.28: zoomed version of Fig. 5.27

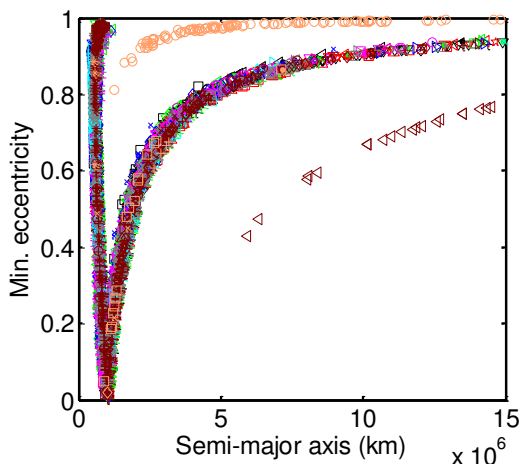


Fig. 5.29: semi-major axis and eccentricity profiles for minimum eccentricity orbit attained by various outer loops

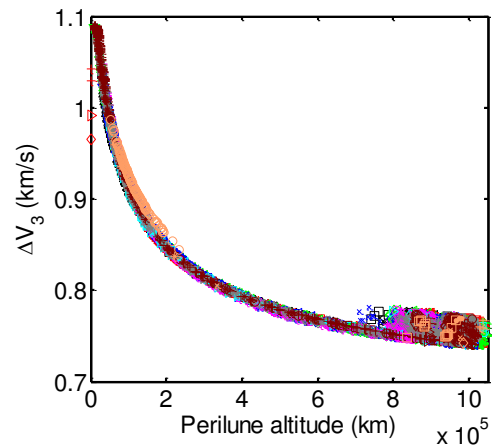


Fig. 5.30: Perilune and ΔV_3 profiles for minimum eccentricity orbit attained by various outer loops

CHAPTER 6

WEAK STABILITY BOUNDARY TRANSFERS TO MARS

6.1. Introduction

Since the successful demonstration of low energy transfers to Moon and Lunar Lagrange points by Hiten in 1991 (Belbruno and Miller, 1993; Uesugi, 1996), SMART-1 in 2003 (Foing and Racca, 1999; Schoenmaekers, 2001), ARTEMIS 2009 (Broschart et al., 2009; Folta et al, 2011) and GRAIL in 2011 (Roncoli and Fujii, 2010; Chung et al, 2010; Hatch et al. 2010), many researchers are working on feasibility of low energy transfers to distant planets for example Mendell (2001); Strizzi et al (2001); Castillo et al (2003); Kulkarni and Mortari (2005); Nakamiya et al. (2008); Topputo and Belbruno (2009; 2015) and so on. In case of Hohmann transfer to Moon, spacecraft's v_∞ is close to the Moon's orbital velocity. But in case of Hohmann transfer from Earth to Mars, the orbital velocity of Mars is much higher than the approach v_∞ of the spacecraft. Hence it took a long time and efforts, since the discovery of WSB transfers to Moon, for researchers to find WSB transfers to Mars.

Topputo and Belbruno (2015) give a new concept for the design of WSB trajectory to Mars by targeting a distant point x_c (few million km from Mars) where a manoeuvre ΔV_C is performed, which finally leads to a capture orbit at Mars (Fig. 6.1). The WSB trajectories are simulated in the framework of planar elliptic restricted three-body problem. They claim 25% saving in ΔV_{MOI} with flight duration exceeding by 1.5 to 2 years when compared with conventional Hohmann transfer. The major advantages of this method reported are lower capture manoeuvres at higher altitudes and flexibility of launch window. Working on the same concept, an algorithm for numerical computation of trajectories to Mars with ballistic capture is developed in this chapter.

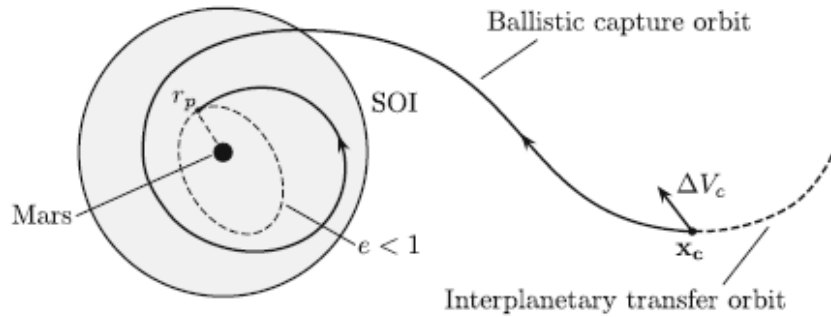


Fig. 6.1: Structure of the ballistic capture transfers to Mars (from Topputto and Belbruno, 2015)

Here, we study the dynamics of capture orbits at Mars and present details of the forward propagation algorithm to find WSB trajectories to Mars in high fidelity force model (including gravitational effects from the central body and third body). Results are obtained for the launch opportunity in 2018. Forward-backward propagation algorithms to find WSB trajectories face major problem of launch vehicle constraint satisfaction especially when the Earth Parking Orbit (EPO) is elliptical. Forward-backward propagated trajectories may lead to a patching point, too expensive for a launch vehicle to satisfy its maximum payload constraints (mainly AOP and inclination). This drawback is eliminated in this case, as the algorithm starts from the required EPO (circular or elliptical). The planet-equatorial declination of incoming asymptote provides the measure of minimum possible inclination of arrival trajectory. For given a departure date and EPO conditions, a number of WSB arrival orbits can be found (irrespective of the declination of incoming asymptote) using the given algorithm with marginal difference in impulse requirements. The one suiting our requirement which is also optimal from energy point of view can be selected. The capture orbits obtained by WSB trajectory are high altitude orbits, mostly unsuitable for interplanetary mission objectives. The discussed algorithm does not stop at the high altitude capture orbit; it waits for the osculating eccentricity to minimize, where another impulse is given to obtain desired mapping orbit. This chapter also details phase space portraits for capture orbits obtained at different periapsis altitudes. These portraits are obtained in restricted three-body problem, and help to understand the

relation between positional phase angle of periapsis of the incoming trajectory and time required for its ballistic capture.

6.2. Dynamics of WSB capture orbits at Mars

Capture orbits at Mars are first studied in the framework of Restricted Three-Body Problem (R3BP) – Sun-Mars-spacecraft system described in Appendix A. The position and velocity of a particle in orbit around smaller primary m_2 (Mars in this case) is given by García and Gómez, (2007) are detailed in Chapter 2, equations (2.4)-(2.6). These are used to find initial conditions with positive and negative velocity (osculating retrograde and direct motions about m_2). The initial conditions obtained from these equations are back propagated for 2000 days using equations of motion in Appendix A, A.17-A.18. Periapsis is fixed at 1000 km (Fig. 6.2), 5000 km (Fig. 6.3), 10,000 km (Fig. 6.4), 25,000 km (Fig. 6.5), 1,00,000 km (Fig. 6.6) and 5,00,000 km (Fig. 6.7). Figs. 6.2-6.7 are obtained in the following manner. The periapsis altitude is kept fixed and the apoapsis altitude is obtained by varying eccentricity from 0 to 0.99. The positional phase angle of periapsis (θ) is varied from 0° to 360° . Starting from an initial condition defined by periapsis altitude, apoapsis altitude and θ , the orbit is back propagated in time for 2000 days. Time of capture, refers to the time when $C3$ wrt Mars becomes positive, is recorded in each case. Each point in the figures (6.2-6.7) represent an orbit around Mars which can be targeted by an incoming trajectory to Mars and will result in a capture orbit. Figs. 6.1-6.6 show the phase space representation of Mars capture trajectories with colour code on time of capture (TOC). Colour code for these figures are - Red: $TOC \leq 60$ days, green: $60 \text{ days} < TOC \leq 120$ days, light blue (cyan): $120 \text{ days} < TOC \leq 180$ days, dark blue: $180 \text{ days} < TOC < 365$ days, black: $365 \text{ days} < TOC \leq 2000$ days. For instance, the regions represented on the phase space by red color will result in capture orbit within 60 days while those in cyan will take 120 to 180 days. It is clearly seen that for lower periapsis altitudes (≤ 1000 km), the capture orbits are clustered in the regions for $-55^\circ \leq \theta \leq 55^\circ$ and $125^\circ \leq \theta \leq 305^\circ$. For intermediate periapsis altitudes ($\leq 10,000$ km), the

capture orbits with less TOC are clustered in the above region. While for high periapsis altitudes (above 10,000 km) all the values of θ yield capture orbits within stipulated time duration.

It is clearly seen that Proposition 2 (Appendix B) is valid from small periapsis altitudes (<5000 km) due to Taylor's series approximation. For higher periapsis altitudes ($\geq 10,000$ km), almost all ranges of θ give capture trajectories.

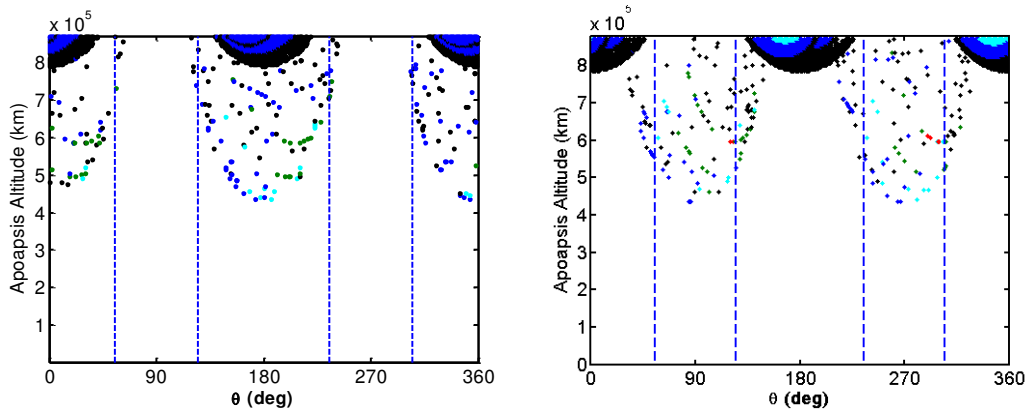


Fig. 6.2: Time of capture (TOC in days) as a function of Apoapsis Altitude and positional phase angle of periapsis (θ) for periapsis altitude 1000 km (a) direct motion about m_2 (b) retrograde motion about m_2 .

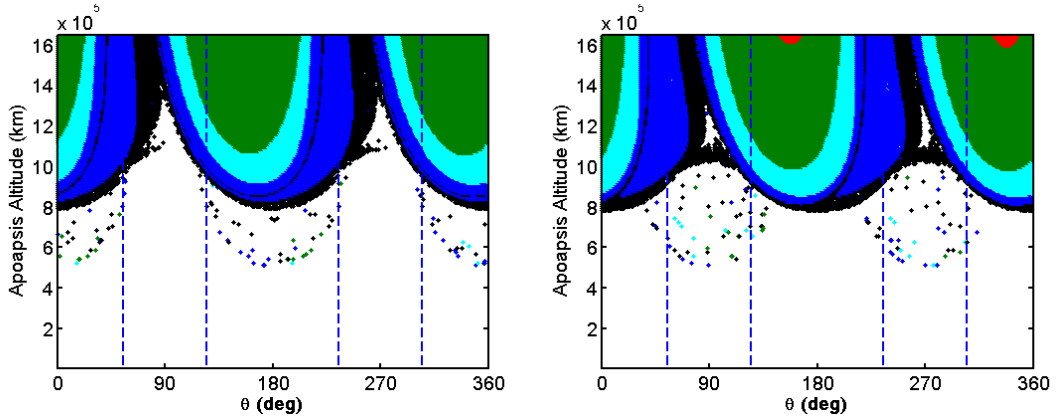


Fig. 6.3: Time of capture (TOC in days) as a function of Apoapsis Altitude and θ for periapsis altitude 5000 km (a) direct motion about m_2 (b) retrograde motion about m_2 .

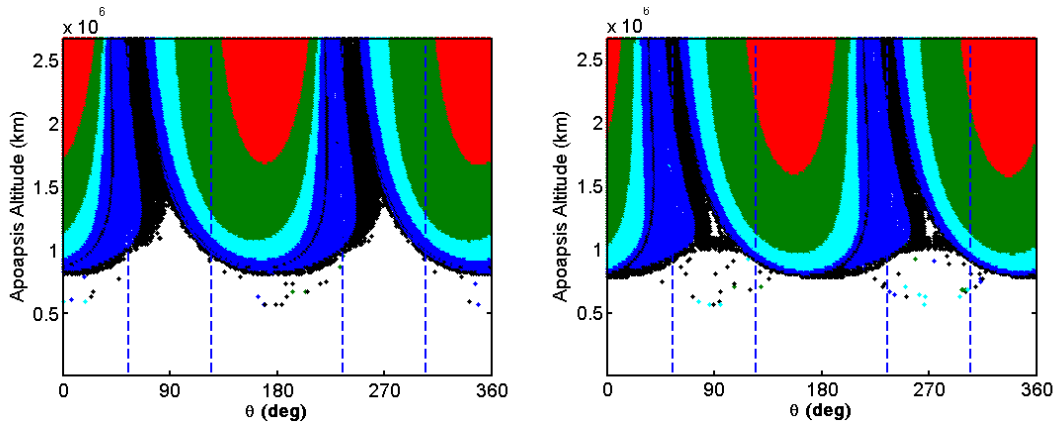


Fig. 6.4: Time of capture (TOC in days) as a function of Apoapsis Altitude and θ for periapsis altitude 10,000 km (a) direct motion about m_2 (b) retrograde motion about m_2 .

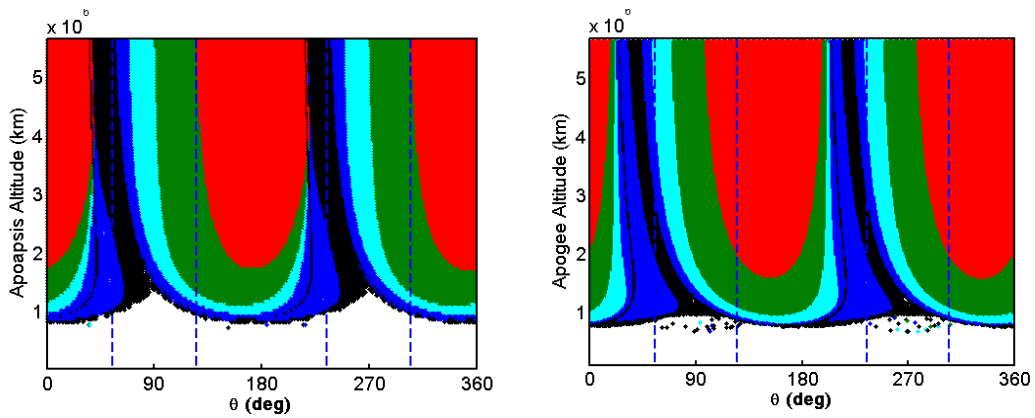


Fig. 6.5: Time of capture (TOC in days) as a function of Apoapsis Altitude and θ for periapsis altitude 25,000 km (a) direct motion about m_2 (b) retrograde motion about m_2 .

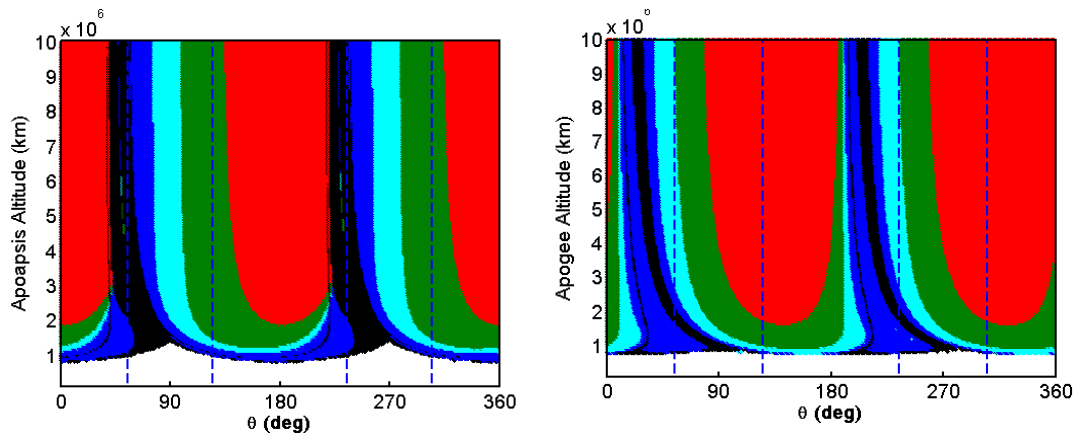


Fig. 6.6: Time of capture (TOC in days) as a function of Apoapsis Altitude and θ for periapsis altitude 1,00,000 km (a) direct motion about m_2 (b) retrograde motion about m_2 .

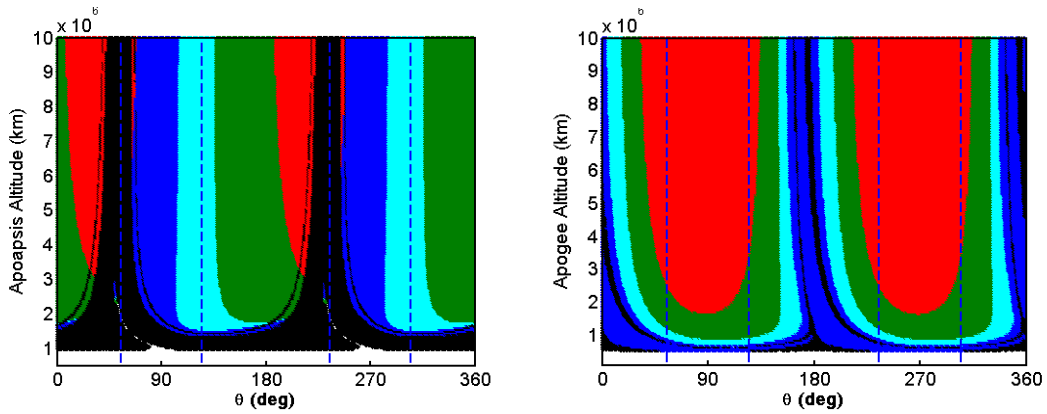


Fig. 6.7: Time of capture (TOC in days) as a function of Apoapsis Altitude and θ for periapsis altitude 5,00,000 km (a) direct motion about m_2 (b) retrograde motion about m_2 .

6.3. Algorithm for Numerical Computation of WSB Trajectories

A new algorithm for numerical computation of WSB trajectories has been developed and used for design of WSB trajectories to Mars. It is inspired by works of Topputo and Belbruno (2015).

First trajectory to Mars is designed using Lambert Conic algorithm and refined using numerical method (Bate, 1971; Battin, 1999; Curtis, 2005; Venkattaramanan, 2006; Conway, 2010). The trajectory starts from an Earth Parking Orbit (EPO) and reaches near Mars to a distance which can vary from few lakh kilometers to several million kilometers from Mars (Figure 6.8). Within WSB of Mars, a manoeuvre ΔV_c (of magnitude about 2-4 km/s) is carried out in such a way that after several months the spacecraft is automatically captured by Mars. In this study the maximum time of propagation after the manoeuvre ΔV_c is fixed to 500 days (assumed to be an upper bound from spacecraft battery and engine point of view). The algorithm consists of two loops with an optimizer (Figure 6.9). The outer loop control variables are namely, LD, the departure epoch from EPO; Ω and ω are Right Ascension of Ascending Node and Argument of Perigee of the EPO; ΔV_{TPI} is the Trans-planetary injection, ie, the impulse in velocity direction given at perigee of

the EPO so that the spacecraft escapes Earth's gravity and starts moving towards Mars in a heliocentric orbit; ΔT is time in days from LD to reach the ΔV_c manoeuvre point. Moreover, all three components of ΔV_{TCM} applied on the way to Mars and time of ΔV_{TCM} application are optional parameters which can be included as control variables (to add more flexibility).

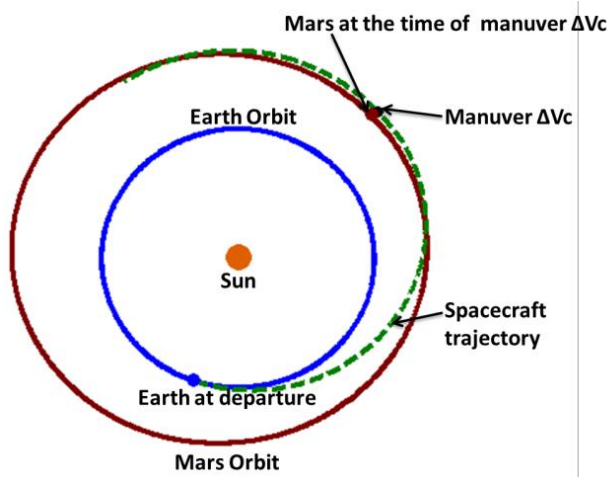


Fig. 6.8 Sample trajectory from Earth to Mars with ΔV_c leading to capture

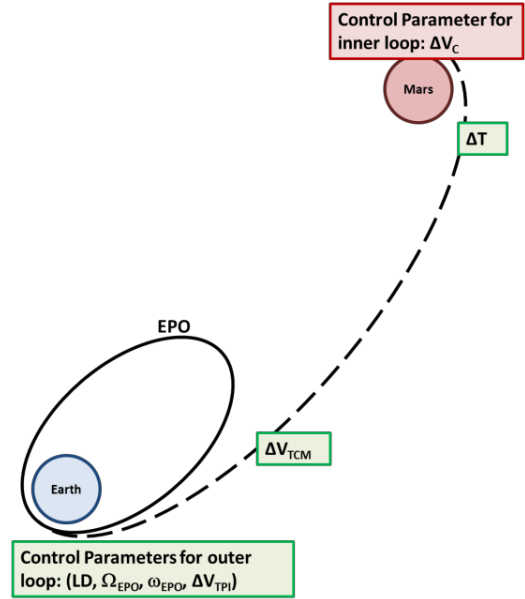


Fig. 6.9 Control variables for WSB trajectory optimization

The objective function to be minimized by the outer loop is:

$$z = y + \text{mag}(\Delta V_{TCM}),$$

where y is obtained from the inner loop. The control variables for inner loop are the three components of $\Delta V_c - \{\Delta V_{c_x}, \Delta V_{c_y}, \Delta V_{c_z}\}$.

The objective function to be minimized by inner loop is:

$$y = \text{mag}(\Delta V_c),$$

whenever a negative value of C_3 (arrival excess hyperbolic energy of the trajectory wrt Mars) is obtained within 500 days of application of ΔV_c . Otherwise, C_3 is always positive till 500 days propagation, in that case y is assigned a large value 1,00,000. The outer loop ensures that a variety of arrival conditions, where ΔV_c can be applied, are obtained. The inner loop searches for minimum ΔV_c so that a capture orbit at

Mars is obtained, for a particular arrival condition. Together with the inner and outer loop the algorithm searches for optimal arrival condition so that a capture orbit at Mars is obtained with minimum ΔV_c .

Propagation is carried out in the full-force model considering major perturbing forces affecting the motion of the spacecraft. The two-body equations of motion are integrated using RKF(7,8) scheme. When the spacecraft is within the sphere of influence (SOI) of Earth, the central body is Earth with 70×70 EGM-96 gravity model, NRLMSIS-00 atmospheric drag (<http://ccmc.gsfc.nasa.gov/modelweb/atmos/nrlmsise00.html>), Sun and Moon third body, solar radiation pressure, solid and ocean tides, albedo. After the spacecraft leaves SOI of Earth, the central body is Sun with Earth and Mars third body. After reaching SOI of Mars, Mars is the central body with Sun and Earth third body. The ephemeris of Sun and other planets are obtained from JPL ephemeris DE421.

The algorithm consists of following steps:

1. Obtain a trajectory from Earth to Mars with specified departure and arrival dates using Lambert Conic method.
2. This trajectory is refined using numerical method so that the required arrival altitude at Mars is achieved. This refined trajectory goes as an input for the present algorithm.
3. The outer loop of the present algorithm varies control variables (LD , Ω , ω , ΔV_{TPI} , ΔT , ΔV_{TCM}) to vary the arrival conditions at Mars.
4. The inner loop varies the ΔV_c so that it results in a capture trajectory within 500 days. A capture trajectory is identified whenever $C3$ crosses $-0.0001 \text{ km}^2/\text{s}^2$ or eccentricity crosses 0.999 decreasing.
5. A suitable optimization method is used to find optimal value of control variables to minimize the objective function.

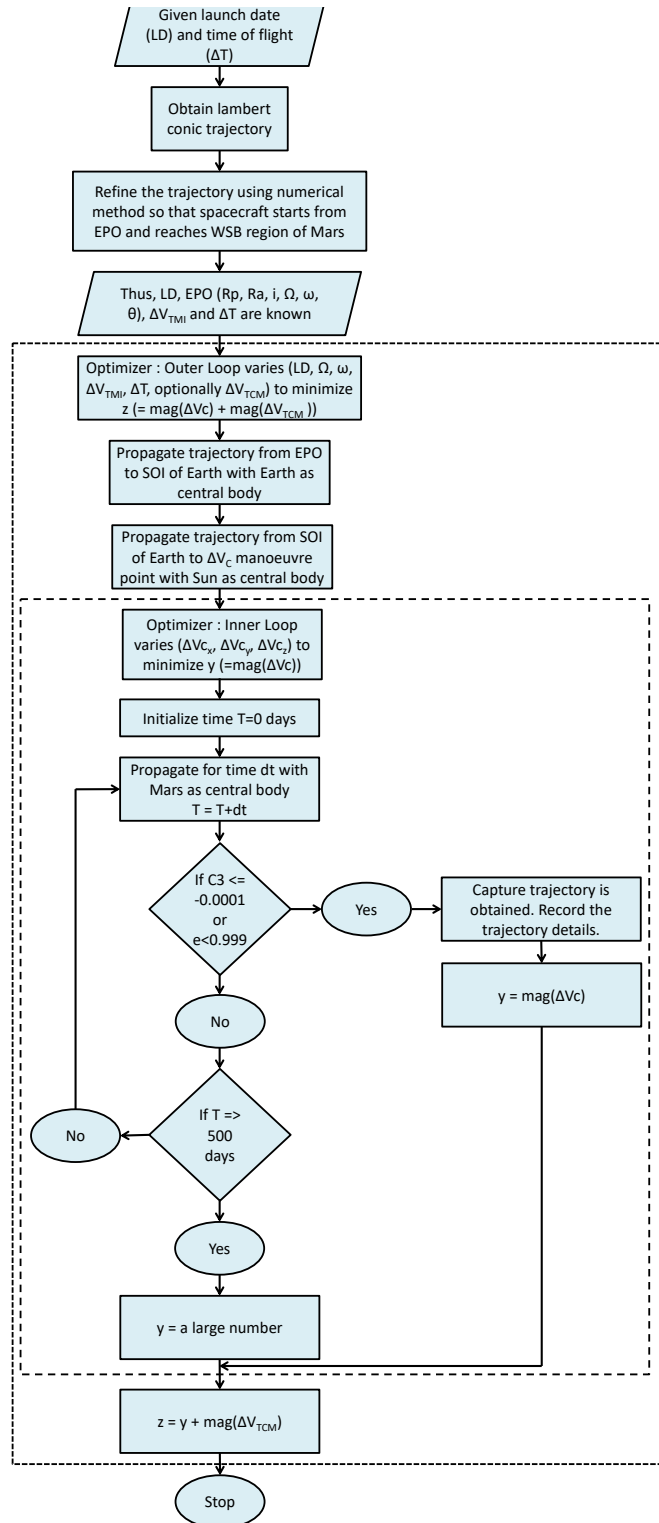


Fig. 6.10: Flowchart of the process to obtain WSB transfers from Earth to Mars

Fig. 6.10 gives the flowchart for the above algorithm. It is observed that after capture if the spacecraft is allowed to continue in the capture orbit, then the eccentricity decreases. For most of the cases the captured orbit's eccentricity decreases for 1-2 days and then it increases till the trajectory becomes parabolic. These are temporary capture orbits. On the other hand for few cases the capture trajectory continues to be elliptical for 100 days also (We have set 100 days threshold on the analysis of captured orbits which is found sufficient later from the analysis of capture orbits in next section). Test cases are presented in the next section.

Any optimization algorithm can be used for inner and outer loops. In this study, genetic algorithm (GA) is used for both inner and outer loops.

6.4. Results

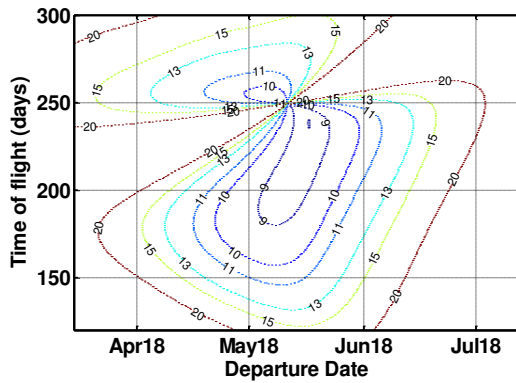


Fig. 6.11: C3 Departure contour plots for the launch opportunity to Mars during 2018

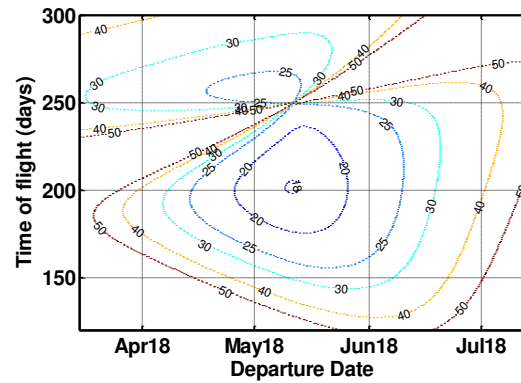


Fig. 6.12: C3 Total contour plots for the launch opportunity to Mars during 2018

Figs. 6.11 and 6.12 give the departure C3 and total C3 contour charts for launch opportunity to Mars during 2018 computed using Lambert conic method. The DE421 ephemeris of Earth and Mars downloaded from www.horizon.com are used for the generation of contour plots. C3 departure decides the Trans-planetary Injection (ΔV_{TPI}) to depart from an EPO towards Mars and C3 arrival decides Mars Orbit Insertion (ΔV_{MOI}) to put the spacecraft into an orbit around Mars. Hence total C3, sum of departure and arrival C3 gives total estimate of ΔV required for an orbiter

mission. These contour charts are obtained by varying launch date from 1 March to 15 July 2018 and time of flight from 120 to 300 days.

For a WSB trajectory, ΔV_{TPI} remains almost the same as for a traditional Lambert conic (LC) trajectory while the ΔV_{MOI} changes according to the capture orbit achieved. Moreover for a WSB trajectory, the time of flight from Earth to Mars remains same as the Hohmann transfer plus an additional capture time (ie, the time required after application of ΔV_c to get ballistic capture orbit around Mars). For the present analysis we have varied launch date from 1 Mar 2018 to 15 June 2018 and found the time of flight corresponding to minimum C3 departure. The trajectory thus obtained from Lambert conic method is refined using numerical simulation so that the periapsis at Mars is less than 15 million km, which is sufficient as an initial condition for generation of a WSB trajectory. The numerically refined trajectory then goes as an input for our present algorithm.

In this analysis, we are presenting 9 test cases, evaluated using the present algorithm. Table 6.1 gives the input trajectory details of these test cases. In all the cases Ω and ω are consistent with an EPO 250 km \times 23,000 km, 18° inclination which is also same as the EPO for MOM-1. The algorithm is valid for all circular and elliptical EPO.

Tables 6.2 - 6.4 gives the details of WSB trajectory thus obtained using the present algorithm. Table 6.2 gives the final value of control parameters - launch epoch, arrival epoch, Ω , ω , ΔV_{TPI} modified by the algorithm (with conditions from Table 6.1 as input) to obtain optimal WSB trajectory. ΔV_C is the impulse given at the WSB region of Mars so that a ballistic capture orbit around Mars is obtained within a specified time duration (we have considered 500 days time duration). Capture time, as mentioned above, is the time required from ΔV_C application till attainment of ballistic capture orbit (ie, C3 wrt Mars is negative). Capture time varies from 40 to 360 days for the cases considered. After a ballistic capture orbit is obtained, the trajectory (for the optimal case only) is further propagated for specified time duration

(100 days is considered here) to find minimum eccentricity conditions. Table 6.3 gives the capture epoch, capture orbit details namely, semi-major axis, eccentricity, C3 energy at arrival and inclination, ΔV_{MOI} (Mars Orbit Insertion manoeuvres if one goes by LC trajectory but prefers the capture orbit obtained by WSB trajectory); ΔV_{Circ_c} is the impulse required to obtain a 1000 km circular orbit from capture orbit; ΔV_{EII_c} is the impulse required to obtain a 500 km \times 80,000 km orbit from capture orbit.

After a ballistic capture orbit is obtained, the trajectory is further propagated for specified time duration (100 days is considered here) to find minimum eccentricity conditions. Table 6.4 gives the epoch when minimum eccentricity is attained; time duration from capture epoch till minimum eccentricity is attained; value of minimum eccentricity; semi-major axis and inclination at that epoch; ΔV_{Circ} is the impulse required at minimum eccentricity point to obtain a 1000 km circular orbit; ΔV_{TO} is the sum of ΔV_{Circ} and ΔV_C which is compared with ΔV_{MOI_circ} (Mars Orbit Insertion manoeuvres for LC trajectory for 1000 km circular orbit); ΔV_{ell} is the impulse required at minimum eccentricity point to obtain a 500 km \times 80,000 km orbit; ΔV_{TO_ell} is the sum of ΔV_{ell} and ΔV_C which is compared with ΔV_{MOI_ell} (Mars Orbit Insertion manoeuvres for LC trajectory for 500 km \times 80,000 km orbit). It is observed that most of the capture orbits obtained have semi-major axis of the order of 4-40 $\times 10^8$ km. On waiting for 2-20 days this semi-major axis often reduces to 5 $\times 10^6$ to 10 8 km and then increases again (temporary capture). Instead of waiting for minimum eccentricity epoch, we can come down to required mapping orbit immediately after capture. By allowing eccentricity to come to minimum automatically, we are saving ΔV upto 50 m/s (for 500 km \times 80,000 km orbit) to 65 m/s (for 1000 km circular orbit) just by waiting upto 2 days in most of the cases, as seen in Table 6.3.

Figures 6.13 to 6.30 give the 2D and 3D representation of WSB trajectories obtained for all the cases mentioned in Table 6.1. In these figures, Earth and Mars at departure epoch (t_0) and arrival epoch (t_f) are shown. Also position of Mars at the time of ΔV_c maneuver (t_c) is also indicated. Figures 6.31 and 6.32, respectively, give

the comparison of distance of the spacecraft from Mars and velocity of the spacecraft with respect to Mars throughout the trajectory for direct transfer and WSB transfer. Table 6.5 gives the detailed comparison of various parameters for both the trajectories.

From Tables 6.2-6.4 it is clear that WSB trajectories result in high altitude capture orbits, which are not a good choice for majority of science payloads for interplanetary missions. These higher orbits might be useful for space weather related studies at Mars. For lower orbit at Mars (eg. 1000 km circular orbits), LC trajectory still remains the best choice in terms of ΔV and time of flight. The present chapter demonstrates that ballistic capture orbits can be obtained at Mars with penalty on time of flight (40 to 500 days). Among all the nine cases considered in the study, only in the last case with launch date on 11 July 2018, WSB is beneficial over LC for getting 500 km \times 80,000 km orbit. The reason is that as we depart away from launch opportunity, C3 arrival increases which translates into higher ΔV_{MOI} for getting into orbit by traditional LC method. While WSB gives various capture orbits with different arrival conditions irrespective of declination of arrival hyperbola.

The main aim of this study is to find possible WSB trajectories for a given LC trajectory. Presently, this algorithm aims to find WSB trajectories with minimum $\Delta V_C + \Delta V_{TCM}$ requirement. The objective function of the algorithm can be modified as per users requirement, for example ΔV_{Circ} or ΔV_{Ell} can also be included in the objective function so that the capture orbit corresponding to lowest total ΔV ($\Delta V_C + \Delta V_{TCM} + (\Delta V_{Circ} \text{ or } \Delta V_{Ell})$) to obtain lower orbit is identified.

All the arrival orbits are analysed for case no. 7 (in Table 6.2). Figures 6.33 to 6.38 show the variation in converged values (obtained after inner loop is completed) of launch epoch, flight duration (from t_0 to t_c), ΔV_{TMI} , RAAN, AOP, ΔV_c and objective function value, respectively, corresponding to the outer loop number. Fig. 6.39 shows the variation in the three components of ΔV_c corresponding to the outer loop for case 7. Fig. 6.40 shows the variation of C3 of the spacecraft with

respect to Mars for some of the outer loops. Fig. 6.41 gives the histogram of semi-major axis of the capture orbits. Fig. 6.42 gives the histogram of inclination of capture orbits. It is observed that all inclination capture orbits are obtained. Fig. 6.43 gives the histogram of capture time (time from t_c to capture epoch). It is observed that most of the capture orbits are obtained within 200-250 days from application of ΔV_C . Hence, the maximum 500 days threshold considered on time limit from application of ΔV_C to capture epoch, seems to be sufficient. Fig. 6.44 gives the histogram of altitude R_c (arrival altitude at which ΔV_C is applied).

Figs. 6.45 gives the plot between ΔV_C and R_c for case 7. It is observed that the arrival altitude for a successful ΔV_C (means ΔV_C for which capture orbit is attained within 500 days) varies from 2-10 million km from Mars. As arrival altitude increases ΔV_C decreases. Fig. 6.46 gives the plot between ΔV_C and capture duration. It is observed that most of the orbits get captured within 200-250 days after application of ΔV_C , and the magnitude of ΔV_C varies from 2-4.5 km/s. Figs. 6.47 gives the plots between minimum eccentricity attained by the captured orbits and time required to attain minimum eccentricity. It is observed that most of the captured orbits attain min. eccentricity by 2-20 days. Even circular orbits are also obtained. Also some orbits remain captured for more than 100 days. Hence, the upper bound of 100 days, considered in this study, to allow the capture orbit to attain minimum eccentricity seems to be sufficient. Fig. 6.48 gives the histogram of periapsis altitude of minimum eccentricity capture orbit. It is seen that most of the capture orbits have periapsis altitude of the order of 10^7 km at minimum eccentricity. Figs. 6.49 give the ΔV requirements to lower from captured orbit to 1000 km circular and $500 \times 80,000$ km orbits for case 7. It is always advantageous to reduce down to $500 \times 80,000$ km compared to 1000 km circular.

It is observed that a number of WSB capture orbits can be obtained by varying the arrival conditions at Mars. These orbits can be obtained by variation in ΔV_C (of the order of 2 km/s) and possess different orbital characteristics (eg. semi-

major axis, minimum eccentricity attained, inclination, capture duration, etc). Among these capture orbits, the one suiting our mission objectives can be selected.

6.5. Conclusion

In the present chapter, we study the dynamics of capture orbits at Mars in the framework of Restricted Three-Body Problem. Capture orbits at Mars are represented on phase space with colour code on time of capture. It is known that capture orbits are obtained when positional phase angle of the periapsis is between -55° to 55° or 125° to 235° in the Sun-Mars fixed rotating frame (Yamakawa, 1992). But this is valid from small periapsis altitudes (<5000 km) only. For higher periapsis altitudes ($\geq 10,000$ km), almost all ranges of positional phase angle gives capture trajectories.

We also develop an algorithm to generate trajectory to Mars with ballistic capture using forward propagation. Forward-backward propagation algorithms to find WSB trajectories face major problem of launch vehicle constraint satisfaction especially when the Earth Parking Orbit (EPO) is elliptical, which is eliminated in this case. Also given a departure date and EPO conditions, a number of WSB arrival orbits can be found using the given algorithm with marginal difference in impulse requirements. The one suiting our requirement can be selected. Another advantage of this algorithm is that we find the WSB trajectories in high fidelity force model which can be used for real missions. This algorithm can be modified suitably to get WSB trajectories to other planets also.

Using this algorithm, we have worked out the launch opportunity of 2018 to evaluate Weak Stability Boundary (WSB) transfer trajectories to Mars. It is found that WSB trajectories to Mars result in high altitude capture orbit (with semi-major axis of the order of $4-40 \times 10^8$ km), which is not a good choice for majority of science payloads for interplanetary missions. For lower orbit at Mars (eg. 1000 km circular orbits), traditional patched conic trajectory still remains the best choice in terms of ΔV and time of flight. Detailed analysis of capture orbits is presented in this study.

Table 6.1: Input trajectory details for the test cases

No.	Launch Epoch (UTC)	Time of flight (days)	Arrival Epoch (UTC)	Ω_{EPO} (degree)	ω_{EPO} (degree)	ΔV_{TPI} (km/s)	Arrival C3 Energy (km ² /s ²)
1.	24 Mar 2018 13:24:00	252.876	5 Dec 2018 00:19:27	312.860	224.514	1.692	14.243
2.	10 Apr 2018 04:30:00	254.037	23 Dec 2018 00:31:49	321.320	220.842	1.585	14.056
3.	24 Apr 2018 13:30:00	178.675	23 Oct 2018 05:56:25	57.050	121.617	1.500	12.662
4.	9 May 2018 16:48:00	186.643	15 Nov 2018 07:36:47	52.306	124.892	1.514	9.235
5.	20 May 2018 13:48:00	211.814	21 Dec 2018 07:05:40	57.197	127.557	1.538	9.987
6.	1 Jun 2018 21:25:58	226.136	17 Jan 2019 00:45:51	93.182	85.094	1.504	12.369
7.	15 Jun 2018 12:55:58	227.577	31 Jan 2019 21:30:29	119.279	59.722	1.591	13.986
8.	27 Jun 2018 12:19:58	233.847	18 Feb 2019 20:04:52	329.391	214.502	1.755	16.001
9.	11 Jul 2018 05:13:58	242.461	12 Mar 2019 21:01:54	318.408	235.778	1.963	18.733

Table 6.2: WSB trajectory details for the test cases

No.	Launch Epoch (UTC)	Time of flight (days)	Ω_{EPO} (degree)	ω_{EPO} (degree)	ΔV_{TPI} (km/s)	ΔV_{TCM} (km/s)	ΔV_C (UTC)	Epoch	Arrival altitude for ΔV_C (km)	ΔV_C (km/s)	Capture time (days)
1.	25-Mar-2018 20:39:46	248.639	144.411	32.006	1.686	0.0069	29 Nov 2018 12:00:08	2018	4.8×10^6	2.968	187.5
2.	10-Apr-2018 15:28:48	241.970	150.904	28.492	1.586	0.0064	8 Dec 2018 14:45:53	2018	6.2×10^6	3.314	359.3
3.	24-Apr-2018 21:52:44	181.291	61.867	126.194	1.499	0.0058	23 Oct 2018 04:51:52	2018	1.7×10^7	3.200	322
4.	09-May-2018 22:59:08	182.949	56.307	124.481	1.513	0.0036	8 Nov 2018 21:46:05	2018	1.1×10^7	3.539	137.8
5.	20-May-2018 23:55:38	213.268	61.812	128.442	1.539	0.0057	20 Dec 2018 06:21:22	2018	1.5×10^7	1.108	168.9
6.	01-Jun-2018 12:17:19	221.879	91.968	89.725	1.505	0.0035	9 Jan 2019 09:23:30	2019	8.6×10^6	2.190	148.5
7.	15-Jun-2018 16:58:40	228.796	123.640	63.662	1.592	0.0055	30 Jan 2019 12:05:41	2019	1.1×10^7	2.159	176.5
8.	27-Jun-2018 10:35:48	72.546	329.359	214.122	1.756	0.0063	7 Sep 2018 23:42:41	2018	4.3×10^7	1.833	42.4
9.	11-Jul-2018 08:57:51	45.190	320.276	240.011	1.962	0.0054	25 Aug 2018 13:30:43	2018	5.0×10^7	0.714	48.4

Table 6.3: WSB trajectory details of orbit obtained at capture for the test cases

S.No.	Capture Epoch (UTC)	Semimajor Axis (km) of capture orbit	Eccentricity of capture orbit	C3 arrival energy (km^2/s^2)	Inclination (deg) of capture orbit	ΔV_{MOI} for capture orbit (km/s)	ΔV_{Circ_c} (km/s)	Gain in ΔV_{Circ_c} (km/s) by waiting for min. ecc.	ΔV_{ell_c} (km/s)	Gain in ΔV_{ell_c} (km/s) by waiting for min. ecc.
1.	4 Jun 2019 22:42:22	3.2×10^9	0.98999999	-1.34×10^{-5}	44.440	3.723	1.343	0.010	0.847	0.011
2.	2 Dec 2019 23:00:39	4.3×10^8	0.99477187	-1.00×10^{-4}	162.747	3.559	1.475	0.065	0.939	0.046
3.	10 Sep 2019 04:52:50.139	4.5×10^8	0.98999999	-9.49×10^{-5}	69.386	3.424	1.424	0.063	0.909	0.053
4.	26 Mar 2019 17:35:26	5.6×10^8	0.99000045	-7.59×10^{-5}	102.883	2.919	1.410	0.061	0.899	0.049
5.	7 Jun 2019 03:58:49	4.2×10^9	0.98999999	-1.02×10^{-5}	50.781	3.116	1.337	0.013	0.841	0.013
6.	6 Jun 2019 21:17:25.560	8.7×10^8	0.98999954	-4.91×10^{-5}	89.493	3.420	1.388	0.039	0.884	0.033
7.	25 Jul 2019 23:10:13	2.4×10^9	0.98999999	-1.76×10^{-5}	10.348	3.681	1.351	0.003	0.853	0.005
8.	20 Oct 2018 09:02:34	4.1×10^9	0.98999969	-1.05×10^{-5}	118.638	3.955	1.338	0.008	0.842	0.008
9.	12 Oct 2018 22:29:59	1.5×10^9	0.98999942	-2.83×10^{-5}	151.698	4.254	1.366	0.001	0.866	0.002

Table 6.4: WSB trajectory details of minimum eccentricity orbit obtained after capture for the test cases

No.	Capture Epoch (UTC)	Duration (days) for min. ecc.	SMA at min. ecc.	Min. ecc.	Inclination (deg)	ΔV_{MOI_circ} (km/s)	ΔV_{Circ} ($\Delta V_{TO} = \Delta V_{Circ} + \Delta V_C$) (km/s)	Gain 1000 km cir ($\Delta V_{MOI} - \Delta V_{TO}$)	ΔV_{MOI_ell} (km/s)	ΔV_{ell} ($\Delta V_{TO_ell} = \Delta V_{ell} + \Delta V_C$) (km/s)	Gain elliptical ($\Delta V_{MOI_ell} - \Delta V_{TO_ell}$)
1	5 Jun 2019 13:40:22.145	0.625	3.5×10^7	0.16730	33.672	2.686	1.333 (4.301)	-1.615	1.436	0.836 (3.804)	-2.368
2	22 Dec 2019 17:00:39.731	19.75	7.2×10^6	0.451556	127.062	2.670	1.410 (4.725)	-2.055	1.421	0.893 (4.207)	-2.787
3	19 Sep 2019 22:52:49.275	9.750	9.1×10^6	0.034346	106.337	2.549	1.360 (4.561)	-2.012	1.303	0.856 (4.056)	-2.753
4	29 Mar 2019 00:35:26.010	2.292	3.4×10^7	0.455058	116.430	2.238	1.349 (4.888)	-2.651	1.005	0.850 (4.390)	-3.385
5	7 Jun 2019 14:58:49.037	0.458	4.5×10^7	0.037267	34.355	2.307	1.324 (2.432)	-0.125	1.071	0.828 (1.937)	-0.865
6	9 Jun 2019 23:17:25.531	3.083	2.6×10^7	0.359212	98.55	2.523	1.350 (3.539)	-1.017	1.278	0.851 (3.040)	-1.762
7	26 Jul 2019 15:10:12.712	0.667	2.9×10^7	0.363516	36.890	2.664	1.347 (3.506)	-0.842	1.415	0.849 (3.008)	-1.593
8	20 Oct 2018 16:02:34.209	0.292	10^8	0.540250	126.316	2.836	1.330 (3.163)	-0.327	1.580	0.834 (2.667)	-1.087
9	13 Oct 2018 08:29:59.028	0.417	3.4×10^7	0.633413	98.788	3.061	1.365 (2.079)	0.982	1.798	0.864 (1.578)	0.220

Table 6.5: Comparison of direct transfer and WSB transfer trajectory for case 1.

	Direct transfer trajectory	WSB transfer trajectory
Epoch (UTC):	25 Mar 2018 12:55:00.000	25 Mar 2018 20:39:46.000
RAAN (deg):	140.807	144.411 deg
AOP (deg):	37.707	32.006 deg
ΔV_{TMI} (km/s):	1.685	1.686
ΔV_{TCM} (km/s):	0.0	0.007
Periapsis Arrival Epoch (UTC):	6 Dec 2018 03:53:03.618	29 Nov 2018 12:00:08.159
Periapsis altitude (km):	586251.917	4.77×10^6
Velocity of s/c at periapsis (km/s):	3.654	3.658
ΔV_c (km/s):	NA	2.968
ΔV_{MOI} (km/s):	3.384	NA
Capture Epoch (UTC):	6 Dec 2018 03:53:03.618	4 Jun 2019 22:42:23.105
Min. eccentricity orbit epoch (UTC):	NA	5 Jun 2019 13:40:22.145
Velocity of s/c in min. eccentricity orbit (km/s):	NA	0.0379

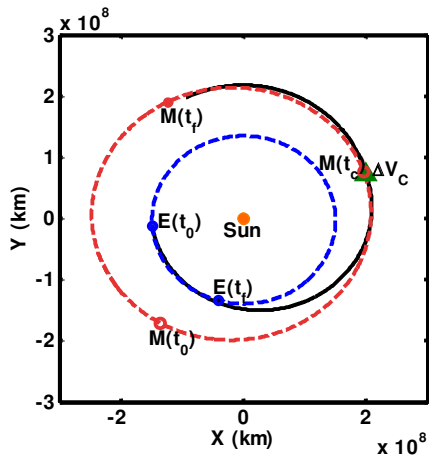


Fig. 6.13: 2D representation of WSB trajectory to Mars case 1 launch date 25 Mar 2018

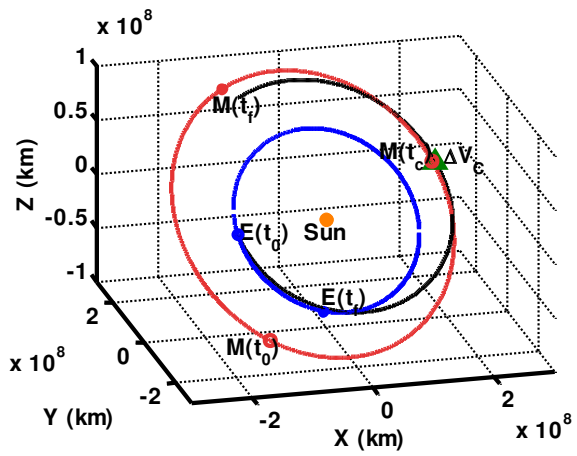


Fig. 6.14: 3D representation of WSB trajectory to Mars case 1 launch date 25 Mar 2018

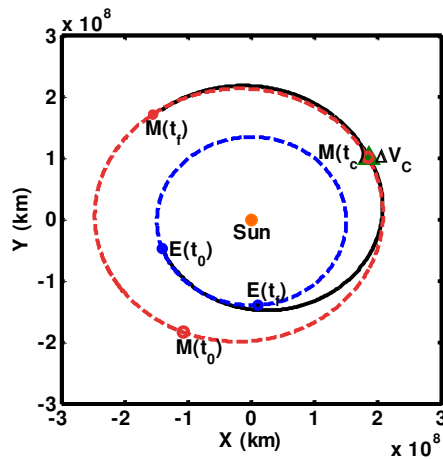


Fig. 6.15: 2D representation of WSB trajectory to Mars case 2 launch date 10 Apr 2018

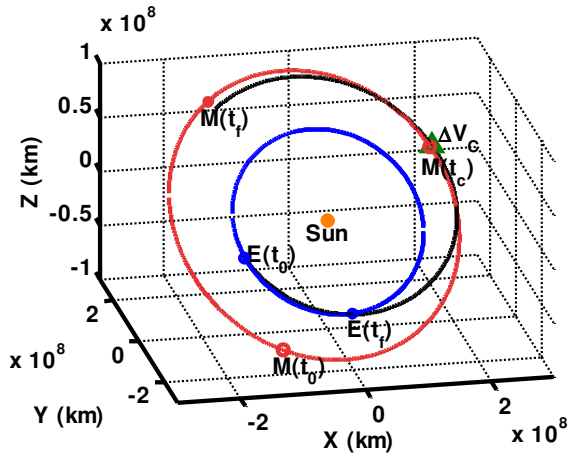


Fig. 6.16: 3D representation of WSB trajectory to Mars case 2 launch date 10 Apr 2018

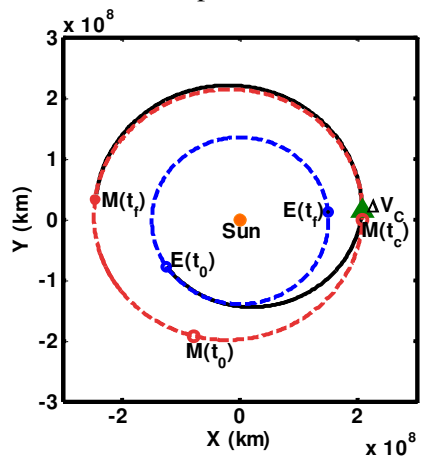


Fig. 6.17: 2D representation of WSB trajectory to Mars case 3 launch date 24 Apr 2018

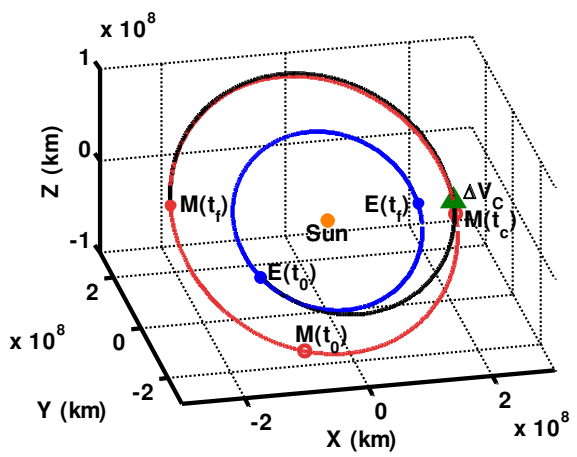


Fig. 6.18: 3D representation of WSB trajectory to Mars case 3 launch date 24 Apr 2018

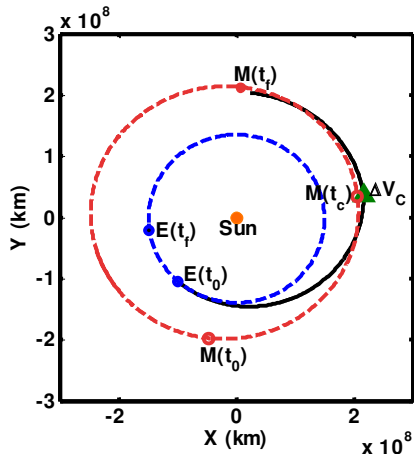


Fig. 6.19: 2D representation of WSB trajectory to Mars case 4 launch date 9 May 2018

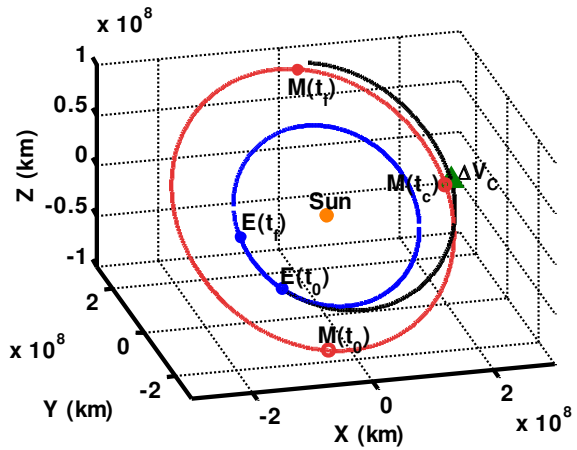


Fig. 6.20: 3D representation of WSB trajectory to Mars case 4 launch date 9 May 2018

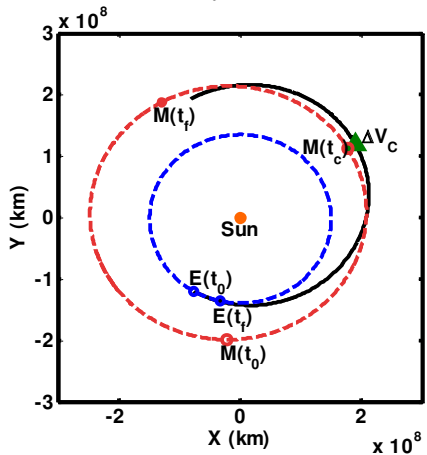


Fig. 6.21: 2D representation of WSB trajectory to Mars case 5 launch date 20 May 2018

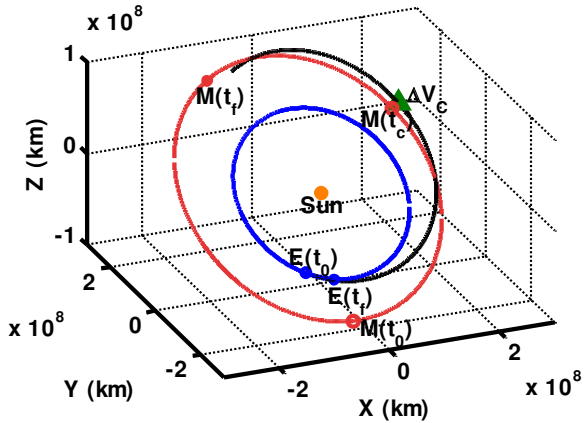


Fig. 6.22: 3D representation of WSB trajectory to Mars case 5 launch date 20 May 2018

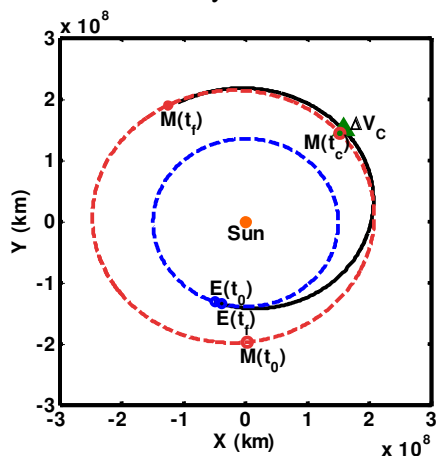


Fig. 6.23: 2D representation of WSB trajectory to Mars case 6 launch date 1 Jun 2018

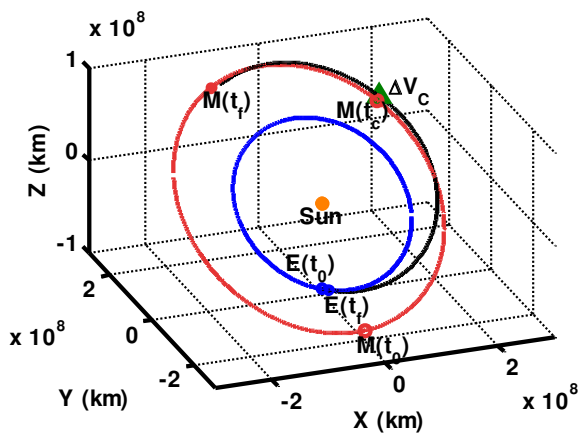


Fig. 6.24: 3D representation of WSB trajectory to Mars case 6 launch date 1 Jun 2018

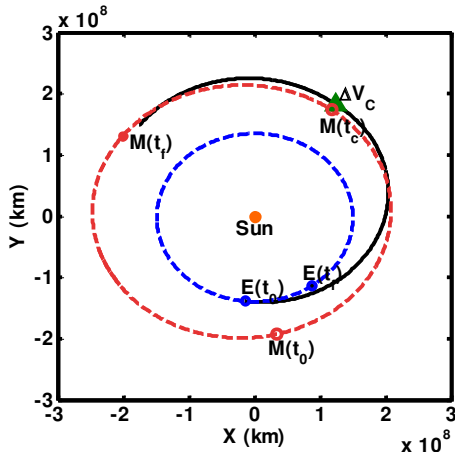


Fig. 6.25: 2D representation of WSB trajectory to Mars case 7 launch date 15 Jun 2018

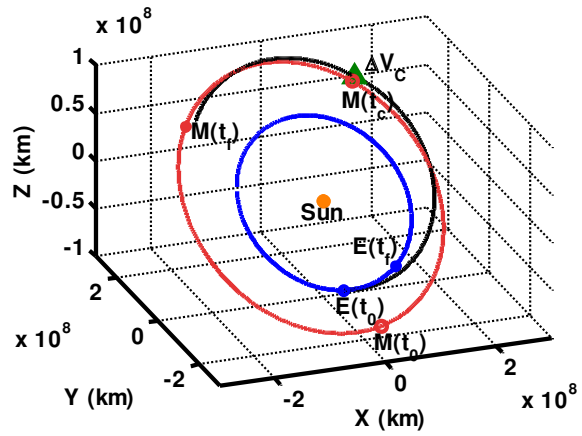


Fig. 6.26: 3D representation of WSB trajectory to Mars case 7 launch date 15 Jun 2018

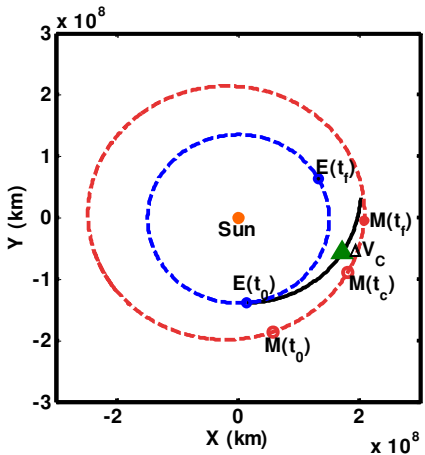


Fig. 6.27: 2D representation of WSB trajectory to Mars case 8 launch date 27 Jun 2018

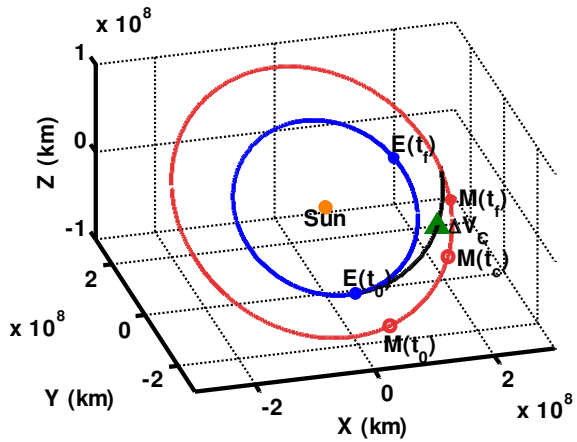


Fig. 6.28: 3D representation of WSB trajectory to Mars case 8 launch date 27 Jun 2018

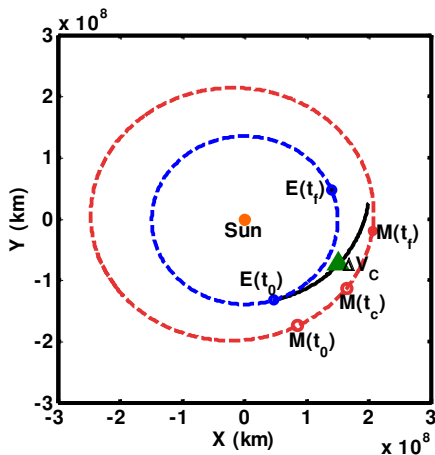


Fig. 6.29: 2D representation of WSB trajectory to Mars case 9 launch date 11 Jul 2018

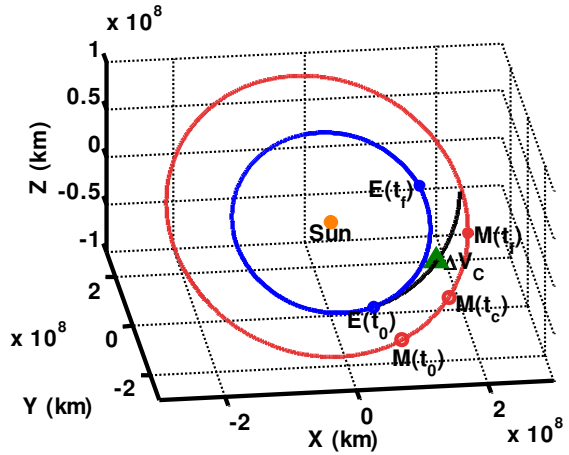


Fig. 6.30: 3D representation of WSB trajectory to Mars case 9 launch date 11 Jul 2018

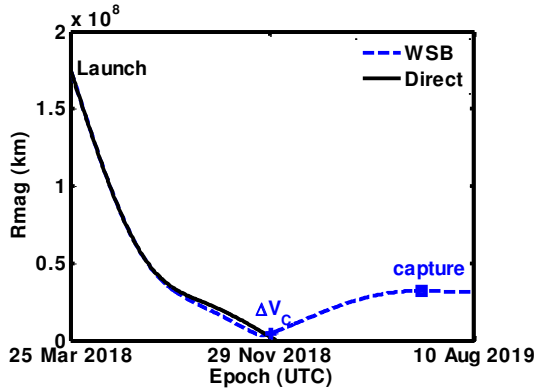


Fig. 6.31: Variation in distance from Mars for direct and WSB trajectories for case 1

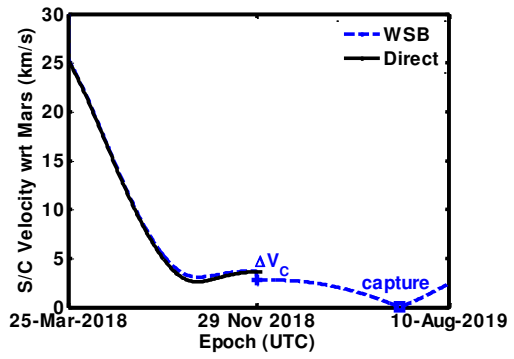


Fig. 6.32: Velocity of the spacecraft with respect to Mars for direct and WSB trajectories for case 1

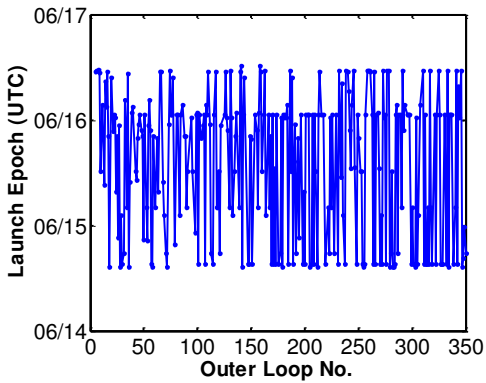


Fig. 6.33: Converged values of launch epoch for each outer loop for case 7

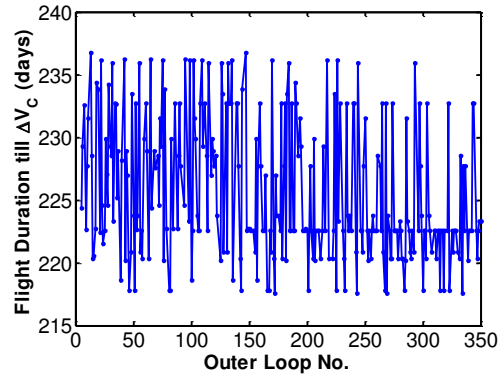


Fig. 6.34: Converged values of flight duration from launch epoch to time of ΔV_c maneuver for each outer loop for case 7

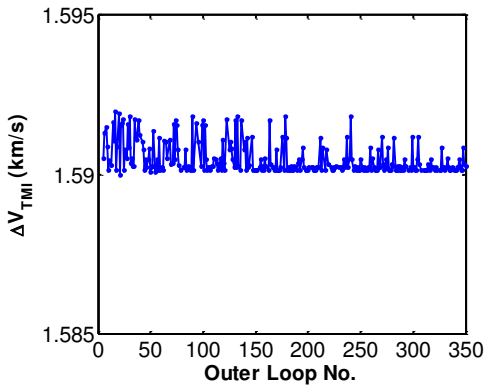


Fig. 6.35: Converged values of ΔV_{TMI} for each outer loop for case 7

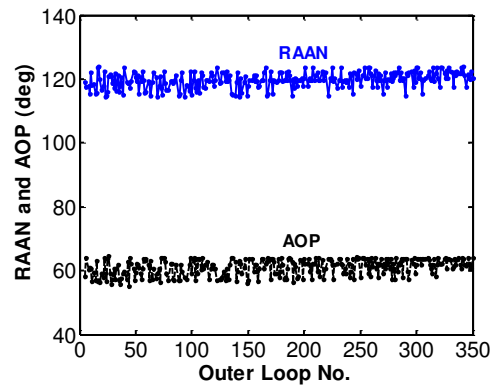


Fig. 6.36: Converged values of RAAN and AOP for each outer loop for case 7

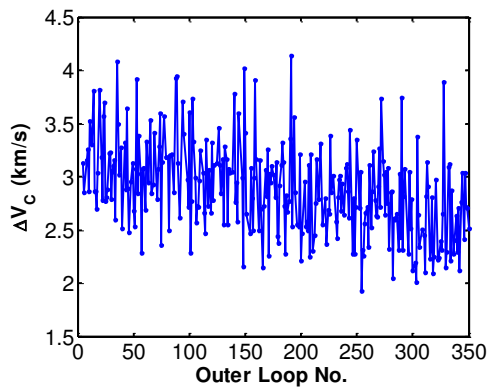


Fig. 6.37: Converged values of ΔV_c for each outer loop for case 7

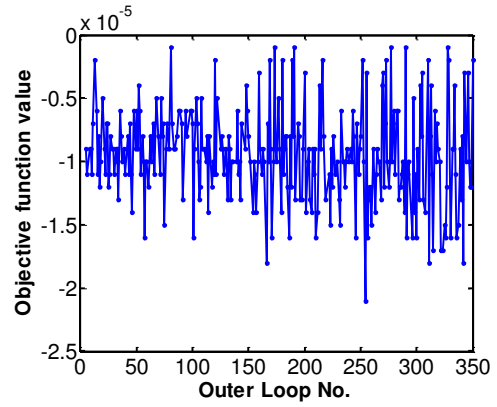


Fig. 6.38: Objective function value for each outer loop for case 7

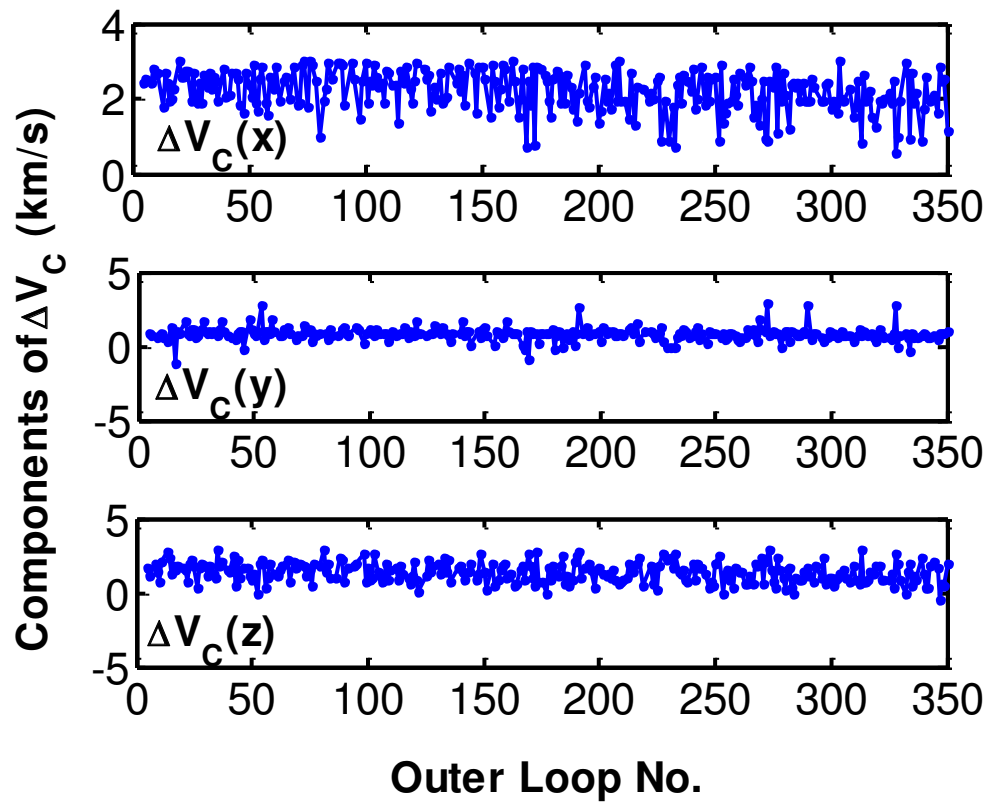
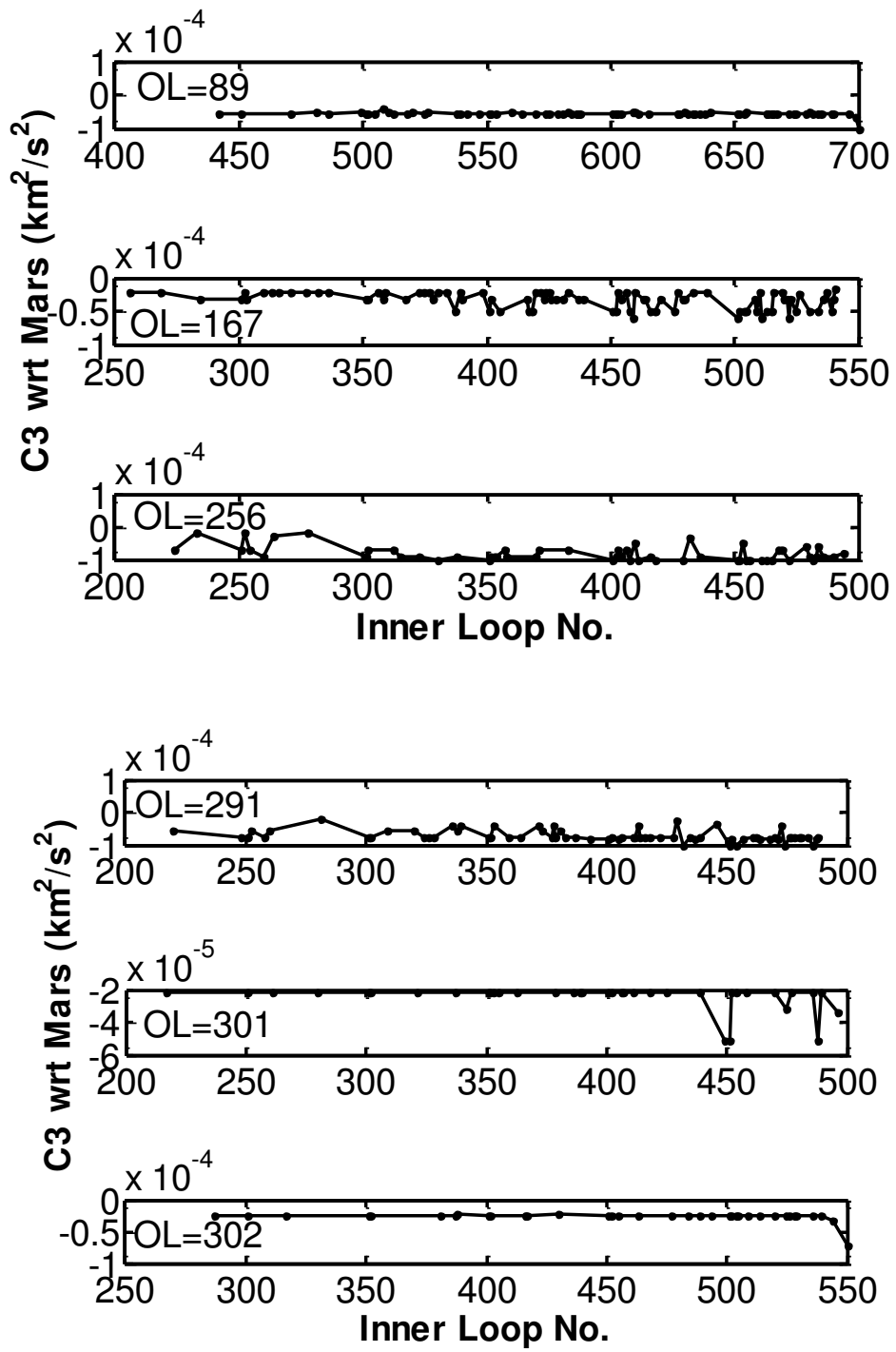


Fig. 6.39: Variation in all the three components of ΔV_c corresponding to each outer loop for case 7



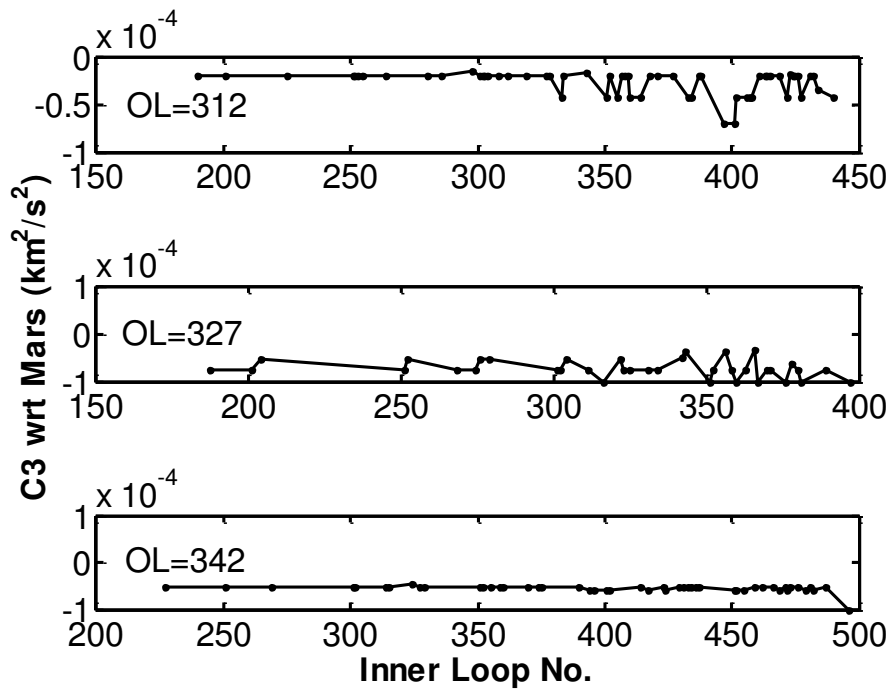


Fig. 6.40: Variation of C3 of the spacecraft wrt Mars by the inner loop for some outer loops (OL) namely, 89, 167, 256, 291, 301, 302, 312, 327, 342.

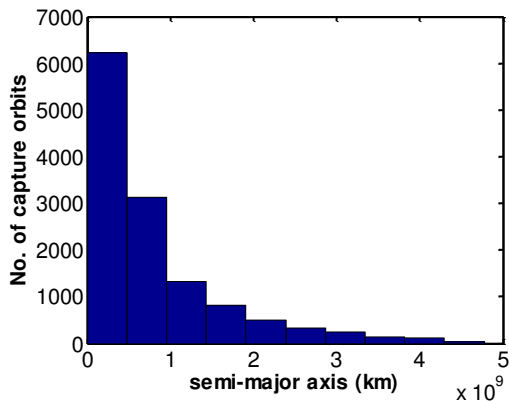


Fig. 6.41: Histogram of semi-major axis of capture orbits for case 7

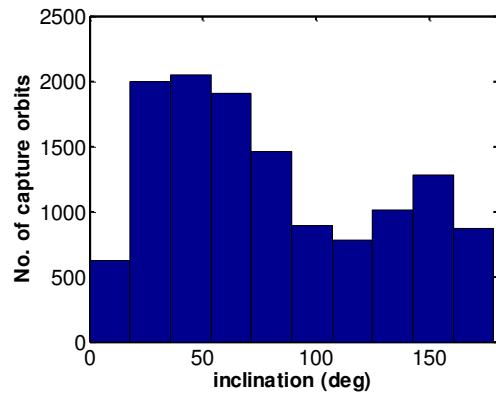


Fig. 6.42: Histogram of inclination of capture orbits for case 7

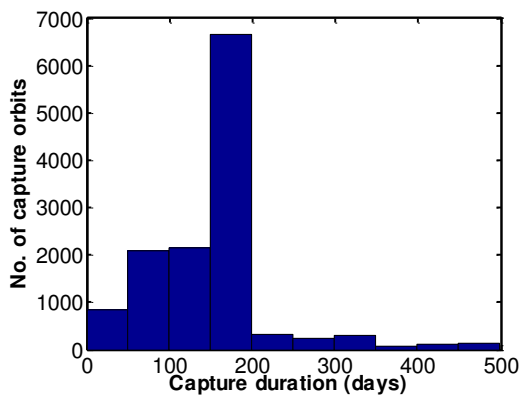


Fig. 6.43: Histogram of capture time (from ΔV_c epoch till capture epoch) for case 7

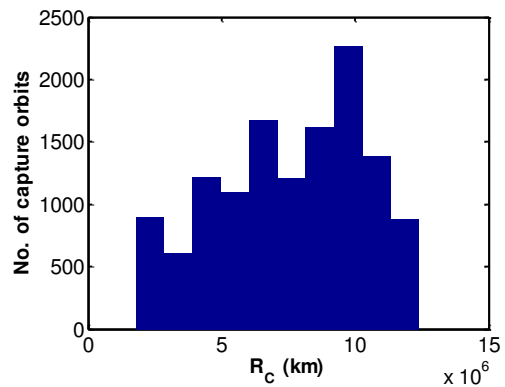


Fig. 6.44: Histogram of altitude R_c at which ΔV_c is applied for case 7

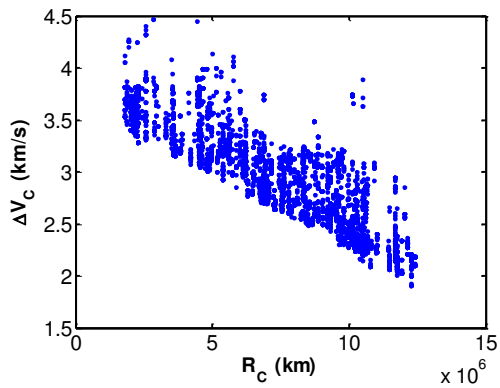


Fig. 6.45: Capture ΔV_c and altitude R_c at which ΔV_c is applied - case 7

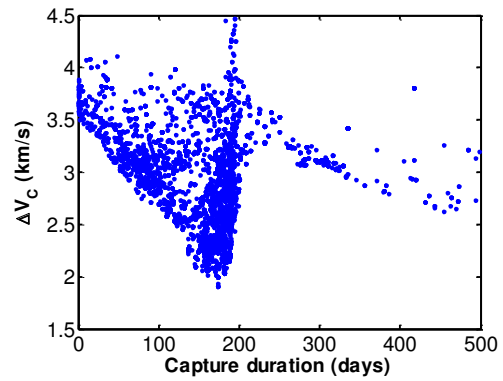


Fig. 6.46: Capture ΔV_c vs capture duration (no. of days from ΔV_c to capture) - case 7

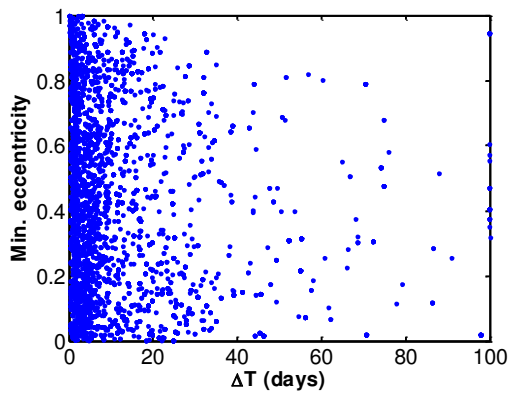


Fig. 6.47: Minimum eccentricity attained after ΔT days after being captured in orbit around Mars - case 7

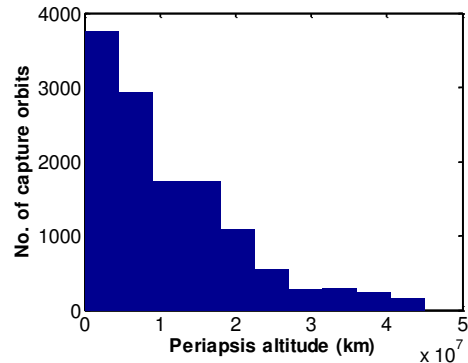


Fig. 6.48: Histogram of periapsis altitude of minimum eccentricity orbits for case 7

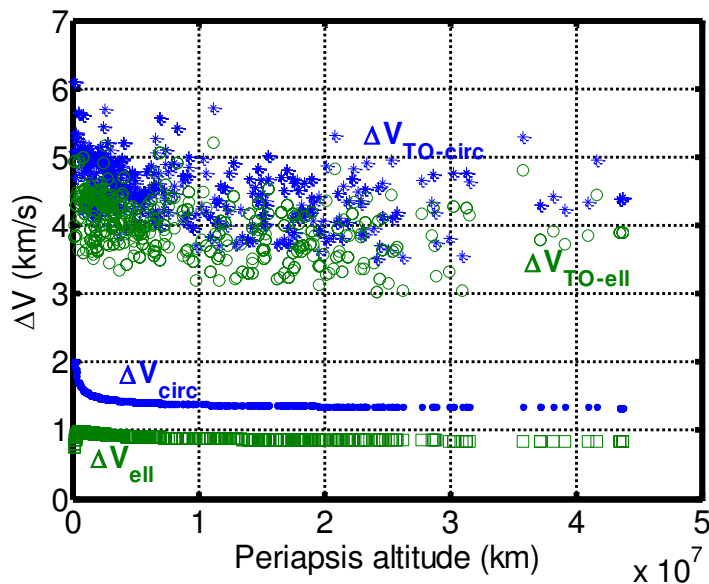


Fig 6.49: DeltaV required to reduce from captured orbit to 1000 km circular and 500X80,000 km orbits- case 7

CHAPTER 7

CONCLUDING REMARKS AND FUTURE WORKS

Weak Stability Boundary (WSB) transfer to Moon was first discovered by Belbruno for the Lunar Get-a-Way Special (LGAS) spacecraft (Belbruno, 1987). Belbruno's WSB theory was demonstrated in 1990 by Japanese Hiten Mission. This theory was again highlighted in salvaging Asiasat3 in 1998. Next ESA's SMART-1 was launched on 27 Sep 2003 and it reached Moon utilizing a low energy trajectory like the one designed for LGAS. NASA's Gravity Recovery and Interior Laboratory (GRAIL) Mission in 2011 was the first mission launched to Moon directly on a WSB transfer.

WSB is explained using the restricted three-body problem. The invariant manifold structure associated with the Lyapunov orbits near the collinear Lagrange points play an important role in these transfers. Using the dynamical system theory, natural phenomena like resonance hopping and capture of comets by Jupiter have been explained.

The works carried out in this thesis mainly concern with the design of WSB transfers to Moon and Mars and studies their dynamics. To begin with the distribution of planar fly-by trajectories to Moon in the phase space is studied. It is found that fly-by trajectories and periodic orbits are clustered and follow some pattern in the phase space. Next, the dynamics and construction of WSB trajectories to Moon is studied in the framework of restricted three-body and four-body problems. Yamakawa (1992) shows analytically that the positional phase angle of perilune in Earth-Moon fixed rotating frame of lunar capture trajectories lies within -55° to 55° and 125° to 235° . In the present work, with the help of numerical simulations it is found that the above result holds good for lower altitudes but it is violated to some extent for higher apolune altitudes.

Proceeding on the same lines, the dynamics of capture orbits at Mars are studied. It is found that for higher periapsis altitudes ($\geq 10,000$ km) almost all ranges positional phase angle of periapsis in Sun-Mars fixed rotating frame yields capture orbits. Hence in order to obtain WSB trajectories to Mars, the algorithm has to be targeted to high periapsis altitudes to increase the possibility of finding capture orbits.

Numerical algorithms are developed to obtain WSB trajectories to Moon and Mars in high fidelity force model. These algorithms start from an Earth Parking Orbit (EPO), use forward propagation to reach a capture trajectory at Moon/Mars. These algorithms can be applied to both circular and elliptical EPO and are designed to satisfy launch vehicle maximum payload constraints. Also given a departure date and EPO conditions, a number of WSB arrival orbits can be found using the given algorithm with marginal difference in impulse requirements but varying arrival orbits. Using these algorithms WSB trajectories were obtained for all the days considered in the study.

It is observed that most of the impulse required to obtain a capture orbit at Mars is spent to reduce the incoming velocity. Possibility of using alternative methods instead to reduce the spacecraft's incoming velocity can be explored. Combination of various methods can be implemented in such a way that major drawbacks like longer flight durations and high altitude capture orbits can be overcome. Classification of capture orbits at Mars and hence WSB transfers to Mars can be attempted. Also analysis of capture corridor at Mars to account for navigational uncertainties is important to complete the trajectory design process.

The numerical algorithms developed here can be extended for the design of WSB transfers to other planets also. Moreover, these algorithms can be modified to take advantage of the inherent manifold theory to reduce the computational time. Presently, the optimizer searches for possible capture orbits by varying the control variables randomly. This in turn leads to many failure cases, which can be avoided by implementation of manifold theory for varying the control variables.

REFERENCES

1. Abramowitz, M., Stegun, I.A. (1972). Handbook of Mathematical Functions with Formulas, Graphs and Mathematical Tables, Dover, New York, (ninth printing), 1972.
2. Abramson, M.A. (2002). Pattern search filter algorithms for mixed variable general constrained optimization problems. Ph.D. thesis, Department of Computational and Applied Mathematics, Rice University.
3. Albrecht, P. (1996). The Runge-Kutta Theory in a Nutshell. *SIAM Journal on Numerical Analysis*, 33(5):1712-1735.
4. Alessi, E.M., Gómez, G., Marsdemont J.J. (2009a). Leaving the Moon by means of invariant manifolds of libration point orbits. *Communications in Nonlinear Science and Numerical Simulation*, 14: 4153-4167.
5. Alessi, E.M., Gómez, G., Marsdemont J.J. (2009b). Transfer Orbits in the Earth-Moon System and Refinement to JPL Ephemerides. 21st International Symposium on Space Flight Dynamics, Toulouse, France.
6. Anderson, R.L., and Lo, M.W. (2004). The Role of Invariant Manifolds in Low Thrust Trajectory Design (Part II). AIAA Paper 2004-5305.
7. Anderson, R.L., and Lo, M.W. (2009). Role of Invariant Manifolds in Low Thrust Trajectory Design. *Journal of Guidance, Control and Dynamics*, 3(6).
8. Anderson, R.L., and Parker, J.S. (2011a). Comparison of Low-Energy Lunar Transfer Trajectories to Invariant Manifolds. AAS/AIAA Astrodynamics Specialist Conference, AAS Paper 11-423, Girdwood, AK.
9. Anderson, R.L., and Parker, J.S. (2011b). A survey of ballistic transfers to the lunar surface. 21st AAS/AIAA Space Flight Mechanics Meeting, AAS Paper 11-278, Orleans, Louisiana.
10. Assadian, N., Pourtakdoust, S.H. (2010). Multiobjective genetic optimization of Earth-Moon trajectories in the restricted four-body problem. *Advances in Space Research*, 45:398-409.
11. Audet, C., Dennis, J.E. Jr. (2003). Analysis of generalized pattern searches. *SIAM Journal of Control and Optimization*, 13(3): 889–903.

12. Bailey, R.W., Hall, J.L., Spilker, T.R., (2003). Titan Aerocapture Mission and spacecraft design overview. 39th AIAA/ASME/SAE/ASEE Joint Propulsion Conference, Von Braun Center, Huntsville, AL.
13. Barrabés, E., Gómez, G., and Rodríguez-Canabal, J. (2004). Notes for the gravitational assisted trajectories Lectures. Advanced Topics in Astrodynamics, Summer Course, Barcelona.
14. Bate, R.R., Mueller, D.D, and White, J.E. (1971). Fundamentals of Astrodynamics. Dover Publication Inc.
15. Battin, R.H. (1999). An introduction to the mathematics and methods of astrodynamics, Rev.ed., AIAA education series.
16. Beerer, J., Broks, R., Esposito, P., Lyons, D., Sidney, W, (1996). Aerobraking at Mars: the MGS Mission, AIAA-96-0334.
17. Belbruno, E.A. (1987). Lunar Capture Orbits, A method of constructing Earth-Moon trajectories and the Lunar GAS Mission. Proceedings of AIAA/DGLR/JSASS, Inter. Propl. Conf., AIAA Paper No 87-1054.
18. Belbruno, E. (1990). Examples of nonlinear dynamics of ballistic capture and escape in the earth-moon system, AIAA Paper No. 90-2896, In Proc. Annual Astrodynamics Conference.
19. Belbruno, E.A, and Miller, J.K. (1993). Sun Perturbed Earth-to-Moon Transfers with Ballistic Capture. Journal of Guidance, Control and Dynamics, 16(4).
20. Belbruno, E.A. and Marsden, B. (1997). Resonance hopping in comets, Astron. Journal 113: 1433-1444.
21. Belbruno, E.A., Humble, R. and Coil, J. (1997). Ballistic Capture Lunar Transfer Determination for the U.S. Air Force Academy Blue Moon Mission, In AAS 97-171.
22. Belbruno, E.A. and Carrico, J.P. (2000). Calculation of Weak Stability Boundary Ballistic Lunar Transfer Trajectories. In AIAA/AAS Astrodynamics Specialist Conference, AIAA 2000-4142.
23. Belbruno, E.A. (2004) Capture Dynamics and Chaotic Dynamics in Celestial Mechanics, Princeton University Press.

24. Belbruno, E.A. (2005). A low energy lunar transportation system using chaotic dynamics. In AAS 05-382.
25. Belbruno, E.A. (2007). *Fly Me to the Moon: An Insider's Guide to the New Science of Space Travel*, Princeton University Press.
26. Belbruno, E. and Gott III, J.R. (2005). Where did the moon come from?. *Astronautical Journal*, 129: 1724-1745.
27. Belbruno, E., Moro-Martin, A. and Malhotra, R. (2008a). Minimal energy transfer of solid material between planetary systems, ArXiv: 0808.3268v2(astro-ph), 1-30.
28. Belbruno, E.A., Topputo, F. and Gidea, M. (2008b). Resonance transitions associated to weak capture in the restricted three-body problem. *Advances in Space Research*, 42(8):1330-1351.
29. Biesbroek, R., Ockels, W. and Janin, G. (1999). Optimization of Weak Stability Boundary Orbits from GTO to the Moon using Genetic Algorithms. In IAF-99-A.6.10, Amsterdam.
30. Biesbroek, R. and Janin, G. (2000) Ways to the Moon?. In ESA Bulletin No. 103:92-99.
31. Biesbroek, R. and Ancarola, B.P. (2003). Study of Genetic Algorithms settings for trajectory optimization, IAC-03-A.P.30.
32. Bollt, E.M., and Meiss, J.D. (1995). Controlling chaotic transport through recurrence, *Physica D: Nonlinear Phenomena*, 81(3): 280, 294.
33. Briozzo, C. B. and Leiva, A. M. (2004). Catálogo de Familias de Orbitas Periódicas de Transferencia Rápida en el RTBP Tierra - Luna. In BAAA 47: 77-80.
34. Broschart, S.B., Chung, M.J., Hatch, S.J., Ma, J.H., Sweetser, T.H., Weinstein-Weiss, S.S., and Angelopoulos, V. (2009). Preliminary Trajectory Design for the ARTEMIS Lunar Mission, Proceedings of the AIAA/AAS Astrodynamics Specialist Conference, Aug. 9-13, 2009, Pittsburgh, Pennsylvania (A.V. Rao, T.A.Lovell, F.K.Chan and L.A.Cangahuala, eds.), Vol. 134, Paper AAS 09-382, *Advances in Astronautical Sciences*, AAS/AIAA, Univelt Inc., San Diego, California.

35. Byrnes, D.V. (1979). Application of the Pseudostate Theory to the Three-Body Lambert Problem. AAS Paper 79-163.
36. Campagnola, S. and Lo, M. (2007). BepiColombo gravitational capture and the elliptic restricted three-body problem. In PAMM, 7, 1030905-1030906.
37. Castellà, E. and Jorba, Á. (2000). On the vertical families of two-dimensional Tori near the triangular points of the bicircular problem. *Celestial Mechanics and Dynamical Astronomy* 76:35–54.
38. Castillo, A., Bello, M., Gonzalez, J.A., Janin, G., Graziani, F., Teofilatto, P. and Circi, C. (2003). Use of Weak Stability Boundary Trajectories for Planetary Capture. IAF-03-A.P.31, In 54th International Astronautical Congress of the International Astronautical Federation, the International Academy of Astronautics, and the Interanational Institute of Space Law, 29 Sep- 3 Oct 2003, Bremen, Germany.
39. Chobotov, V.A. (1996). *Orbital Mechanics*, 2nd Edition, AIAA Education Series.
40. Chung, M.J., Hatch, S.J., Kangas, J.A., Long, S.M., Roncoli, R.B. and Sweetser, T.H. (2010) Trans-Lunar Cruise Trajectory Design of GRAIL (Gravity Recovery and Interior Laboratory) Mission, AIAA 2010-8384. In AIAA Guidance, Navigation and Control Conference, Toronto, Ontario, Canada, 2-5 Aug 2010.
41. Circi, C. and Teofilatto, P. (2001). On the Dynamics of Weak Stability Boundary Lunar Transfers, *Celestial Mechanics and Dynamical Astronomy*, 79:41-72.
42. Circi, C. and Teofilatto, P. (2006). Weak Stability Boundary Trajectories for the Deployment of Lunar Spacecraft Constellations. *Celestial Mechanics and Dynamical Astronomy*, 95:371-390.
43. Coffee, T.M., Anderson, R.L. and Lo, M.W. (2011). Multiobjective optimization of low-energy trajectories using optimal control on dynamical channels (Part-1), AAS 11-129.
44. Conley, C. (1968). Low Energy Transit Orbits in the Restricted Three Body Problem, *SIAM Journal Applied Mathematics*, 16(4):732-746.
45. Conway, B.A. (2010). *Spacecraft Trajectory Optimization*. Cambridge University Press.

46. Cook, R.A., and Lyons, D.T., (1992) Magellan aerobraking periapse corridor design, AAS 92-159.
47. Curtis, H., (2005), *Orbital Mechanics for Engineering Students*, Elsevier Aerospace Engineering Series.
48. Dachwald, B. (2004). Low Thrust Trajectory Optimization and Interplanetary Mission Analysis using Evolutionary Neurocontrol, Deutscher Luft- und Raumfahrtkongress, Dresden, Germany.
49. Doody, David F., (1995). Aerobraking the Magellan Spacecraft in Venus Orbit, *Acta Astronautica*, 35:475-480.
50. Dumitras, Elena, D. (1997). A Runge-Kutta-Fehlberg procedure for numerical integration of differential equations systems. *Computational Applied Mathematics* 6(2): 42-45.
51. Dutt, P. and Sharma, R.K. (2010). Analysis of periodic and quasi-periodic orbits in the Earth-Moon system, *Journal of Guidance, Control and Dynamics*, 33 (3): 1010-1017.
52. Dutt, P. and Sharma, R.K. (2011). Evolution of periodic orbits near the Lagrangian point L2. *Advances in Space Research*, 47 (11):1894-1904.
53. Egorov, V.A. (1958). Certain Problems of Moon Flight Dynamics, in *The Russian Literature of Satellites, Part 1*, International Physical Index, Inc., New York.
54. Fantino, E., Gómez, G., Masdemont, J.J. and Ren, Y. (2010). A note on libration point orbits, temporary capture and low-energy transfers. *Acta Astronautica* 67:1038-1052.
55. Fehlberg, E. (1969). Low-order classical Runge-Kutta formulas with step size control and their application to some heat transfer problems, NASA Technical Report 315.
56. Foing, B.H., and Racca, G.R. (1999). The ESA SMART-1 Mission to the Moon with Solar Electric Propulsion, *Advances in Space Research*, 23(11):1865-1870.
57. Folta, D.C., Webster, C.M., Bosanac, N., Cox, A.D., Guzzetti, D. and Howell, K.C. (2016). Trajectory Design Tools for Libration and Cislunar Environment, 6th International Conference on Astrodynamics Tools and Techniques, 2016.

58. Folta, D., Woodard, M., Sweetser, T., Broschart, S.B. and Cosgrove, D. (2011). Design and Implementation of the ARTEMIS Lunar Transfer using Multi-body Dynamics, AAS 11-511.
59. García, F. and Gómez, G. (2007). A note on weak stability boundaries, *Celestial Mechanics and Dynamical Astronomy*, 97:87-100.
60. Gómez, G. and Masdemont, J. (2000). Some zero cost transfers between libration point orbits, AAS/AIAA Space Flight Mechanics Meeting, Clearwater, Florida, Paper No. AAS 00-177.
61. Gómez, G., Koon, W.S., Lo, M.W., Marsden, J.E., Masdemont, J. and Ross, S.D. (2004). Connecting orbits and invariant manifolds in the spatial restricted three-body problem. *Nonlinearity* 17:1571-1606.
62. Graziani, F., Teofilatto, P., Circi, C., Porfilio, M., Mora, M.B. and Hechler, M. (2000). A strategy to find weak stability boundary lunar transfers. In AIAA 2000.
63. Griesemer, P.R., Ocampo, C. and Cooley, D.S. (2011). Targeting Ballistic Lunar Capture Trajectories Using Periodic Orbits, 34(3): 893-902.
64. Grover, P. and Andersson, C. (2012). Optimized three-body gravity assists and manifold transfers in end-to-end lunar mission design, AAS 12-184.
65. Gurfil, P. and Kasdin, N.J. (2002). Characterization and design of out-of-ecliptic trajectories using deterministic crowding genetic algorithms, *Computational Methods Applied Mechanics Engineering*. 191:2141-2158.
66. Gurzadyan, G.A., (1996) *Theory of Interplanetary Flights*, Gordon and Breach Publishers.
67. Hadjidemetriou, J.D. (1968). A classification of orbits through L1 in the Restricted three body problem. *The Astronomical Journal*, 73(2), Part I.
68. Hairer, E., Norsett, S. and Wanner, G. (1993). *Solving Ordinary Differential Equations I: Nonstiff Problems*, II edition, Springer-Verlag, Berlin. ISBN 3-540-56670-8.
69. Hatch, S.J., Roncoli, R.B. and Sweetser, T.H. (2010). GRAIL Trajectory Design: Lunar Orbit Insertion through Science, *Proceedings of the AIAA/AAS Astrodynamics Specialist Conference*, August 2-5, 2010, Toronto, Ontario, Paper AIAA 2010-8385.

70. Heaton, A.F., Strange, N.J., Longuski, J.M. and Bonfiglio, E.P. (2002). Automated Design of the Europa Orbiter Tour, *Journal of Spacecraft and Rockets*, 39(1).
71. Hénon, M. (1965a). Exploration Numérique du Problème Restreint. I. Masses égales, Orbites périodiques, *Annales d'Astrophysique*, 28(2): 499-511.
72. Hénon, M. (1965b). Exploration Numérique du Problème Restreint. II. Masses égales, stabilité des orbites périodiques, *Annales d'Astrophysique*, 28(2): 992-1007.
73. Heppenheimer. (1978). A mass-catcher for large scale lunar material transport, *Journal of Spacecraft and Rockets*, 15:242-249.
74. Howell, K.C., Mains, D.L., Barden, B.T. (1994). Transfer trajectories from Earth parking orbits to Sun-Earth halo orbits. In *AAS/AIAA Space Flight Mechanics Meeting*, Cocoa Beach, Florida, Paper No. AAS 94-160.
75. Howell, K.C., Barden, B. and Lo, M. (1997). Application of Dynamical Systems Theory to Trajectory Design for a Libration Point Mission, *JAS* 45(2).
76. Howell, K.C., Marchand, B.G., Lo, M.W. (2000). Temporary Satellite Capture of short-periodic Jupiter family comets from the perspective of dynamical systems, *AAS/AIAA Space Flight Mechanics Meeting*, Clearwater, Florida USA, Paper No. 00-155.
77. Huang, T.-Y. and Innanen, K.A. (1983). The gravitational escape/capture of planetary satellites, *Astronomical Journal*, 88:1537-1548.
78. Hunter, R. (1967). Motions of satellites and asteroids under the influence of Jupiter and the Sun, *Monthly Notices of the Royal Astronomical Society*, 136:245-277.
79. http://www.opencourse.info/astronomy/introduction/05.motion_planets/
80. <http://star.arm.ac.uk/research/solarsystem/jma/hohmann.html>
81. [https://en.wikipedia.org/wiki/Sphere_of_influence_\(astrodynamics\)](https://en.wikipedia.org/wiki/Sphere_of_influence_(astrodynamics))
82. Ivashkin V.V. (2002). On Trajectories of the Earth-Moon Flight of a Particle with its Temporary Capture by the Moon. *Doklady Physics, Mechanics* 47(11):825-827.

83. Ivashkin V. V. (2003). On the Earth-to-Moon Trajectories with Temporary Capture of a Particle by the Moon. In 54th International Astronautical Congress, Bremen, Germany, September 29 – October 3. Paper IAC-03-A.P.01 pp. 1-9.
84. Ivashkin V. V. (2004) On Trajectories for the Earth-to-Moon Flight with Capture by the Moon. In Proceedings of the International Lunar Conference 2003 / International Lunar Exploration Working Group 5 – ILC2003/ILEWG 5, 16-22 November 2003 in Waikoloa Beach Marriott Hotel, Hawaii Island, USA. Eds: Steve M. Durst, et al. American Astronautical Society AAS. Vol. 108, Science and Technology Series. Published for the AAS and Space Age Publishing Company, Paper AAS 03-723:157-166.
85. Jefferys, W.H. (1971). An atlas of surfaces of section for the restricted problem of three bodies, University of Texas, Austin.
86. Jehn, R., Campagnola, S., Garcia, D. and Kemble, S. (2004). Low thrust approach and gravitational capture at mercury. In 18th International Symposium on Space Flights Dynamics, Munich, Germany, 11-15 Oct 2004.
87. Jehn, R., Companys, V., Corral, C., Yarnoz, D.G. and Sanchez, N. (2008). Navigating BepiColombo during the weak stability capture at Mercury. *Advances in Space Research*, 42:1364-1369.
88. Johannesen J.R., and D’Amario, L.A. (1999). Europa Orbiter Mission Trajectory Design, AAS Paper 99-360.
89. Jorba, Á. (2000). A numerical study on the existence of stable motions near the triangular points of the real Earth–Moon system. *Astronomy and Astrophysics*, 364 (1): 327–338.
90. Kawaguchi, J., Yamakawa, H., Uesugi, T. and Matsuo, H. (1995). On making use of lunar and solar gravity assists in LUNAR-A, PLANET-B missions. *Acta Astronautica*, 35(9-11): 633-642.
91. Kluever, C.A. (1997). Optimal Earth–Moon trajectories using combined chemical–electric propulsion. *Journal of Guidance, Control and Dynamics*, 20 (2): 253–258.
92. Koon, W.S., Lo, M.W., Marsden, J.E. and Ross, S.D. (2007). *Dynamical Systems, the Three-Body Problem, and Space Mission Design*, Springer-Verlag, New York.
93. Krish, V. (1991). An Investigation into Critical Aspects of a New Form of Low Energy Lunar Transfer, the Belbruno-Miller Trajectories, M.Sc. Thesis, Massachusetts Institute of Technology.

94. Kulkarni, T.R. and Mortari, D. (2005). Low energy interplanetary transfers using halo orbit hopping method with STK/Astrogator, AAS 05-111.
95. Lagarias, J.C., Reeds, J.A., Wright, M.H., Wright, P.E. (1998). Convergence properties of the Nelder-Mead simplex method in low dimensions. *SIAM Journal on Control and Optimization*, 9(1): 112–147.
96. Lantoine, G., Russell, R.P. and Campagnola, S. (2009). Optimization of low-energy resonant hopping transfers between planetary moons, IAC-09.C1.1.1.
97. Lee, K.H. (2011) Lunar Orbiter Trade Study and Conceptual Design of Onboard Propulsion Systems, *Journal of Spacecrafts and Rockets*, 48(2).
98. Lizia, P.D., Radice, G., Izzo, D., and Vasile, M. (2005). On the solution of Interplanetary Trajectory Design Problems by Global Optimisation Methods, *Proceedings of GO*: 1-7.
99. Llibre, J., Martinez, R. and Simo, C. (1985). Transversality of the invariant manifolds associated to the Lyapunov family of periodic orbits near L2 in the restricted three-body problem, *Journal of Differential Equations*, 58:104-156.
100. Lo, M.W. and Chung, M.K. (2002). Lunar Sample Return via the Interplanetary Superhighway, *AIAA/AAS Astrodynamics Specialist Meeting*, Monterey, CA, Paper No. AIAA 2002-4718.
101. Lo, M.W., Anderson, R.L., Whiffen, G. and Romans, L. (2004). The Role of Invariant Manifolds in Low Thrust Trajectory Design (Part I), AAS Paper 04-288.
102. Lo, M.W., Anderson, R.L., Lam, T., Whiffen, G. (2006). The Role of Invariant Manifolds in Low Thrust Trajectory Design (Part III), AAS Paper 06-190.
103. Lo, M.W. and Parker, J.S., (2005). Chaining Simple Periodic Three Body Orbits, AAS 05-380.
104. Lo, M. and Ross, S. (1997). SURFing the solar system: invariant manifolds and the dynamics of the solar system, *JPL IOM 312/97:2-4*.
105. Longuski, J.M. and Williams, S.N. (1991). Automated Design of Gravity-Assist Trajectories to Mars and the Outer Planets, *Celestial Mechanics and Dynamical Astronomy* 52: 207-220.

106. Luo, Y.Z., Tang, G.J. and Li, H.Y. (2006). Optimization of multiple-impulse minimum-time rendezvous with impulse constraints using a hybrid genetic algorithm, *Aerospace Science Technology*, 10(6):534-540.
107. Luo, Y.Z., Lei, Y.J. and Tang, G.J. (2007). Optimal multi-objective nonlinear impulsive rendezvous, *Journal of Guidance Control and Dynamics*, 30(4):994-1002.
108. Lyons, D.T., (2000). Aerobraking Trajectory Options for the first Mars Micro-Mission Telecom orbiter, AAS 00-199.
109. Markellos, V.V., (1974). Numerical investigation of the planar restricted three body problem, *Celestial Mechanics and Dynamical Astronomy*, 10(1): 87-134.
110. McGehee, R. (1969). Some homoclinic orbits for the restricted three-body problem, PhD thesis, University of Wisconsin, Madison.
111. Melo, C.F., Macau, E.E.N., Winter, O.C. and Neto, E.V. (2007). Numerical study about natural escape and capture routes by the Moon via Lagrangian points L1 and L2, *Advances in Space Research*, 40:83-95.
112. Mendell, W.W. (2001). A gateway for human exploration of space? The weak stability boundary, *Space Policy* 17: 13-17.
113. Miller, J.K. and Belbruno, E.A. (1991). A method for the construction of a Lunar Transfer Trajectory using Ballistic Capture, AAS/AIAA Spacecraft Mechanics Meeting, AAS 91-100.
114. Miller, J.K. (2003). Lunar transfer trajectory design and the four body problem, ASS 03-144.
115. Mingotti, G., Topputo, F. and Bernelli-Zazzera, F. (2003). Hybrid propulsion transfers to the Moon, IAA-AAS-DyCoSS1-03-01.
116. Mingotti, G., Topputo, F. and Bernelli-Zazzera, F. (2009). Low-energy, low-thrust transfers to the Moon, *Celestial Mechanics and Dynamical Astronomy*, 105: 61-74.
117. Moore, A. (2009). Two approaches utilizing invariant manifolds to design trajectories for DMOC optimization. Geometric Mechanics Project Archives, California Institute of Technology, Pasadena, CA. <http://www.cds.caltech.edu/~marsden/projects/geomech>.

118. Mora, M.B., Graziani, F., Teofilatto, P., Circi, C., Porfilio, M. and Hechler, M. (2000). A systematic analysis on weak stability boundary transfers to the Moon, IAF-00-A.6.03.
119. Murison, M.A. (1989). The Fractal Dynamics of Satellite Capture in the Circular Restricted Three-Body Problem, *The Astronomical Journal*, 98(6).
120. Nakamiya, M., Yamakawa, H., Scheeres, D.J. and Yoshikawa, M. (2008). Analysis of capture trajectories into periodic orbits about libration points, *Journal of Guidance, Control and Dynamics*, 31(5).
121. Nakamiya, M., Yamakawa, H., Scheeres, D.J. and Yoshikawa, M. (2010). Interplanetary transfers between Halo orbits: connectivity between escape and capture trajectories, *Journal of Guidance, Control and Dynamics*, 33(3).
122. Neto, E.V. and Prado, A.F.B.A. (1998). Time-of-Flight Analyses for the Gravitational Capture Maneuver. *Journal of Guidance, Control and Dynamics*, 21(1):122-126.
123. Neto, E.V. and Winter, O.C. (2001). Time analysis for temporary gravitational capture: satellites of Uranus, *The Astronomical Journal*, 122: 440-448.
124. Ocampo, C. (2005). Trajectory Analysis for Lunar Flyby Rescue of Asiasat-3/HGS-1, *New Trends in Astrodynamics and Applications*, *Annals of New York Academy of Sciences*, 1065:232-253.
125. Ockels, W.J. and Biesbroek, R. (1999). Genetic Algorithms used to determine WSB trajectories for LunarSat Mission. In *Proceedings of Fifth International Symposium on Artificial Intelligence, Robotics and Automation in Space*, 1-3 June 1999.
126. Parker, J.S. and Anderson, R.L. (2013). *Low-Energy Lunar Trajectory Design*, *Deep Space Communication and Navigation Series*, Wiley.
127. Peng, L., Wang, Y., Dai, G., Chang, Y., Chen, F. (2010). Optimization of the Earth-Moon low energy transfer with differential evolution based on uniform design. In *IEEE Congress on Evolutionary Computation (CEC)*, 18-23 July 2010.
128. Peng, L., Dai, G., Wang, M., Hu, H., Chang, Y. and Chen, F. (2011). Self-adaptive uniform differential evolution for optimizing the initial integral point of the Earth-Moon low-energy transfer, *Journal of Aerospace Engineering*, 225(11): 1263-1276.

129. Parker J.S. and Anderson, R.L. (2013). Surveying Ballistic Transfers to Low Lunar Orbit, *Journal of Guidance, Control and Dynamics*, 36(5).
130. Parker, T.S. and Chua, L.O. (1989). *Practical Numerical Algorithms for Chaotic Systems*, Springer-Verlag, New York.
131. Prado, A.F.B. (1996). Powered Swing-by, *Journal of Guidance, Control and Dynamics*, 19(5):1142-1147.
132. Prado, A.F.B. (2005). Numerical and analytical study of the gravitational capture in the bicircular problem. *Advances in Space Research* 36:578–584.
133. Radice,G. and Olmo,G., Ant colony algorithms for two-impulse interplanetary trajectory optimization, *Journal of Guidance, Control and Dynamics*, 29 (6):1440–1444.
134. Ramanan, R.V.(2013). Interplanetary Mission Opportunities, *PLANEX*, 3(2).
135. Repic, E.M., Boobar, M.G, Chapel, F.G., (1968) Aerobraking as a potential planetary capture mode. *Journal of Spacecraft and Rocketry*, 5(8).
136. Romagnoli, D. and Circi, C. (2009). Earth-Moon Weak Stability Boundaries in the restricted three and four body problem, *Celestial Mechanics and Dynamical Astronomy*, 103:79-103.
137. Roncoli, R.B. and Fujii, K.K. (2010). Mission Design Overview for Gravity Recovery and Interior Laboratory (GRAIL) Mission, *Proceedings of AIAA/AAS Astrodynamics Specialist Conference*, August 2-5, 2010, Toronto, Ontario, Paper AIAA 2010-8383.
138. Ross, S.D., Koon, W.S., Lo, M.W. and Marsden, J.E. (2003). Design of a multi-moon orbiter. In 13th AAS/AIAA Space Flight Mechanics Meeting, Puerto Rico.
139. Ross, S.D., Koon, W.S., Lo, M.W., Marsden, J.E. (2004). Application of Dynamical Systems Theory to a Very Low Energy Transfer, AAS 04-289.
140. Safiya Beevi, A. and Sharma, R.K. (2011). Analysis of periodic orbits in the Saturn-Titan system using the method of Poincaré section surfaces. *Astrophysics and Space Science*, 333(1): 37-48.

141. Schoenmaekers, J., Horas, D. and Pulido, J.A. (2001). SMART-1: with solar electric propulsion to the moon. In 16th International Symposium on Space Flight Dynamics, Pasadena, CA, 3-7 Dec 2001.
142. Schroer, C.G. and Ott, E. (1997). Targeting in Hamiltonian systems that have mixed regular/chaotic phase spaces. *Chaos*, 7: 512-519.
143. Schy, A.A. and White, J.A. (1969). Deceleration control systems for aerobraking and skipout to orbit at Mars, *Journal of spacecraft and Rockets*, 6(7):831-834.
144. Sergeyevsky, A.B., Snyder, G.C. and Cunniff, R.A. (1983). *Interplanetary Mission Design Handbook, Vol 1, Part 2, Earth to Mars Ballistic Mission Opportunities, 1990-2005*, JPL Publication 82-43.
145. Strizzi, J.D., Kutrieb, J.M., Dampousse, P.E. and Carrico, J.P. (2001). Sun-Mars Libration Points and Mars Mission Simulations, AAS 01-159.
146. Sweetser, T., Maddock, R., Johannesen, J., Bell, J., Penzo, P., Wolf, A., Williams, S., Matousek, S. and Weinstein, S. (1997). Trajectory Design for a Europa Orbiter Mission: A Plethora of Astrodynamical Challenges. In AAS/A IAA Space Flight Mechanics Meeting. Huntsville, Alabama. Paper No. AAS 97- 174.
147. Striepe, S.A., Braun, R.D., Powell, R.W., (1993) Influence of Interplanetary Trajectory Selection on Mars Atmospheric Entry Velocity, *Journal of Spacecraft & Rockets*, 30(4).
148. Szebehely, V. (1967). *Theory of Orbits*, Academic Press, New York.
149. Topputo, F. (2013). On optimal two-impulse Earth Moon transfers in a four-body model, *Celestial Mechanics and Dynamical Astronomy*, 117: 279-313.
150. Topputo, F. and Belbruno, E. (2009). Computation of Weak Stability Boundaries: Sun-Jupiter System, *Celestial Mechanics and Dynamical Astronomy*, 105(1-3):3-17.
151. Topputo, F. and Belbruno, E. (2015). Earth-Mars transfers with ballistic capture, *Celestial Mechanics and Dynamical Astronomy*, 121: 329-346.
152. Topputo, F., Belbruno, E. and Gidea, M. (2008). Resonant motion, ballistic escape, and their applications in astrodynamics, *Advances in Space Research*, 42:1318-1329.

153. Topputo, F., Vasile, M. and Finzi, A.E. (2004). An approach to the design of low energy interplanetary transfers exploiting invariant manifolds of the restricted three-body problem. AAS 04-245.
154. Topputo, F., Vasile, M. and Bernelli-Zazzera F. (2005). Earth-to-Moon low energy transfers targeting L1 hyperbolic transit orbits, *Ann. N.Y.Acad Sci.* 1065: 55-76.
155. Uesugi, K. (1996). Results of the Muses-A “Hiten” Mission, *Advances in Space Research*, 18(11):69-72.
156. Vallado, D.E. (2001). *Fundamentals of Astrodynamics and Applications*, Kluwer.
157. Vasile, M., Summerer, L. and Pascale, P.D. (2005) Design of Earth Mars transfer trajectories using evolutionary-branching technique. *Acta Astronautica*, 56(8): 705-720.
158. Venkattaramanan, R., (2006), *Lunar Transfer Trajectories*, PhD thesis, University of Kerala.
159. Vetrignano, M., Vander Weg, M. and Vasile, M. (2012). Navigating to the Moon along low-energy transfers, *Celestial Mechanics and Dynamical Astronomy*, 114(1-2): 25-53.
160. Villac, B.F. and Scheeres, D.J. (2004). A simple algorithm to compute hyperbolic invariant manifolds near L1 and L2, AAS 04-243.
161. Wilson, S. W. (1970). A Pseudostate Theory for the Approximation of Three-Body Trajectories, AIAA Paper 70-1061, In AIAA Astrodynamics Conference, Santa Barbara, Calif., Aug . 1970.
162. Winter, O.C. (2000). The stability evolution of a family of simply periodic lunar orbits, *Planetary Space Science* 48(1): 23-38.
163. Winter, O.C. and Neto, E.V. (2001). Time analysis for temporary gravitational capture, *Astronomy and Astrophysics*, 377: 1119-1127.
164. Wiggins, S. (1994). *Normally Hyperbolic Invariant Manifolds in Dynamical Systems*, Springer-Verlag, New York.
165. Yagasaki, K. (2004a). Computation of low energy Earth-to-Moon transfers with moderate flight time. *Phys. D: Nonlinear Phenom*, 197: 313–331.

166. Yagasaki, K. (2004b). Sun-perturbed Earth-to-Moon transfers with low energy and moderate flight time, *Celestial Mechanics and Dynamical Astronomy*, 90 (3–4): 197–212.
167. Yam, C.H., Biscani, F. and Izzo, D. (2009). Global Optimization of Low-Thrust Trajectories via Impulsive Delta-V Transcription, 2009-d-03, In 27th International Symposium on Space Technology and Science.
168. Yamakawa, H. (1992). On Earth-Moon Transfer Trajectory with Gravitational Capture, PhD thesis, University of Tokyo.
169. Yamakawa, H., Kawaguchi, J., Ishii, N. and Matsuo, H. (1992). A numerical study of gravitational capture orbit in the Earth-Moon system, AAS 92-186.
170. Yamakawa, H., Kawaguchi, J., Ishii, N. and Matsuo, H. (1993). On Earth-Moon Transfer Trajectory with Gravitational Capture, AAS 93-633.
171. Yokoyama, N. and Suzuki, S. (2005). Modified genetic algorithm for constrained trajectory optimization, *Journal of Guidance, Control and Dynamics*, 28 (1):139–144.